Travail de Fin d'Etudes : Behaviour of steel joints under dynamic actions

Auteur : Golea, Tudor
Promoteur(s) : Jaspart, Jean-Pierre; Demonceau, Jean-Francois

Faculté : Faculté des Sciences appliquées
Diplôme : Master en ingénieur civil des constructions, à finalité spécialisée en "civil engineering"
Année académique : 2019-2020
URI/URL : http://hdl.handle.net/2268.2/9101

UNIVERSITY OF LIÈGE

FACULTY OF APPLIED SCIENCES

Behaviour of Steel Joints Under Dynamic Actions

Graduation Studies conducted for obtaining the Master's degree in

Civil Engineering

by

Tudor Golea

MEMBERS OF THE JURY
Jean-Pierre Jaspart
Jean-François Demonceau
Vincent Denoël
Adrien Corman
Alexandru Aldea

SUPERVISORS
Jean-Pierre Jaspart
Jean-François Demonceau

Academic year 2019-2020

Abstract

The extensive use of steel framed structures as a solution for fast, efficient and well-controlled construction process has stimulated the research on the behaviour of steel connections under static and seismic loading regimes. Nonetheless, there is a limited amount of knowledge around the response of steel joints subjected to transient dynamic loads. Exceptional loading situations due to explosions or impact can lead to the failure of structural elements directly exposed or in the proximity of the loading source. When a joint between two or more structural elements has failed, potential progressive collapse of the structure may occur as a result of the propagation of initial failures. Therefore, to make the built environment safe, it is important to evaluate accurately the resistance capacities and ductility of steel joints.

Current design standards provide a very limited guidance for the design of joints subjected to transient loads, mainly due to the lack of investigations conducted on this topic. The present thesis addresses these aspects by exploring several methods of assessment of the joints non-linear response under quasi-static and impact loading. Experimental, analytical and numerical approaches are employed to predict the observed real behaviour of steel connections. The analytical and numerical procedures are validated against tests results available from the experimental campaign conducted within the research project RobustImpact.

More than 20 specimens of double-sided beam-to-column joint configurations were tested under quasi-static and dynamic loading regimes. The analytical procedures used for the characterisation of the behaviour of steel joints under monotonic loads tend to estimate accurately the response experimentally observed. A specific limitation of the analytical model implemented in Eurocde 3 has been highlighted in this study. For static conditions, the equivalent T-stub model is likely to underestimate the ultimate resistance capacity when it is used for components with thin plates.

The FE modelling techniques allow for the accurate simulation of the response of steel joints under both static and impact loading scenarios. Within the framework of this thesis several FE models that incorporate the material rate sensitivity were developed and validated against experimental results. A good agreement between the simulations and the physical tests results was obtained. The strain rate effects expressed in terms of Dynamic Increase Factors were quantified relying on two assessment methods - analytical and numerical.

The analytical method used for the estimation of maximum impact forces leads to generally accurate predictions. Consequently, this method is used for the estimation of strain rate effects. The values found for the DIFs were in partial-to-good agreement with the ones estimated from the FE results, allowing for the identification of basic active components mostly susceptible to be affected by the deformation rate.

Acknowledgement

I would like to express my deep and sincere gratitude to my research supervisors, Prof. Jean-Pierre Jaspart and Prof. Jean-François Demonceau for giving me the opportunity to conduct this study under their guidance. The completion of this work could have not been accomplished without their advice and continuous support.

Besides my advisors, I would like to thank to the rest of my thesis committee:
Prof. Vincent Denoël, Ing. Adrien Corman and Prof. Alexandru Aldea for their feedback and insightful comments.

I would like to express my special appreciations to the students of the doctoral program of the University of Liège, namely to Marina D'Antimo and Adrien Corman for their continuous support and experience sharing. Without their help this study might not have been possible.

Last but not least, I am truly grateful to my family and friends for supporting me unconditionally, either morally, physically or financially.

Contents

List of Figures

List of Tables

1 | Introduction

1.1 Background & Context

In the past three decades, particularly after such catastrophic events as natural hazards or terrorist attacks, the interest of research community into investigation of the structural response of steel members and steel connections subjected to extreme dynamic loads has increased considerably. After the terrorist attack and the collapse of the World Trade Center in 2001, the necessity of understanding and quantifying the connections as critical components in structural frames subjected to impact loads has become indisputable.

In a framed structure, the beam-to-column joints should exhibit adequate strength and ductility allowing to resist and transmit the loads without failing. The accidental dynamic loads are not an exception and as stated in UFC 3-340-02 (DOD, 2008): *"the main frame connections must be designed for strength, stiffness, and rotational capacity in the case of blast loading"*. The adequate measures taken in the design phase should prevent the local failure of the connections that could eventually lead to a progressive collapse of the structure.

Notwithstanding the proven importance of understanding the behaviour of steel connections subjected to accidental loads, there is observed a lack of knowledge concerning their dynamic capacities, mostly due to the limited amount of research studies conducted in this field. A few general guidelines and recommendations on the design of beam-to-column connections under severe loading conditions are provided by the current design codes, the dynamic effects being considered in a very simplified manner by most of structural engineers, or even worse - simply disregarded. Specific parts of the Eurocodes are suggesting practical measures and simplified approaches on dealing with accidental actions and their potential effects. EN 1991-1-7 (EC1, 2006) identifies and classifies the accidental actions due to internal explosions and impact, providing also some general strategies for accidental design situations. EN 1998-1:2004 (EC8, 2004) deals with the design of structures for seismic resistance, thus treating the subject of dynamic loading scenarios induced by seismic events. These current design standards allow to account for the effects of accidental actions by means of equivalent static forces, recommending to consider the strain rate effects at the material level. The design of steel joints is currently treated by EN 1993-1-8 (EC3, 2005) (hereafter denoted Eurocode 3), but the provisions of this standard are valid for the quasi-static conditions, as the analyses and the experimental campaigns on which it relies were conducted for monotonic loads, the applicability of these provisions in the characterisation of the behaviour of steel joints subjected to extreme impact loads being questionable. The limited amount of knowledge and the uncertainties related to dynamic phenomena and material behaviour represent thus the stimulus for the enhancement of studies on the response of steel connections under extreme impulsive loading.

Currently, the joints are classified based on their stiffness, resistance and rotation capacity. Eurocode 3 classifies the joints according to their rotational stiffness into three main categories: *rigid, pinned* and *semi-rigid* joints (see Figure 1.1). Most of the joints exhibit in reality an intermediate behaviour between that of a pinned or rigid joint. This fact has contradicted the common practice among the designers to consider the joints to be either pinned or rigid only, as the joint behaviour is proven to have a significant effect on the overall response of a framed structure. However, the provisions and the guidelines provided by Eurocode 3 allow the assessment of the rotational stiffness and bearing capacity for a wide range of joint typologies using an analytical approach based on the component method. Concerning the seismic behaviour of steel structures, the guidance to perform a safe design is provided by Eurocode 8 (EC8, 2004), treating the matter of ductility and energy dissipation capacity of steel joints subjected to seismic action.

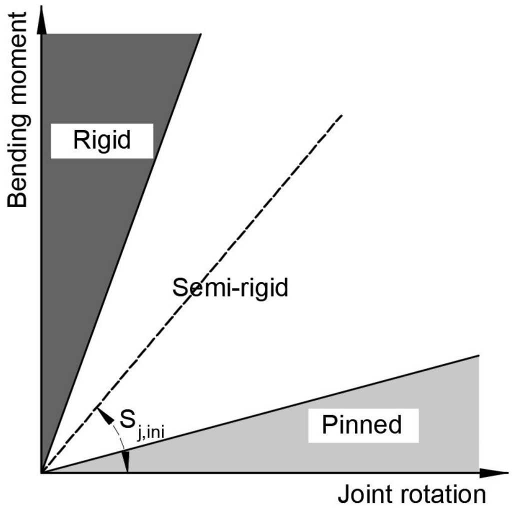

Figure 1.1: Classification of joints based on the rotational stiffness

Real evidences concerning the influence of joints on the overall ductility and deformation capacity of structural frames have been revealed in FEMA's (McAllister, 2002) report. It was concluded that a joint subjected to extreme impulsive loading may exhibit enhanced resistance, whereas its ductility is negatively affected.

Like most materials, when subjected to rapidly applied loads, the mild steel's behaviour is different when compared to the one considered in usual applications under quasi-static loading. Higher strain rates are causing an increase of steel's strength due to its visco-plastic behaviour, but in the same time, it can reduce its toughness, causing a premature fracture. The effects of the loading rate on the behaviour of steel connections was reported in a review by Arup (Arup, 2011) *"... the strain rate enhancement of yield strengths in connections could still be important. It is recommended that research is undertaken to examine this effect using rate-sensitive material models"*.

Usually, the effects related to the loading dynamic nature are quantified by means of Dynamic Increase Factors - DIFs, which represent the ratio between dynamic and static resistances of an element. The use of DIFs allows, in a simplified manner, for the estimation of dynamic effects on a structure, structural elements or even on the material mechanical properties.

Looking forward to understanding and quantifying the effects of extreme dynamic loads on the overall behaviour of steel joints, a research project entitled "RobustImpact" was funded by the Research Fund for Coal and Steel. The main objective was to investigate the behaviour and to provide additional guidance for the design of steel and steel-concrete composite structures under impulsive loading scenarios. As a part of this project, an experimental campaign, focused on the response of steel joints subjected to impact loads, was conducted at the University of Liège. The results of this experimental campaign will serve as a reference database for this thesis.

1.2 Objectives

The uncertainties related to the response of steel joints subjected to natural hazards and accidental loading are the main stimulus for conducting more and more research on this topic. Exploiting the results of physical tests conducted within the aforementioned research project "RobustImpact", the main objective of this study is to enhance the knowledge on the performance of steel joints under dynamic actions.

The present thesis aims at highlighting the discrepancies between the static and dynamic response of steel joints, with the main purpose of quantifying the effects of loading rates on the overall behaviour of connections. The approach is employing the use of finite element models that would be able to reproduce with high accuracy the experimentally observed behaviour. The finite element models have to be firstly validated against data collected throughout physical static tests and used afterwards for dynamic impact simulations. Additionally, once the numerical simulations provided the response of joints under dynamic actions, the results have to be confronted to the ones obtained during the experimental campaign, aiming at highlighting and quantifying the strain rate effects.

The behaviour of several joint configurations is investigated and the dynamic effects are assessed by means of dynamic increase factors - DIFs. It is intended to identify the joints typologies and basic joint components that are susceptible to exhibit a behaviour substantially influenced by the elevated strain rates.

In order to accomplish the main goals of this study, there are required knowledge and skills around finite element modelling techniques and FE analyses for both quasi-static and dynamic loading conditions.

1.3 Thesis outline

The complete thesis is outlined over six main chapters. To assist the reader, the following section provides a short survey of the key aspects addressed in each chapter.

In Chapter 1, the general aspects concerning the research motivation, main objectives and the relation to the research project RobustImpact are briefly presented.

Chapter 2 evaluates the available theoretical support for the characterisation of steel connections subjected to quasi-static and dynamic loading conditions. The most recent research investigations conducted on this topic and their outcome are presented briefly in this chapter.

In Chapter 3, the experimental campaign conducted within the research project RobustImpact is presented in detail. The main assumptions concerning the testing conditions are briefly reported and a survey of physical tests results is provided.

Chapter 4 presents the applicability of the component method in the assessment of joints response under quasi-static regime. A complementary approach is explored to enhance the prediction capacity of the analytical method proposed in Eurocode 3. Later, FE models are developed and validated against static tests results.

Chapter 5 describes the approaches used to estimate the dynamic effects on steel joints. A graphic method for the evaluation of strain rate effects is explored and afterwards is confronted with the FE predictions. The influence of strain rates on various joint components is clearly highlighted by comparing their static and dynamic behaviour.

Finally, Chapter 6 presents the conclusions drawn from the study identifies the aspects to be addressed for the improvement of prediction accuracy.

2 | Literature review

2.1 Steel joints - general aspects

Steel framed structures consist of beams and columns assembled in a specific network and linked by means of connections. Frequently, there is noticed a common misunderstanding of the two terms related to the link between structural elements in steel structures: *connection* and *joint*. A *connection* comprises the physical components which ensure the mechanical fastening of two or more connected elements. In the case of beam-to-column joints, the connection is considered to be concentrated at the interface between the beam end and the column. The term *"joint"* is used to describe the region comprising the connection itself and the corresponding zone of interaction between the fastened elements.

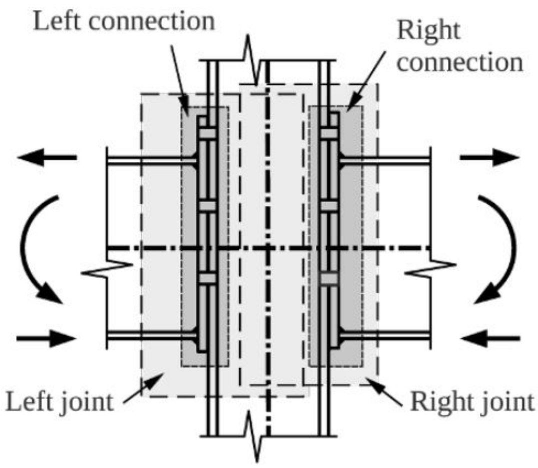

Figure 2.1: Typical double sided beam-to-column joint (Jaspart and Weynand, 2016)

As previously mentioned, in reality, when referring to their rotational stiffness, most of the joints exhibit an intermediate behaviour between that of fully rigid and pinned joints. When referring to its strength, according to Eurocode 3, a joint can be classified as *full-strength*, *partial strength* and *pinned*. Considering the joints properties related to their rotational stiffness and resistance, there could be adopted three main joint modelling approaches:

- rigid/full-strength;
- rigid/partial-strength;
- pinned.

Designing a joint as fully rigid or pinned leads to economically inefficient solutions. A joint modelling based on the semi-rigid behaviour would be thus more suitable from the economical point of view. Therefore, some new joint modelling possibilities were derived starting from the aforementioned ones:

- semi-rigid/full-strength;
- semi-rigid/partial-strength.

With a view to simplifying the problematics around the modelling procedure, three models which account for these possibilities were introduced in Eurocode 3:

- continuous, that is covering the case of rigid/full-strength joints;
- semi-continuous, that is covering the rigid/partial-strength, the semi-rigid/full-strength and the semi-rigid/partial-strength cases;
- simple, covering the case of pinned joints.

These joint models allow for the characterisation of a certain joint for different types of analysis performed by the designer (elastic, rigid-plastic, or elastic-perfectly plastic analysis). Whatever modelling possibility adopted, the assessment of joint's behaviour relies on its moment-rotation curve. The real behaviour of a joint is strongly nonlinear and is rather complex to predict in practice. With a view to simplification, Eurocode 3 idealizes the real moment-rotation curve using three different possibilities, adopted in such a way that would fit the frame analysis with different levels of complexity. Three idealisation possibilities are proposed by Eurocode 3, intending to cover the full range of analyses performed by designers:

- elastic, for an elastic analysis;
- rigid-plastic, for a rigid-plastic analysis;
- non-linear, for an elastic-plastic analysis.

For the latter, being the most complex, one can identify different idealisation possibilities (see Figure 2.2).

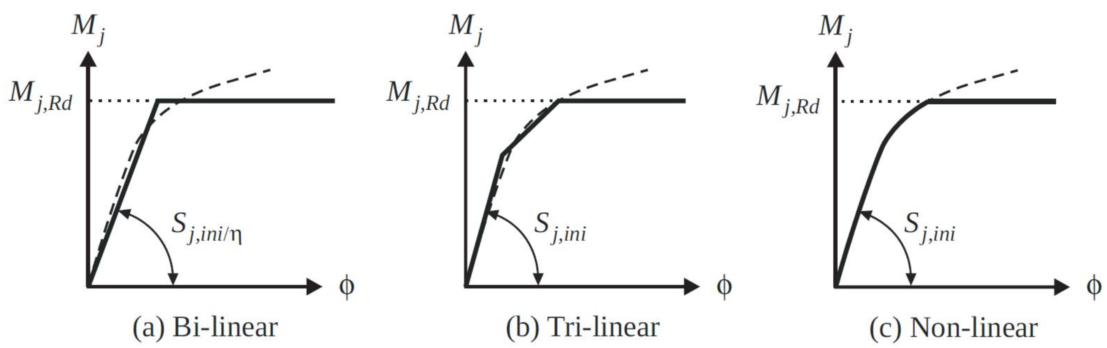

Figure 2.2: Non-linear representations of a M-ϕ curve (Jaspart and Weynand, 2016)

Despite its complexity of evaluation, the behaviour of joints is considered to be essential when the structural stability is assessed, or potential causes leading to progressive collapse are investigated. Although more and more recent studies and reported evidences from real cases (McAllister, 2002) have highlighted the joint as a critical component limiting the ductility and deformability of structural frames, currently, the guidance provided by the design standards (EC3, 2005) refers mostly to the stiffness and resistance of joints under quasi-static conditions.

2.2 Characterisation of the behaviour of steel joints

In the second half of the 20th century, the extensive use of steel elements as a solution for fast, reliable and well-controlled construction process has stimulated the efforts in the investigation of solutions for steel joints and their behaviour. Initially, the characteristics related to the resistance and stiffness of joints were of main interest for the research community (Zoetemeijer, 1974; Jaspart, 1991; Swanson and Leon, 2002). These research efforts led eventually to the development of current analytical methods, implemented in Eurocode 3 as the *"component method"*, for the assessment of joint's resistance and stiffness.

The component method aims at predicting the moment-rotation curve of a joint by discretising it into different physical components which contribute to the overall strength and stiffness with respect to their individual characteristics (stiffness, resistance and ductility). Each active component is modelled as a spring that reproduces its actual behaviour through a force-displacement non-linear curve. Currently, Eurocode 3 provides the analytical formulae to estimate the strength and stiffness properties for different types of components.

Following an assembly procedure based on the characteristics of its basic components, the joint is represented through a mechanical model. Subsequently, the moment-rotation curve is drafted by evaluating the stiffness and the resistance of basic active components, which can work either in series or in parallel. An example of such a mechanical model is depicted in Figure 2.3 for a typical beam-to-column bolted connection.

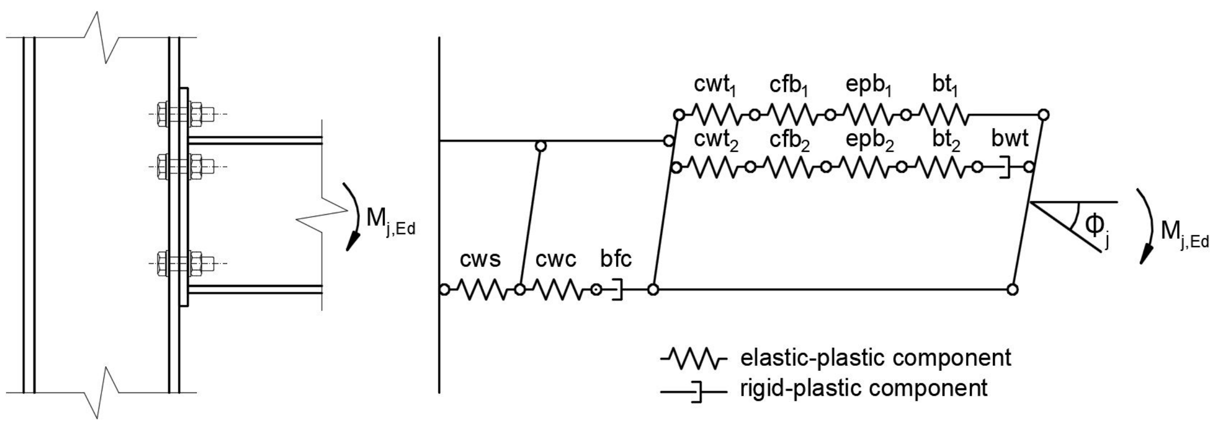

Figure 2.3: Mechanical model of a typical beam-to-column bolted joint

In a typical beam-to-column bolted joint, the basic active components covered by Eurocode 3 are:

- column web in shear (cws);
- column web panel in compression (cwc);
- column web in tension (cwt);

- column flange in bending (cfb);
- end-plate in bending (epb);
- beam flange and web in compression (bfc);
- beam web in tension (bwt);
- bolts in tension (bt).

Generally, the procedure to assess the behaviour of a specific joint through the component method implies the following 3 steps:

1. Identification of the active components;
2. Characterisation of the behaviour of each constitutive component through a F-Δ spring model;
3. Assembly of the active elements in a mechanical model comprising the elastic-plastic and the rigid-plastic components. By assembling the constitutive components, an equivalent element is obtained, for which the F-Δ characteristics are used to generate the global M-ϕ curve.

The characterisation of the non-linear response of a joint based on its mechanical model implies the estimation of an equivalent initial stiffness ($S_{j,ini}$) and an equivalent bending resistance ($M_{j,Rd}$) referring to the basic active components in the joint. The initial stiffness is evaluated using the elastic stiffness coefficients (k_i) of each ith contributing component, the lever arm (z) and the steel's Young modulus (E) as follows:

$$S_{j,ini} = \frac{E \cdot z^2}{\sum_i \frac{1}{k_i}} \tag{2.1}$$

The design moment resistance is evaluated according to the equilibrium equation:

$$M_{j,Rd} = \sum_r h_r \cdot F_{r,Rd} \tag{2.2}$$

where, h_r is the distance from the compression center to the rth bolt row and $F_{r,Rd}$ is the resistance of the rth bolt row taken as the minimum of the basic component resistances as follows:

$$F_{r,Rd} = min(F_{cwt}, F_{cfb}, F_{epb}, F_{bwt}, F_{bt}) \tag{2.3}$$

Based on these two characteristics of a joint ($S_{j,ini}$ and $M_{j,Rd}$), its design moment-rotation curve is generated following the model depicted in Figure 2.4 applying the following relations and limitations:

$$S_j = S_{j,ini} \quad \text{for} \quad M_{j,Ed} \leq \frac{2}{3} M_{j,Rd} \tag{2.4}$$

$$S_j = \frac{S_{j,ini}}{\mu} \quad \text{for} \quad \frac{2}{3} M_{j,Rd} \leq M_{j,Ed} \leq M_{j,Rd} \tag{2.5}$$

where, μ is the stiffness ratio determined as $\mu = \left(\frac{1.5M_{j,Ed}}{M_{j,Rd}}\right)^{\psi}$, with the coefficient ψ varying between 2.7 to 3.1 depending on the type of connection.

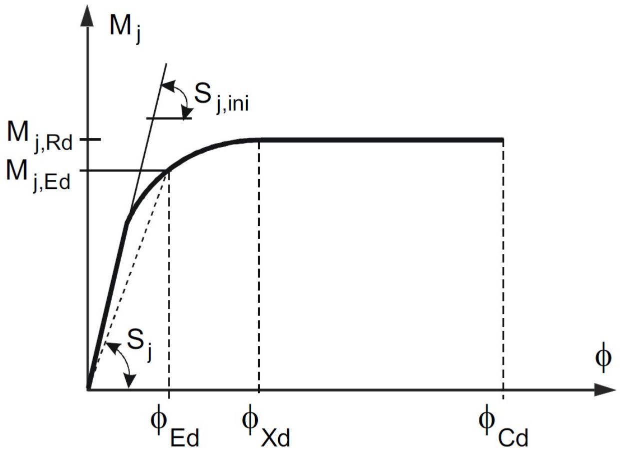

Figure 2.4: Moment-rotation curve according to EC3 (2005)

It is worth noting that the rotation capacity is directly dependent to the ductility of the joint's weakest basic components. Eurocode 3 provides general design conditions that would ensure that a specific joint will possess sufficient rotation capacity for a plastic global analysis. However, these provisions are leading to a rather qualitative evaluation of the rotational capacity (ϕ_{Cd}). As depicted Figure 2.5, the joint's rotational behaviour assessed using this procedure is mostly an idealisation of its real response.

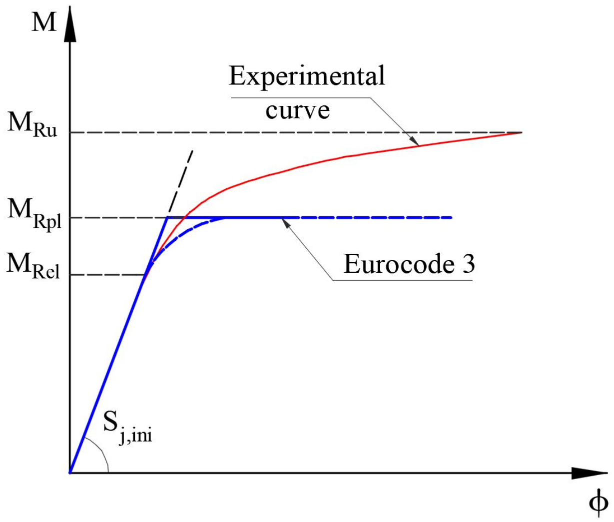

Figure 2.5: Experimental vs. design moment-rotation curve

This idealisation of the rotational behaviour is suitable for usual design practice, providing designers with a practical and reliable tool for the design of steel joints. However, its simplicity is leading to potential underestimations of the real capacities, that could have significant effects when some special rules of design, for example the "*Capacity Design*" concept, are applied or when a plastic analysis of structures with partial-strength joints is performed.

In order to improve the prediction accuracy for the resistance and rotational capacities of a steel joint, several studies were conducted on the extension of the component method applicability. Japsart et al. (2019) developed an analytical procedure to evaluate the ultimate and plastic rotational capacities. This simplified analytical approach is built around four key parameters: the initial stiffness ($S_{j,ini}$), the plastic bending resistance (M_{Rpl}), the stain-hardening stiffness ($S_{j,st}$) and the ultimate bending resistance (M_{Ru}).

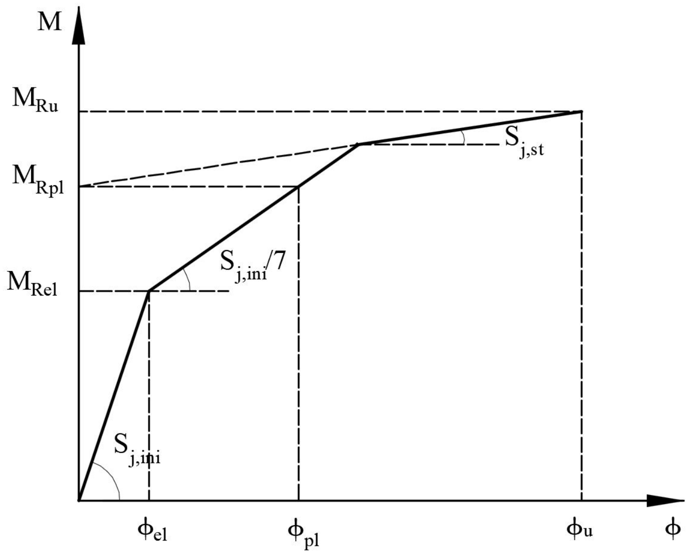

Figure 2.6: Joint $M-\phi$ curve according to Japsart et al. (2019)

Based on these parameters, several mathematical expressions have been developed, in order to approximate closely the non-linearity of the actual moment-rotation (M-ϕ) curve. While the current guidance provided by Eurocode 3 refers only to the evaluation of the initial stiffness ($S_{j,ini}$) and bending resistance (M_{Rpl}) of joints, this method aims at providing the analytical expressions for the estimation of the strain-hardening stiffness ($S_{j,st}$), ultimate bending resistance (M_{Ru}) and rotational capacity (ϕ_u). Its applicability can be seen as a complementary approach to the provisions of Eurocode 3.

The method proved to be efficient for various connection types, a good agreement between the experimental results and the analytical predictions being generally achieved. However, taking into account that the analytical approach is based on the component method, its accuracy for dynamic applications requires further investigations on the response of basic components under dynamic loading regimes.

2.3 Steel joints under dynamic actions

A proper assessment of the structural stability could play a significant role in preventing the progressive collapse. When the accurate assessment of structural capacities is sought, the behaviour of joints has to be explicitly considered Therefore, its precise characterisation is of great importance for a safe exploitation of a structure. The previous sections have briefly described the procedures used to evaluate the behaviour of steel joints under quasi-static loading conditions. Currently, the scientific community is preoccupied with investigating the performance of joints subjected to severe dynamic actions. However, most of the studies concerning the dynamic effects on the joints are focused on seismic action (Xu and Ellingwood, 2011) and fire (Santiago et al., 2008). Recently, the effects of impact and blast loads have become an investigation focus for some research groups.

The full-scale dynamic physical tests may provide useful information for understanding the response of steel joints. The limitations of this approach, related to its costs and difficulty to be performed in a controlled manner, are however important. Finite element models proved to be a feasible alternative to the physical tests. Moreover, this robust tool can be employed in the study of joints subjected to any type of loading scenarios, without requiring high economical and computational effort. Sabuwala et al. (Sabuwala et al., 2005) investigated typical beam-to-column joints subjected to blast loads by performing numerous 3D finite element (*FE*) analyses. A single-sided, beam-to-column joint was modelled using FE techniques and a pressure load simulating an internal explosion was imposed in the numerical environment. Dynamic increase factors (*DIFs*) were used to account for the strain rate influence on steel's mechanical properties. The study has proven that the recommendations of the design code precursor to UFC 3-340-02 (DOD, 2008) were defective. However, one may qualify the results of the study as being questionable, as the FE models were validated only against static tests results. In 2009, the study was enhanced by Yim and Krauthammer (2009) performing additional finite element analyses with solid elements on joints subjected to blast loads with variable time duration (5 - 20 ms) and variable load magnitude. A good agreement was observed between the results of physical tests and those acquired from numerical simulations, certifying the rather simplified frame models as an efficient tool with a low computational cost.

Grimsmo et al. (2015, 2016) investigated the response of steel joints subjected to high loading rates. The study implied the use of experimental and numerical approaches for beam-to-column connections under an impact load applied axially on the column. In order to highlight the dynamic effects and to validate the numerical models, Grimsmo et al. (2015) performed quasi-static and dynamic tests on double-sided bolted beam-to-column joint configurations. The 3D FE model of the specimen depicted in Figure2.7a was developed using the commercial FE software Abaqus/Explicit.

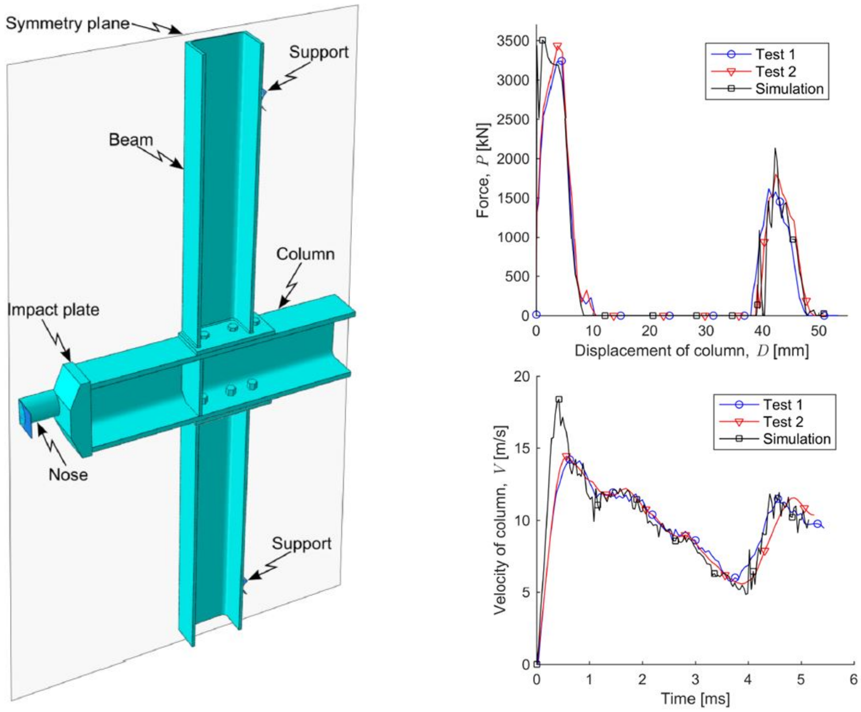

(a) FE model (b) Tests vs. simulations

Figure 2.7: FE model developed by Grimsmo et al. (2016)

The assembly was modelled using solid elements and the implemented material model incorporate the strain-rate sensitivity and damage criteria calibrated against data collected from tests on the coupons extracted from the specimen's elements. For both loading scenarios, the failure occurred as a combination of the tensile bolt fracture and the bending of the end-plate, the numerical simulations being able to provide accurately the deformation and failure modes observed in the tests. The global response in the terms of force-displacement and velocity-time curves, reported here in Figure 2.7b, has been as well captured by the numerical simulations.

Recently, D'Antimo et al. (2019) studied the effects of severe dynamic impact loads on simply supported steel beams. An experimental impact test campaign has been carried out for a variety of impact loads with different levels of energy. The finite element solutions were employed in the study of strain-rate and dynamic effects, highlighting the importance of material modelling and the accurate calibration of material constants used for the definition of the material behaviour laws. The outcome of the study demonstrates the reliability of some constitutive models formulations such as the Johnson-Cook or Cowper-Symonds formulations for dynamic applications, when the stain-rate effects have to be accounted for.

An innovative joint solution for seismic design has been investigated by D'Antimo (2020) for applications under quasi-static and, particularly, under impact loads. Once again, the behaviour of the joint was studied using two approaches - physical tests and numerical simulations. The FE models were developed considering the outcomes of the previous study of simply supported beams subjected to impact loads (D'Antimo et al., 2019).

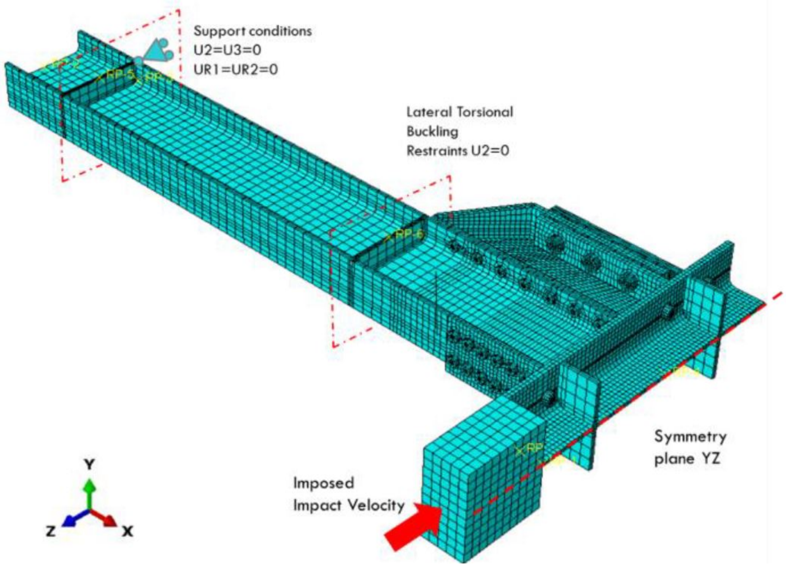

Figure 2.8: FE model of the test specimen (D'Antimo, 2020)

The strain-rate sensitivity of the material was implemented in the numerical models using the Johnson-Cook formulation. Firstly, the model was validated against the results from the static tests and subsequently, against dynamic tests results and used for further parametric studies. The Explicit solver of the commercial software Abaqus was used for the simulations of the impact tests, in order to optimize the analysis time and to avoid convergence related problems due to complex contact involved in the model. The global response of the joints under impact loads has been assessed based on the results provided by physical tests and numerical simulations, and subsequently, compared in terms of displacement-time curves.

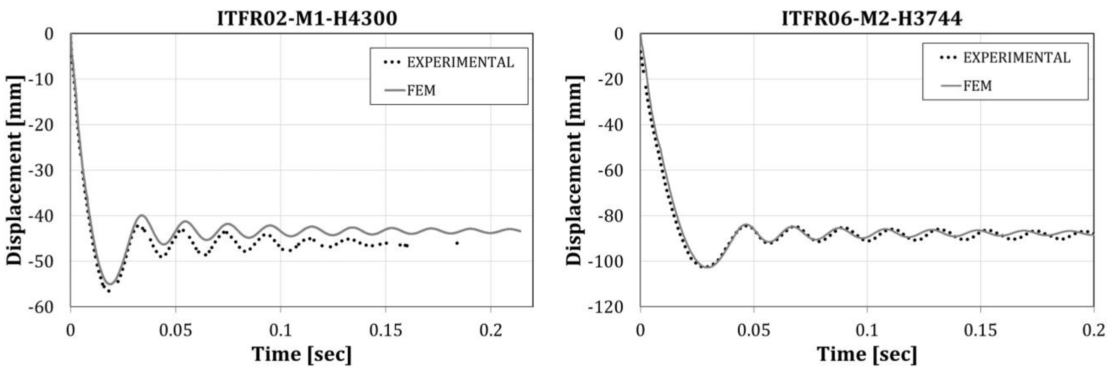

Figure 2.9: Experimental tests vs FE modelling (D'Antimo, 2020)

The agreement between the actual registered behaviour and the one predicted by the numerical simulation allows to identify the FE simulations as an accurate method in the assessment of the behaviour of joints under dynamic actions.

3 | Experimental campaign

3.1 Context

Aiming at investigating the response of various joint typologies under static and dynamic loads, an experimental campaign was conducted at the University of Liège. Integrated in the framework of the aforementioned research project RobustImpact, this experimental programme provided the physical test results required for the preparation of this thesis. The response of various configurations of beam-to-column joints and of steel-to-concrete column bases connections was investigated within the research project. In the framework of this thesis only the beam-to-column steel joints will be addressed, thus the information concerning the testing setup and the test specimens will be provided exclusively for this joint typology. The experimental programme, including the testing setup and the specimens' geometry, is presented in detail in the deliverables of the research project, namely in (Hoffmann et al., 2014, 2016), only a brief survey of it being provided here.

A total of 22 physical specimens of double-sided beam-to-column joints with different configurations were tested under quasi-static and impact loading, in order to highlight the magnitude of the strain rate influence on different joint components. The response of five joint configurations subjected to impact loading has been investigated. For each joint configuration, one quasi-static test and several impact tests with different levels of energy were performed and the strain rate effects were identified by comparing the static response of the specimens with the one exhibited under impact.

The test specimens were designed so that a specific failure mode, corresponding to the failure of different basic active components of the investigated joints, would occur under monotonic loading. Accordingly, an actual joint configuration (real joint - RJ) has been designed and afterwards, this joint configuration has been subjected to several modifications, that would ensure the failure of a specific component within the joint. Therefore, five different joint configurations have been designed, allowing to investigate the behaviour of basic components, as follows:

- RJ - the real joint: 4 specimens;
- EPB - the end-plate in bending: 5 specimens;
- CFB - the column flange in bending: 5 specimens;
- BFC - the beam flange in compression: 4 specimens;
- CWC - the column web in compression: 4 specimens.

3.2 Testing setup

3.2.1 Static tests

Throughout quasi-static tests, the double-sided beam-to-column joints were symmetrically loaded by applying a monotonic load at the top of the column. A hydraulic jack with displacement control loaded the specimen up to its failure and the evolution of the displacements and deformations experienced by the specimen were recorded using specific instrumentation, such as displacement transducers and extensometers. As the column's vertical displacement is not restrained, during the test the joint is mainly subjected to bending moments and shear forces.

A schematic view of the test specimens and the experimental setup is illustrated in Figure 3.1; a more detailed presentation, including the used specific instrumentation is available in (Hoffmann et al., 2016).

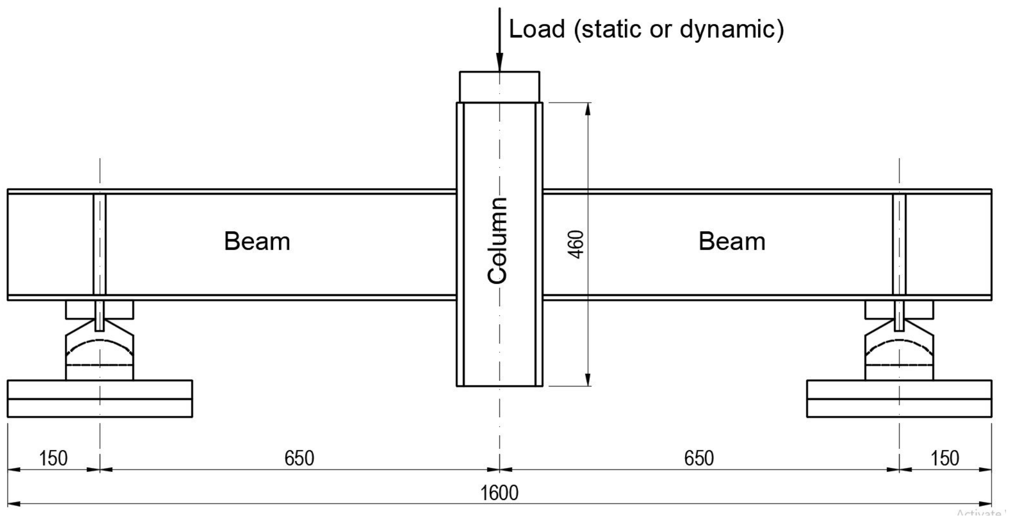

Figure 3.1: Schematic view of the test specimens

3.2.2 Impact tests

As previously mentioned, a total 22 specimens of five beam-to-column joint configurations were tested during the experimental programme; 19 physical tests were performed under impact loading conditions. The test specimens used for the impact tests were identical with the ones employed the static experiments. The main difference between the quasi-static and the impact tests was the load application. The impact load has been applied through a dropping mass, which in order to induce different levels of impact energies, hits the column head with variables speeds. Moreover, the impact energy can be controlled by modifying two parameters - the dropping height of the impactor and its weight.

Based on previously assessed response of specimens under quasi-static loads, their behaviour under impact loads has been investigated for the elastic and plastic ranges. Thus, the energy levels induced by the impact were adjusted so that for each specimen at least one test was performed in the elastic range. The methods to evaluate the required levels of energy and the corresponding dropping heights for the impactor are presented in detail in (Hoffmann et al., 2016). For the sake of brevity, here will be reported only the representative values used for the physical tests. Three masses were used for the physical tests (M1=100 kg, M2=167 kg and M3=211 kg) and the dropping heights varied between 80 and 4505 mm.

The specimens were subjected to impact by simply hitting the column head with a dropping weight. While the dropping height is constrained by the limitations of the testing rig, the maximum dropped weight could be adjusted, at least theoretically, according to a wide range of particular needs. In this specific case, the dropped weights were released from a certain height by using the system pictured in Figure 3.2a, consisting of two tubular guides which are holding and driving the weight. The mass hanged at a particular height is suddenly released through a quick-release mechanism using a hook equipped with a spring, which once pulled by a connected cable causes the instantaneous drop of the mass.

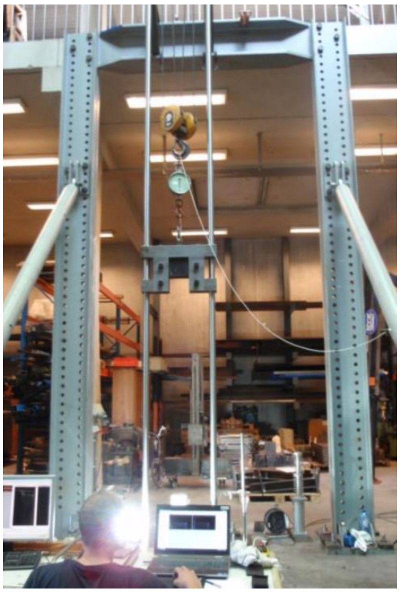

(a) Testing rig

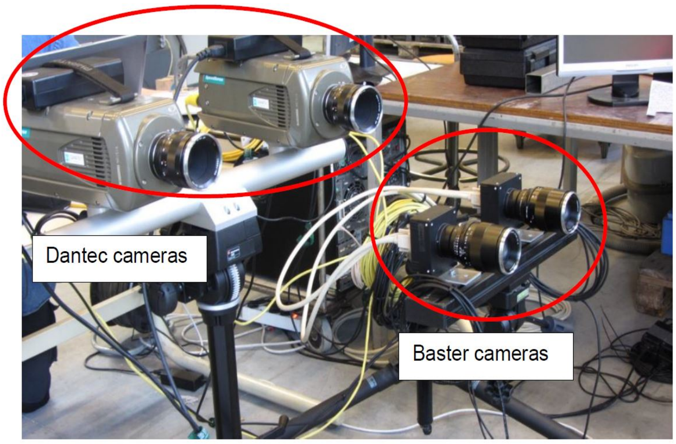

(b) High speed cameras

Figure 3.2: Testing setup

Similar to the quasi-static tests, during the impact tests the vertical displacement and the deformation of the specimens were recorded. The acquisition system in the case of the impact test is however different. Two pairs of high speed cameras were used to capture the response of the specimens under impulsive loading. The pair of Dantec cameras (5000 Hz), with a higher frequency of acquisition, was used to catch the global behaviour of the specimen, while Baster cameras (400 Hz) were used to capture the local behaviour of key joint components.

3.3 Test specimens

The global dimensions of the specimens were governed by the limitations of the available setup, a distance of maximum 1.6 m between the supports of the beams being available. The specimens consisted of rolled HEA and IPE profiles in S355 steel grade for both column and beams. In order to avoid the local buckling of the beam web under associated concentrated loads, web stiffeners were provided on the beam at the level of its supports. A specific system has been designed for the beam's supports with the main purpose of avoiding problems related to the rebound of the specimen when subjected to the impact load and to create the adequate supporting conditions for a simply supported element (allowing the rotations and the horizontal displacements). The length of the column has been established at the value of 460 mm in order to provide an adequate diffusion of the transverse compression forces transferred from the beams. The redistribution of the load (static or dynamic) on the entire cross-section of the column was ensured by providing a "loading plate", with a thickness of 50 mm, at the top of the column.

3.3.1 Real joint specimen (RJ)

As previously mentioned, this joint was used as a reference configuration from which the other specimens derived through specific modifications on the components geometrical properties or by providing additional stiffening elements to the joint. The specimen consists of two beams - IPE 180 profiles and a HEA 140 profile - column. Two 15 mm thick extended end-plates were welded to the beams by fillet welds with a throat thickness of 5 mm for the beam flanges and 3 mm for the beam web. The two beams were connected to the column by means of four partially threaded M16 bolts of grade 10.9. A detailed view of the specimen is provided in Figure 3.3.

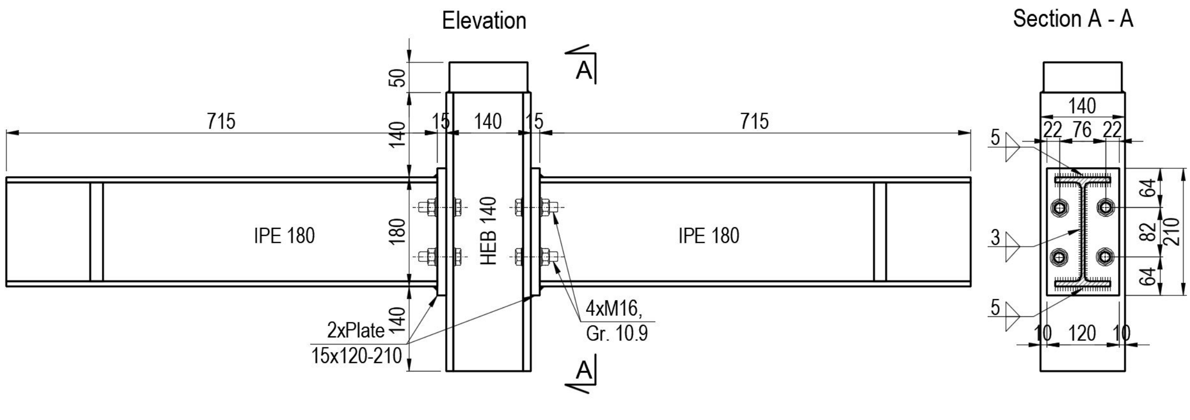

Figure 3.3: RJ specimen

3.3.2 End-plate in bending specimen (EPB)

In order to activate the failure of the "end-plate in bending" (*epb*) component, the overall configuration of the real joint has been used, the only modified parameter being the thickness of the end-plate which has been reduced from 15 mm to 8 mm as depicted in the figure below.

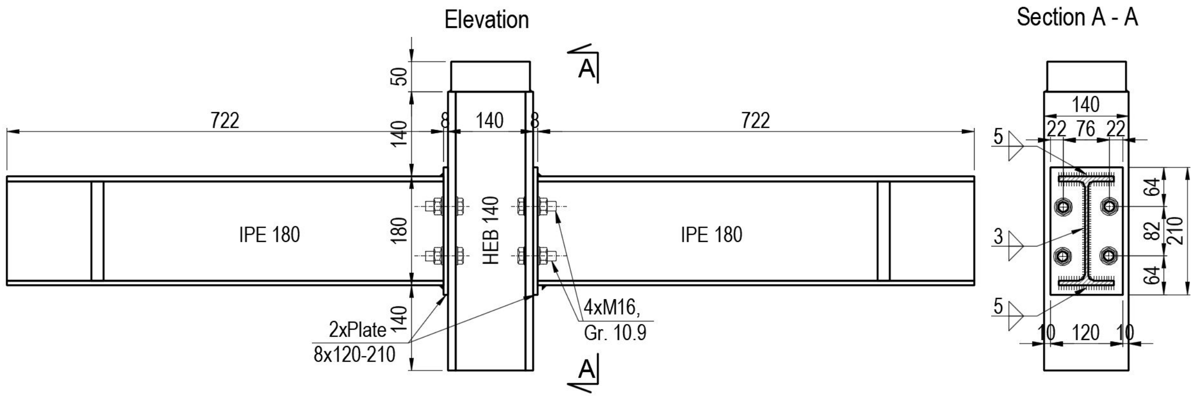

Figure 3.4: EPB specimen

3.3.3 Column flange in bending specimen (CFB)

The failure of the "column flange in bending" (*cfb*) component was induced by increasing the resistance capacity of two other active components - "end-plate in bending" (*epb*) and "beam flange in compression" (*bfc*). An additional 6 mm thick plate has been welded to the beams flanges in compression and, in order to avoid the failure of the end-plate in bending its thickness has been increased to 18 mm.

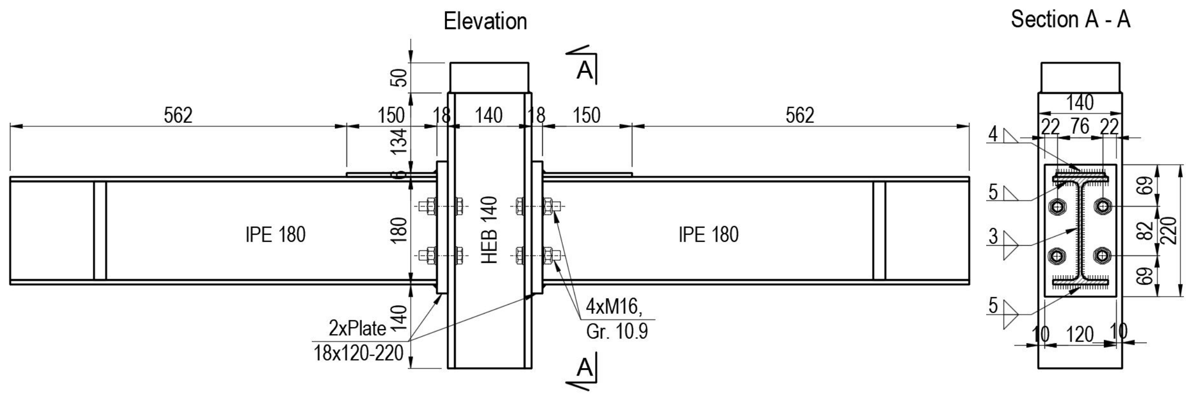

Figure 3.5: CFB specimen

3.3.4 Beam flange in compression specimen (BFC)

Aiming at inducing a failure mode associated to the failure of the "beam flange in compression" (*bfc*) component, the RJ configuration has been subjected to several modifications, the most important being the transition from a bolted connection to a fully welded one. The beams have been directly welded to the column and, in order to prevent the failure of the column web during the test, additional 12 mm thick stiffeners were provided as illustrated in Figure 3.6.

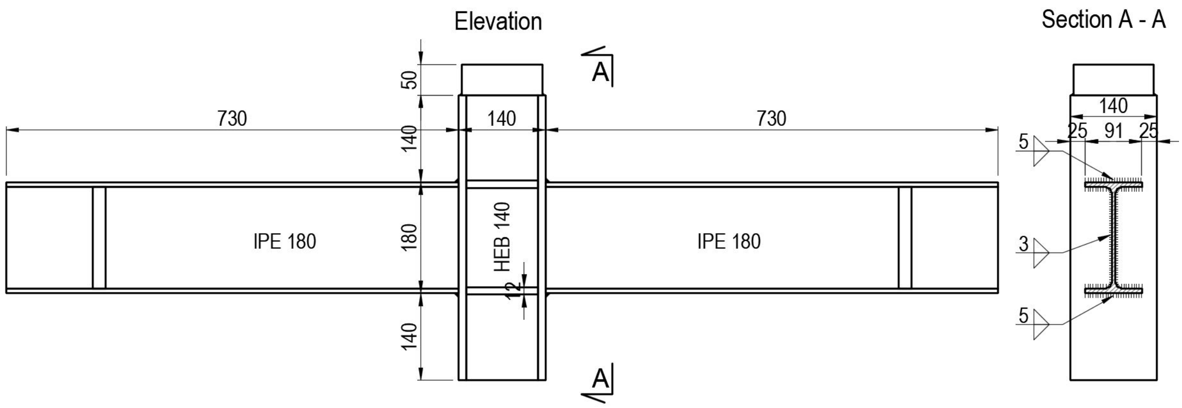

Figure 3.6: BFC specimen

3.3.5 Column web in compression specimen (CWC)

The "column web in compression" component could be activated only by reducing the thickness of the column web. In this particular case, an IPE 180 profile was used for the column as well. In order to prevent the failure of the column web region in tension, a 10 mm thick stiffener has been welded to the profile as depicted in the figure below.

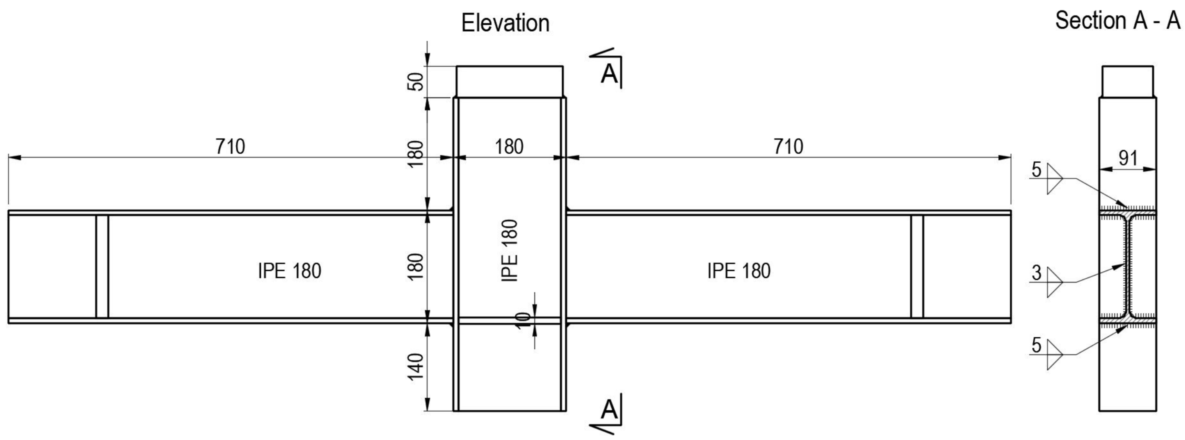

Figure 3.7: CWC specimen

3.4 Material properties

Quasi-static uniaxial tension tests on coupons extracted form the plates of all constitutive elements of the specimens were performed in order to evaluate the actual material properties. Full thickness coupon specimens were extracted from beams and columns flanges and webs, as well as from all end-plates used for the bolted connections. From the experimental recordings, for each coupon extracted, the stress-strain curves were generated. The latter will be used hereinafter in the FE simulations. The variance and uncertainties incurred in the coupon test results were mitigated by processing the experimental data and reporting the mean values from several tests as presented in Table 3.1.

Element	Coupon	f_y [MPa]	ε_y [%]	f_u [Mpa]	ε_u [%]
IPE 180	Flange	413.3	1.97	537.7	21
	Web	435.5	2.07	545.2	25
HEB 140	Flange	385.3	1.83	539.6	20.6
	Web	433.7	2.06	544	22
End-plates	8 mm	409.3	1.95	594.8	18
	15 mm	416.6	1.98	588.7	23
	18 mm	384.5	1.83	556.2	22

Table 3.1: Actual mechanical properties of the material

The figures below display the representative engineering stress-strain curves acquired from the coupon tests under quasi-static loading rate. Afterwards, these curves will be used for the definition of the non-linear material behaviour in the finite element model, by generating the true stress-logarithmic plastic strain curves.

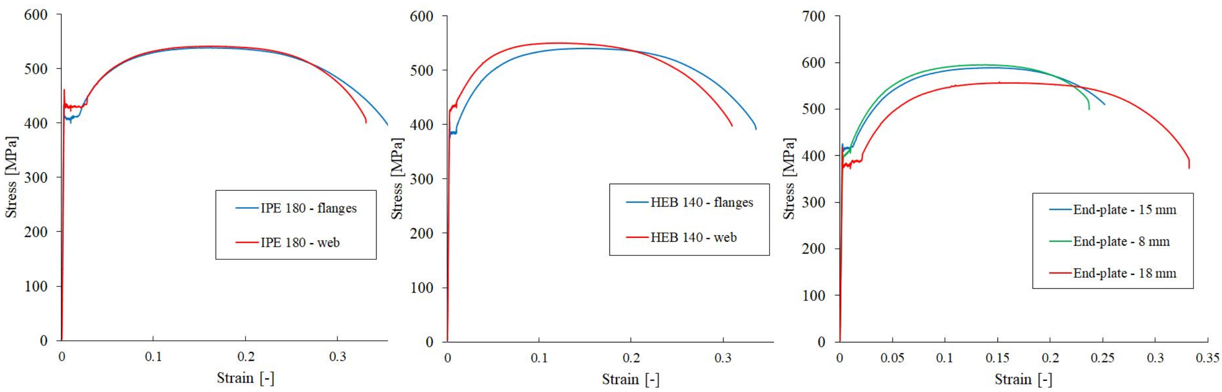

(a) IPE 180 (b) HEB 140 (c) End-plates

Figure 3.8: Engineering stress-strain curves for the used materials

The properties for M16 grade 10.9 bolts were not available from the coupon tests. Nonetheless, in the framework of the same research project, some coupon tests were performed for M20 grade 10.9 bolts and reported in (Hoffmann et al., 2016). The values for the yield strength f_{yb} and ultimate strength f_{ub} for bolts material will be considered as:

$$f_{yb} = 1020 \text{ N/mm}^2 \qquad \text{and} \qquad f_{ub} = 1080 \text{ N/mm}^2$$

3.5 Experimental results

3.5.1 Static tests

As previously described, a monotonic load has been applied at the top of the column during the quasi-static tests. The evolution of the applied force and the vertical displacement of the column were recorded, providing the required data to generate the force-displacement (F-Δ) curve of the joints. Usually, the behaviour of joints is assessed by means of moment-rotation (M-ϕ) curves, this approach being also prescribed by Eurocode 3; therefore, using the experimentally obtained data, the M-ϕ curve of each specimen has been generated.

When computing the joint rotation, a special attention has been paid as the displacement measured at the column's level is the sum of two contributions: one vertical displacement associated to the elastic deformation of the beam and another associated to the rotation of the joint, as depicted in Figure 3.9.

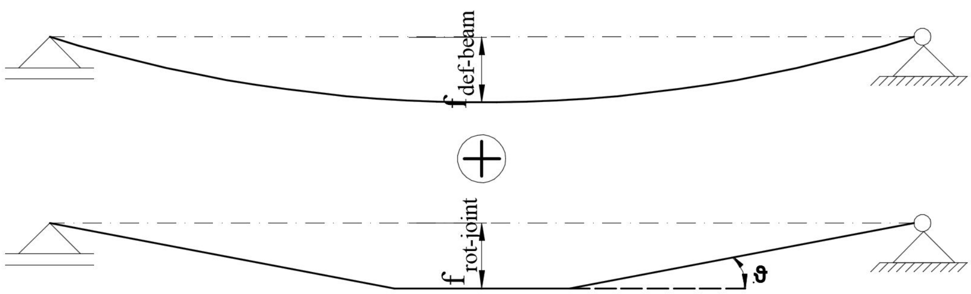

Figure 3.9: Joint rotation - displacement contributions

Thus, the rotation of the joint was determined by extracting the displacement induced by the elastic deformation of the beam from the total vertical displacement measured at the column's level as follows:

$$\phi = \frac{f_{rot-joint}}{L} = \frac{f_{total} - f_{def-beam}}{L} \tag{3.1}$$

where, $f_{rot\text{-}joint}$ is the displacement associated to the rotation of the joint, f_{total} is the vertical displacement experimentally measured at the top of the column, $f_{def\text{-}beam}$ is the displacement associated to the elastic deformation of the beam and L is the distance from the supports to the center line of the column's flange.

For the RJ specimen, two loading-unloading sequences were performed during the test, in order to estimate accurately the initial stiffness of the joint. At first, the joint was monotonically loaded until a force level of F=90 kN; at this loading level the joint still behaves in an elastic way. The second loading-unloading sequence was performed in the plastic range of the specimen. at a load value of F=130 kN. The behaviour of RJ joint configuration under quasi-static conditions is depicted in Figures 3.10a and 3.10b by means of force-displacement and moment-rotation curves. The initial stiffness of the RJ joint configuration, experimentally evaluated through the loading-unloading cycles, is approximately 3581 kNm/rad, being estimated as the average value of the two loading-unloading sequences. The maximum bending moment developed in the joint is estimated at a value of 47.5 kNm. The failure mechanism observed during the static test is a combination of the failure of two basic active components of the joint: at the level of the first bolt row, the yielding of the column flange in bending was observed, whereas, for the second bolt row, yielding occurred in the beam's top flange in compression.

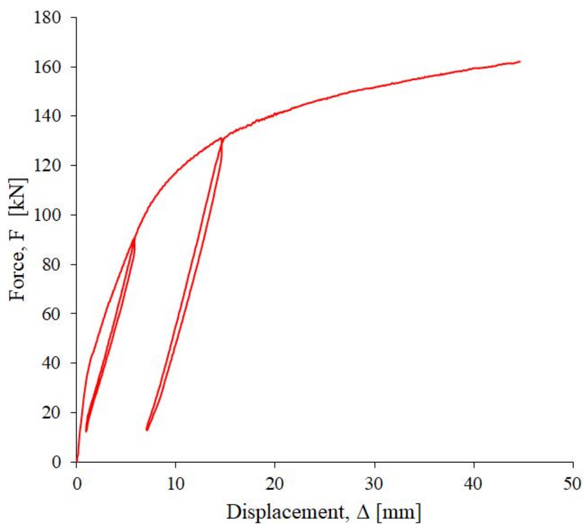

(a) Force - displacement curve

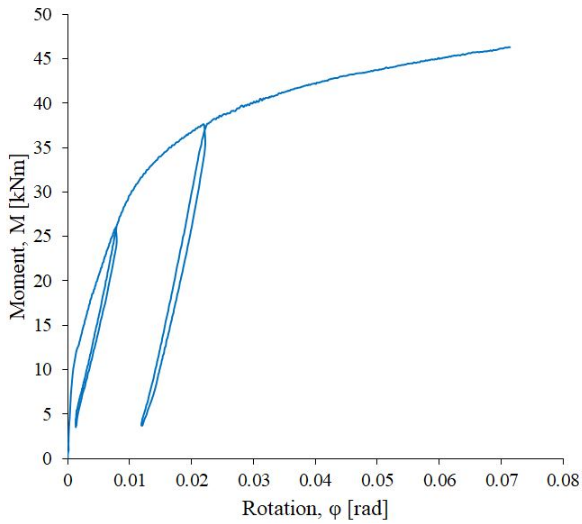

(b) Moment - rotation curve

Figure 3.10: RJ static behaviour

A similar procedure was performed for the EPB specimen, the two loading-unloading cycles being performed at a value of F=63 kN and F=85 kN, respectively. Based on these two cycles, the initial stiffness of the joint has been estimated at a value of 2518.6 kNm/rad. The maximum value of the bending moment experienced by the EPB joint configuration under quasi-static loading conditions is 38.7 kNm. The failure of the "end-plate in bending" (*epb*) component has occurred during the test at the level of both bolt rows. The overall behaviour of the investigated joint is illustrated in Figures 3.11a and 3.11b.

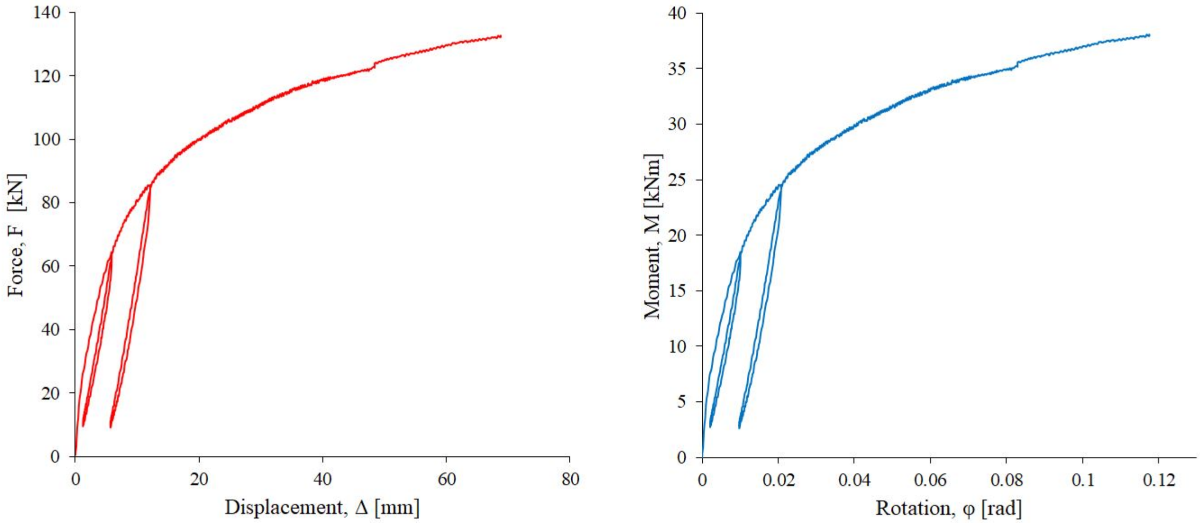

(a) Force - displacement curve

(b) Moment - rotation curve

Figure 3.11: EPB static behaviour

The initial stiffness of the CFB specimen has been evaluated following the procedure previously presented. As depicted in Figures 3.12a and 3.12b, two loading-unloading sequences were performed when the applied force reached 100 kN and 135 kN, respectively. The initial stiffness is estimated at the value of 4413 kNm/rad, while the maximum bending moment developed is 51.4 kNm. During the test, significant yielding has developed in the column flanges in the compressed zone, this failure mode being the governing one.

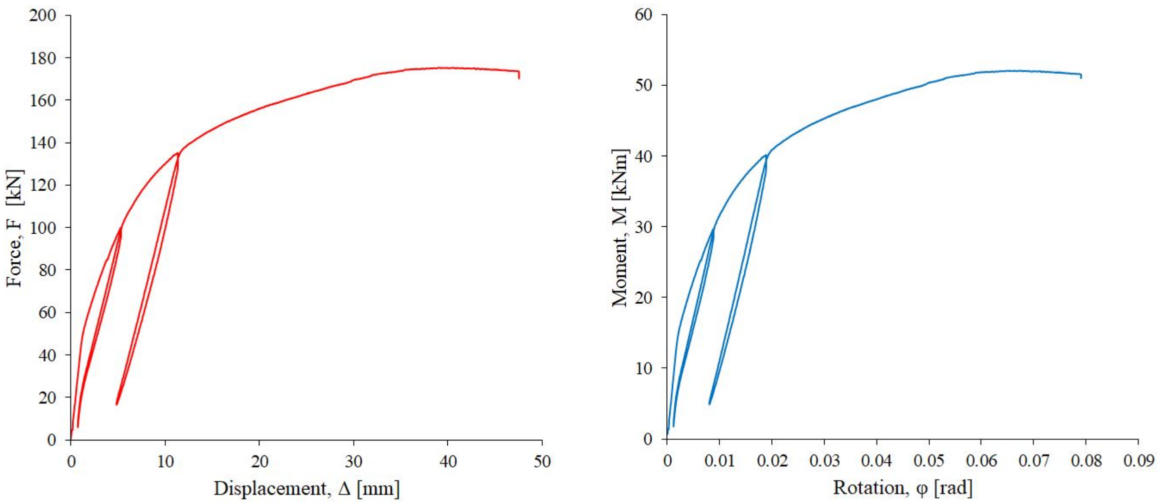

(a) Force - displacement curve

(b) Moment - rotation curve

Figure 3.12: CFB static behaviour

The fully welded joint configurations were tested following the same procedure performed for the bolted configurations. The BFC specimen has been monotonically loaded until the force level F=200 kN, when the first loading-unloading cycle was performed. The second cycle has been performed at F=240 kN and the initial stiffness, obtained as the average value from the loading-unloading sequences, is estimated to be 95241 kNm/rad. The static response in terms of $F-\Delta$ and $M-\phi$ curves is depicted in Figures 3.13a and 3.13b.

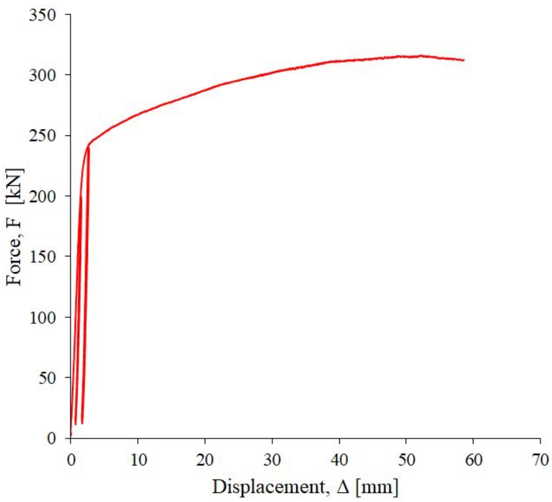

(a) Force - displacement curve

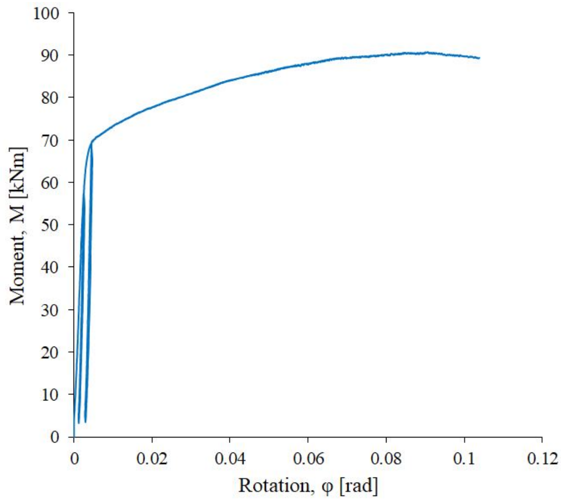

(b) Moment - rotation curve

Figure 3.13: BFC static behaviour

As expected, this joint configuration is much stiffer when compared to the bolted joint configurations. The bending capacity has also significantly increased, the maximum registered bending moment being 92.6 kNm, value that corresponds to the failure of the "beam flange in compression" (*bfc*) component.

The behaviour of the last joint configuration is illustrated in Figures 3.14a - 4.21b.

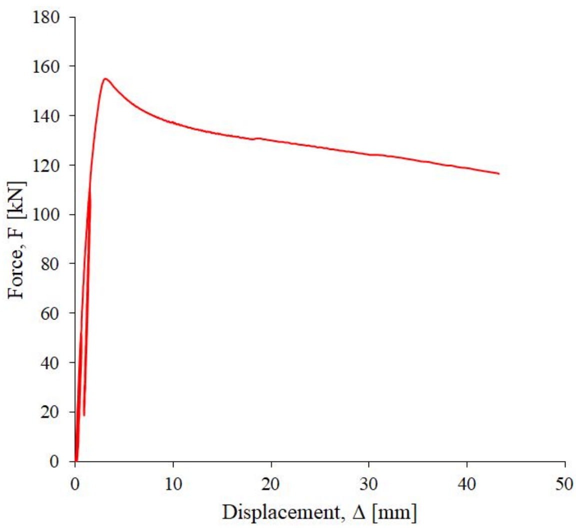

(a) Force - displacement curve

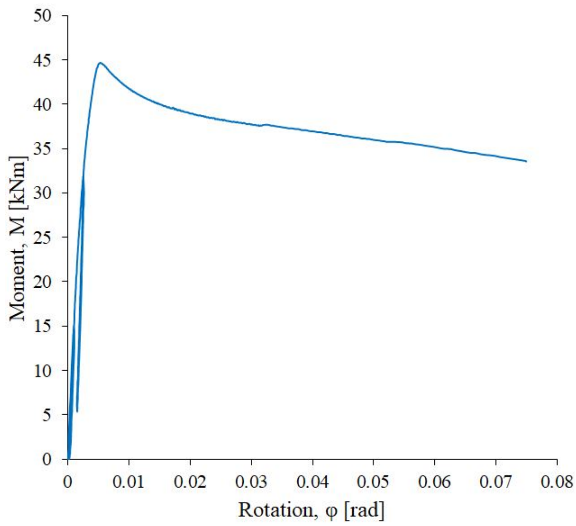

(b) Moment - rotation curve

Figure 3.14: CWC static behaviour

The CWC specimen proved to be also stiffer than the previously presented bolted connections.

One loading-unlaoding sequence has been performed during the test and the initial stiffness has been evaluated at 28342 kNm/rad. The local buckling of the column web in compression has limited drastically the bending capacity of the joint, a maximum bending moment of 45.4 kNm being developed.

3.5.2 Impact tests

A brief survey of the impact tests results is provided in this section. The dynamic responses of tested joint configurations are reported in terms of vertical displacement - time curves. Minimum three tests were conducted for each of the specimens with the main purpose to investigate their response under impulsive loading with different levels of energy. The energy associated to the impact can be readily evaluated using the kinetic energy expression:

$$E_k = \frac{1}{2} m v_{imp}^2 \tag{3.2}$$

where, m is the weight of the dropped mass and v_{imp} is the impact velocity captured by the acquisition system.

The RJ specimen was subjected to a series of four impact tests. One test was conducted in the elastic domain with a mass of 211 kg dropped from a small height $h = 80$ mm. Under this small impact energy no plasticity occurred in any components of the joint, thus there is no permanent displacement observed. Tests T2, T3 and T4 were performed in the plastic domain, inducing in the impacts different levels of energy by adjusting either the dropping height or the dropped mass as summarized in Table 3.2. The evolution in time of the joint's vertical displacement is depicted in Figure 3.15.

Test	M [kg]	h [mm]	v_{imp} [m/s]	v_{reb} [m/s]	Δ_{max} [mm]	Δ_{perm} [mm]
T1	211	80	1.27	0.96	2.73	0.1
T2	211	1505	5.23	1.94	18.89	6.5
T3	211	2005	6.03	2.03	23.94	10.64
T4	167	2005	5.89	2.14	19.82	7.1

Table 3.2: RJ - experimental results

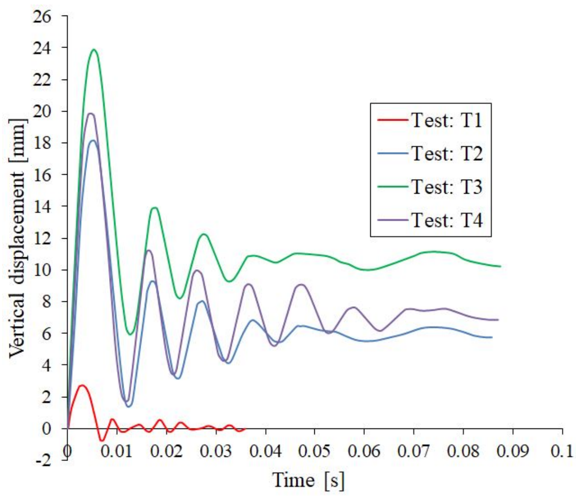

Figure 3.15: RJ - Δ-t curve

Similarly, four impact tests were performed for the EPB specimen. The small impact energy induced during the first test did not lead to the development of plasticity, thus the specimen exhibits an elastic response as can be seen in Figure 3.16. For the plastic domain, high plasticity was induced by increasing considerably the dropping height. A maximum vertical displacement of approx. 40 mm and a permanent displacement of 25 mm, respectively, have been recorded during the 3rd test (see Table 3.3).

Test	M [kg]	h [mm]	v_{imp} [m/s]	v_{reb} [m/s]	Δ_{max} [mm]	Δ_{perm} [mm]
T1	211	85	1.23	0.91	3.87	0
T2	211	1910	5.84	1.66	29.36	16.16
T3	211	3000	7.38	1.77	39.83	25
T4	167	3000	7.41	2.1	32.47	18.33

Table 3.3: EPB - experimental results

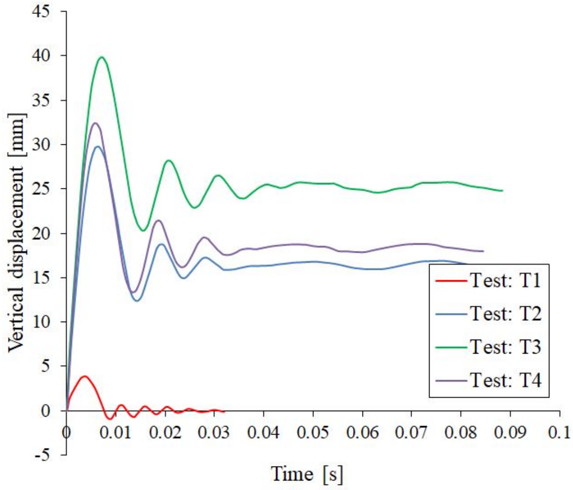

Figure 3.16: EPB - Δ-t curve

Lower impact energies were applied to the CFB specimen. Accordingly, two tests were carried out in the elastic domain, the joint exhibiting no permanent deformations after the tests. The small weight of 100 kg used for the first three tests was not enough to produce significant amounts of energy that would entrain material's plasticity, thus the permanent deformations experienced by the joint are modest to negligible for these tests. Only test T4 seems to provide reliable data for the study of joint's post yielding behaviour.

Test	M [kg]	h [mm]	v_{imp} [m/s]	v_{reb} [m/s]	Δ_{max} [mm]	Δ_{perm} [mm]
T1	100	259	2.1	0.84	2.65	0
T2	100	720	3.53	1.16	5.13	0
T3	100	1654	5.3	2.19	18	3.7
T4	211	2057	6.19	1.78	25.25	9.5

Table 3.4: CFB - experimental results

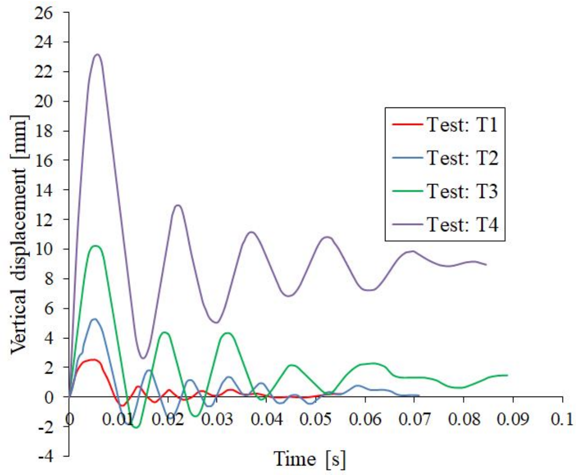

Figure 3.17: CFB - Δ-t curve

Since it was the joint configuration with the highest rotational stiffness and bending capacity, the BFC specimen has been subjected to impacts with higher energy levels. The joint exhibits an elastic behaviour during the first test, while for the other two, a plastic response is observed, a maximum permanent displacement of approx. 16 mm being recorded. In order to activate the plasticity in the joint components, as presented in Table 3.5, the maximum available dropping height has been used for this particular specimen.

Test	M [kg]	h [mm]	v_{imp} [m/s]	v_{reb} [m/s]	Δ_{max} [mm]	Δ_{perm} [mm]
T1	211	110	1.86	0.72	2.52	0
T2	211	2002	6.04	1.93	13.46	8
T3	167	4505	8.89	2.44	21.09	15.86

Table 3.5: BFC - experimental results

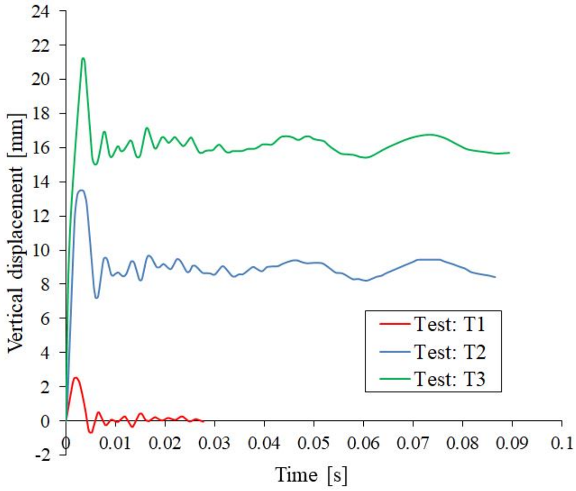

Figure 3.18: BFC - Δ-t curve

For the CWC joint configuration four impact tests were carried out using the same mass of 100 kg and adjusting the levels of impact energy only by increasing the dropping height. As summarized in Table 3.6, the dropping height varied from 0.52 to 2.93 m, the specimen being hit with a maximum impact velocity of 6.79 m/s. A maximum permanent displacement of 6.5 mm was reached during the 4th test. However, it seems that the impact energy was not high enough to trigger the failure of column web in compression. Even if the specimen exhibits a clear post-elastic response, the loading rate is too high and the application time is too short for potential buckling phenomena to occur.

Test	M [kg]	h [mm]	v_{imp} [m/s]	v_{reb} [m/s]	Δ_{max} [mm]	Δ_{perm} [mm]
T1	100	524	3.04	1.71	4.19	0
T2	100	916	4.24	2.23	5.63	1.3
T3	100	2040	5.78	2.26	8.93	4.2
T4	100	2927	6.79	2.27	11.66	6.5

Table 3.6: CWC - experimental results

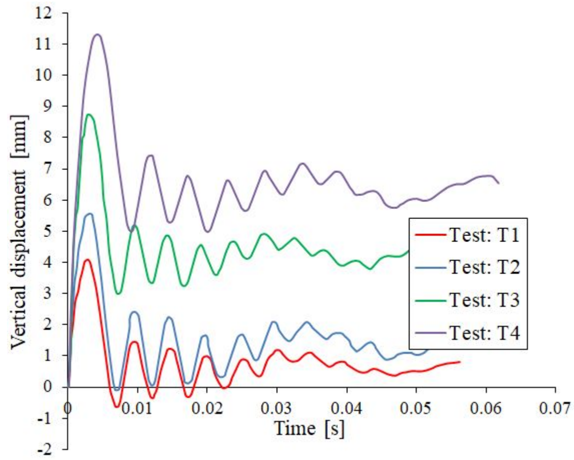

Figure 3.19: CWC - Δ-t curve

The results of the static and impact tests will be used in further investigation of dynamic effects on the global behaviour of beam-to-column joints. The rebound velocity v_{reb} reported for each test can be used afterwards to estimate the impact force applied on the column head .

4 | Behaviour under static loading

Nowadays, the dynamic effects on the behaviour of steel joints are quantified by means of Dynamic Increase Factors (*DIFs*), which, as previously stated, are the ratio between the dynamic and static resistance of the joint. Therefore, the joint behaviour under static loading conditions becomes a reference matter when the dynamic effects are assessed. The static conditions are usually considered to correspond to the normal exploitation of a structure, hence most of the design rules and guidance are focused on the static behaviour of steel joints.

4.1 Application of the component method

As mentioned in the introductory chapter of this thesis, the double-sided beam-to-column joint consists of a "left joint" and a "right joint". Theoretically, their non-linear behaviour can be assessed using the analytical formulae proposed in Eurocode 3. This section provides an overview on the application of the component method to different joint configurations. A comparison is made between the analytically predicted M-ϕ curve with the actual one derived from the outcomes of physical tests .

The actual material properties and geometrical characteristics were used for the characterisation of the joints' non-linear response through the component method. The M-ϕ curve of each joint typology is generated based on the assembly procedure of basic active components using a semi-automatic Excel routine - specifically developed with this purpose. The activated components and the assembly procedure for each joint specimen is presented briefly hereafter, whereas in the appendices of this paper a detailed presentation of the procedure is provided.

4.1.1 Active components

The stiffness and resistance capacities of a joint are estimated relying on the influence of its active basic components. The initial stiffness is evaluated on the basis of the elastic stiffness (k_i) of each i$^{\text{th}}$ active component, whilst the moment resistance is derived from their individual resistance capacity.

Considering the general layout of the joints addressed in this paper and the fastening method employed in their assembly, one may classify the test specimens in two main categories:

- Bolted joints: RJ, EPB and CFB specimens;
- Welded joints: BFC and CWC specimens.

The basic active components of these two specimen categories are presented in Table 4.1.

Joint category	Bolted joints		Welded joints	
Component	Resistance	Stiffness	Resistance	Stiffness
1. Column web in compression (cwc)	✓	✓	✓	✓
2. Column web in tension (cwt)	✓	✓		
3. Column flange in bending (cfb)	✓	✓		
4. End-plate in bending (epb)	✓	✓		
5. Beam flange and web in compression (bfc)	✓	*	✓	*
6. Beam web in tension (bwt)	✓	*		
7. Bolts in tension (bt)	**	✓		

Table 4.1: Active components for the two joint types

Note:

* The component is considered in the deformation of the beam;

** The component is considered in the equivalent T-stub.

4.1.2 Determination of the component properties

a) Component 1 - Column web in compression (cwc)

The resistance of the unstiffened column web subjected to transverse compression is determined from the following expression:

$$F_{c,wc,Rd} = \frac{\omega k_{wc}\, b_{eff,c,wc}\, t_{wc}\, f_{y,wc}}{\gamma_{M0}} \quad \text{but} \quad F_{c,wc,Rd} \leq \frac{\omega k_{wc}\, \rho\, b_{eff,c,wc}\, t_{wc}\, f_{y,wc}}{\gamma_{M1}} \tag{4.1}$$

Since the transformation parameter for a double-sided symmetrically loaded joint is $\beta = 0$, the reduction factor ω in equation 4.1 can be taken as $\omega = 1$. In most of the cases, the maximum longitudinal compressive stress $\sigma_{com,Ed}$ due to axial force and bending moment in the column web is $\sigma_{com,Ed} \leq 0.7 f_{y,wc}$ and the reduction factor k_{wc} can be taken as 1.0. The resistance in compression of the column web is limited by local buckling through a reduction factor (ρ) which accounts for potential buckling occurrence. This factor is evaluated based on the slenderness of the column web ($\bar{\lambda}_p$) as follows:

$$\rho = \begin{cases} 1.0 & \text{if} \quad \bar{\lambda}_p \leq 0.72 \\ (\bar{\lambda}_p - 0.2)/\bar{\lambda}_p^2 & \text{if} \quad \bar{\lambda}_p > 0.72 \end{cases} \tag{4.2}$$

The slenderness of the web is estimated as:

$$\bar{\lambda}_p = 0.932\sqrt{\frac{b_{eff,c,wc}\, d_{wc}\, f_{y,wc}}{E t_{wc}^2}} \qquad \text{where} \qquad d_{wc} = h_c - 2(t_{fc} + s) \tag{4.3}$$

The resistance to compression of the column web depends on the dispersion length ($b_{eff,c,wc}$) of the compression force through the end-plate and column flange. The area of the web providing resistance to compression is given by the effective width ($b_{eff,c,wc}$) illustrated in Figure 4.1.

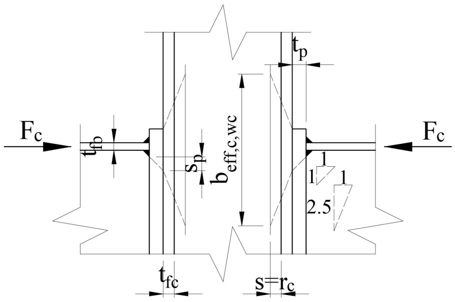

Figure 4.1: Force dispersion for column web in compression

According to Figure 4.1, the effective width of the column web in compression is evaluated:

$$b_{eff,c,wc} = t_{fb} + 2\sqrt{2}a_p + 5(t_{fc} + s) + s_p \tag{4.4}$$

where, s_p is the length obtained by dispersion at 45° through the end-plate. In this particular case, because the length of the end-plate bellow the flange is less than $2t_p$, s_p was considered as one end-plate thickness.

b) Component 2 - Column web in tension (cwt)

The resistance of an unstiffened column web subjected to transverse tension is determined according to eq. 6.10.

$$F_{t,wc,Rd} = \frac{\omega\, b_{eff,t,wc}\, t_{wc}\, f_{y,wc}}{\gamma_{M0}} \tag{4.5}$$

Once again, the reduction factor ω which accounts for the interaction with shear in the column web panel will be taken as 1.0, corresponding to the situation of a double-sided joint symmetrically loaded. For bolted connections, the effective width $b_{eff,t,wc}$ of column web in tension is evaluated based on the equivalent T-stub representing the column flange, therefore the effective length l_{eff} of the equivalent T-stub is estimated for each bolt rows acting individually or in a combination with the other bolt rows. The use of the equivalent T-stub model implies the estimation of several geometrical parameters that allows to evaluate its equivalent length.

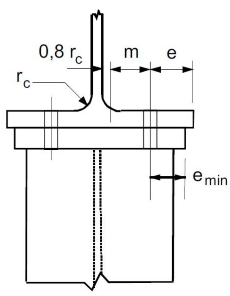

Figure 4.2: Geometrical parameters for the equivalent T-stub (EC3, 2005)

For this particular joint configuration the geometrical parameters are estimated as follows:

$$m = \frac{p_2}{2} - \frac{t_{wc}}{2} - 0.8r_c \qquad e = \frac{b_c}{2} - \frac{p_2}{2} \qquad e_{min} = \min(e;\ e_2) \tag{4.6}$$

Having two bolt rows on the elevation of the connection implies the computation of l_{eff} for bolt rows 1 & 2 acting individually or as a part of a group.

Bolt row 1

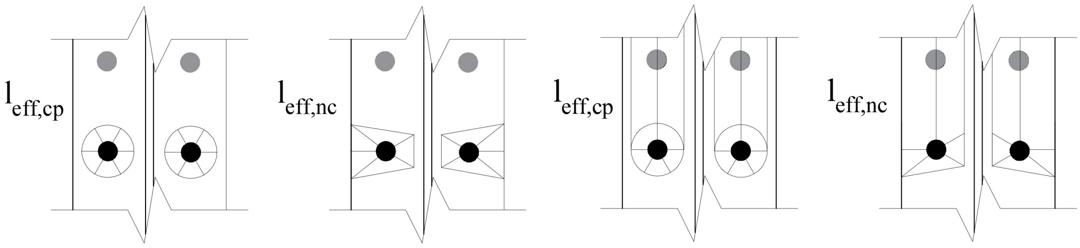

(a) Individual (b) As first row of a group

Figure 4.3: Effective lengths for bolt row 1

- Individual effective lengths

$$l_{eff,cp} = 2\pi m \qquad l_{eff,nc} = 4m + 1.25e \tag{4.7}$$

-Effective lengths as first bolt row of a group

In this case, for bolt row 1 combined with row 2, both bolt rows are considered as "end bolt rows" and the effective lengths for the unstiffened column flange should be taken as the minimum value as follows:

$$l_{eff,cp} = \min(\pi m + p;\ 2e_1 + p) \tag{4.8}$$

$$l_{eff,nc} = \min(2m + 0.625e + 0.5p;\ e_1 + 0.5p) \tag{4.9}$$

Bolt row 2

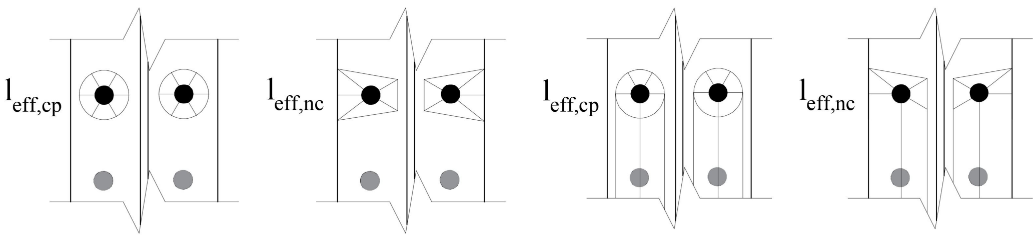

(a) Individual (b) As first row of a group

Figure 4.4: Effective lengths for bolt row 2

- Individual effective lengths

$$l_{eff,cp} = 2\pi m \qquad l_{eff,nc} = 4m + 1.25e \tag{4.10}$$

-Effective lengths as first bolt row of a group

$$l_{eff,cp} = \min(\pi m + p;\ 2e_1 + p) \tag{4.11}$$

$$l_{eff,nc} = \min(2m + 0.625e + 0.5p;\ e_1 + 0.5p) \tag{4.12}$$

c) Component 3 - Column flange in bending (cfb)

The resistance and the failure mode of an unstiffened column flange in bending are evaluated using the equivalent T-stub model for both - individual and group bolt rows. Associated resistances are calculated for three possible failure modes and the overall resistance is taken as the minimum of the three. In the figure below, the possible failure modes of the equivalent T-stub are illustrated. Failure mode 1 corresponds to the complete yielding of the column flange. Failure mode 2 is associated to a combined failure of the bolts and yielding in the flange whereas the 3rd mode is totally associated to the bolt fracture.

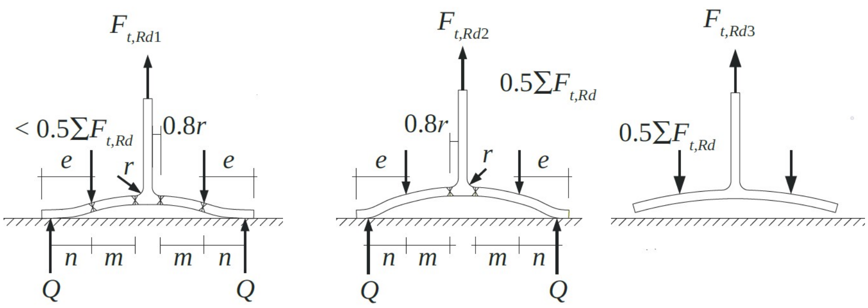

(a) Failure mode 1 (b) Failure mode 2 (c) Failure mode 3

Figure 4.5: Equivalent T-stub failure modes (Jaspart and Weynand, 2016)

EN 1993-1-8 provides the analytical formulae for the evaluation of the resistance for each of the three failure modes as follows:
- for Mode 1 (alternative method)

$$F_{t,1,Rd} = \frac{(8n - 2e_w)M_{pl,1,Rd}}{2nm - e_w(m+n)} \tag{4.13}$$

- for Mode 2

$$F_{t,2,Rd} = \frac{2M_{pl,2,Rd} + n\Sigma F_{t,Rd}}{m+n} \tag{4.14}$$

- for Mode 3

$$F_{t,3,Rd} = \Sigma F_{t,Rd} \tag{4.15}$$

where:

$$M_{pl,1,Rd} = \frac{0.25\Sigma l_{eff,1}\, t_f^2\, f_y}{\gamma_{M0}} \qquad \text{and} \qquad M_{pl,2,Rd} = \frac{0.25\Sigma l_{eff,2}\, t_f^2\, f_y}{\gamma_{M0}} \tag{4.16}$$

Figure 4.6 depicts the geometrical parameters from eq. 6.22 and 6.23. Previously estimated parameter m will remain unchanged, while e_w and n are determined as follows:

$$e_w = \frac{d_w}{4} \qquad n = \min(e_{min};\ 1.25m) \tag{4.17}$$

where, d_w is the diameter of the washer.

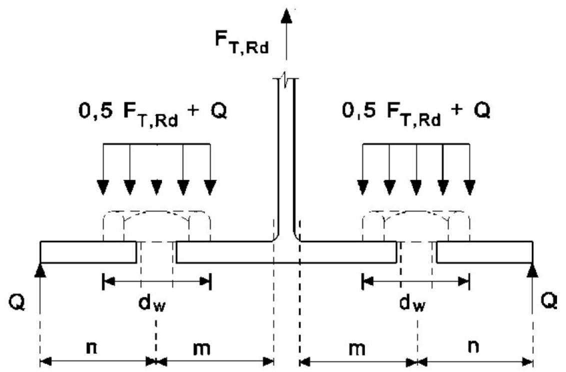

Figure 4.6: Geometrical parameters for the equivalent T-stub (EC3, 2005)

For mode 2 and 3, the bolts failure limits the overall resistance of the T-stub. The resistance of a bolt in tension is evaluated as:

$$F_{t,Rd} = \frac{0.9 f_{ub}\, A_s}{\gamma_{M2}} \tag{4.18}$$

The resistances associated to the cfb component are determined once again for two possible cases when the bolts are working individually or in a group. The effective lengths $l_{eff,1}$ and $l_{eff,2}$ employed in eq. 4.16 are derived as follows:

$$l_{eff,1} = \min(l_{eff,cp};\ l_{eff,nc}) \qquad \text{and} \qquad l_{eff,2} = l_{eff,nc} \tag{4.19}$$

d) Component 4 - End-plate in bending (epb)

Similar to a column flange in bending in a bolted connection, the resistance and the failure mode of the end-plate in bending are assessed once again by referring to the equivalent T-stub model. The fact that the first bolt rows is adjacent to the beam flange in tension implies the estimation of an additional parameter m_2 as depicted in Figure 4.7

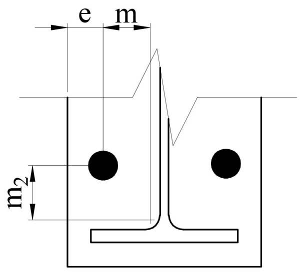

Figure 4.7: Geometrical parameters for the equivalent T-stub

The effective lengths of the T-stub element are evaluated based on the following parameters:

$$m = \frac{p_2}{2} - \frac{t_{wb}}{2} - 0.8a_w\sqrt{2} \qquad m_2 = \frac{h_b}{2} - \frac{p_1}{2} - t_{fb} - 0.8a_f\sqrt{2} \qquad n = \min(e_{min};\ 1.25m)$$

The effective lengths for bolt row 1 require the estimation of an α coefficient as this bolt row is under the beam flange in tension; the two following parameters are needed for the estimation of this coefficient (see Figure 4.8):

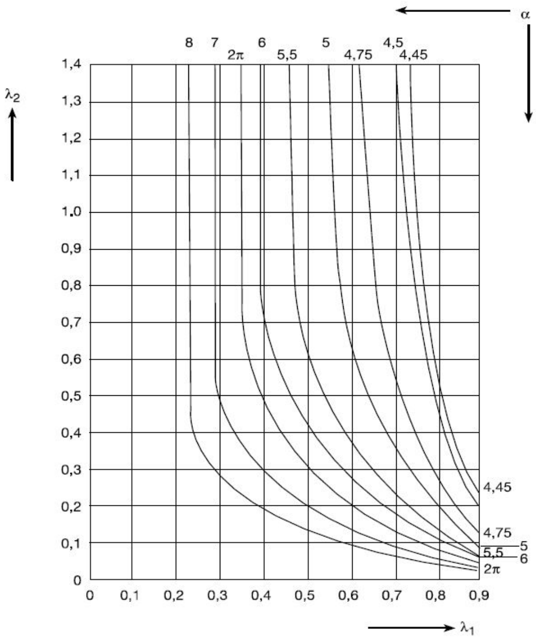

$$\left.\begin{aligned} \lambda_1 &= \frac{m}{m+e} \\ \lambda_2 &= \frac{m_2}{m+e} \end{aligned}\right\} \Rightarrow \alpha \qquad (4.20)$$

Figure 4.8: Estimation of α coefficient (EC3, 2005)

Bolt row 1

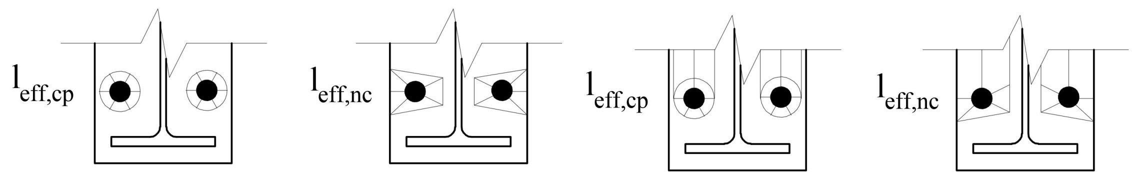

(a) Individual

(b) As first row of a group

Figure 4.9: Effective lengths for bolt row 1

- Individual effective lengths

$$l_{eff,cp} = 2\pi m + p \qquad l_{eff,nc} = \alpha m \tag{4.21}$$

-Effective lengths as first bolt row of a group

$$l_{eff,cp} = \pi m + p \qquad l_{eff,nc} = 0.5p + \alpha m - (2m + 0.625e) \tag{4.22}$$

Bolt row 2

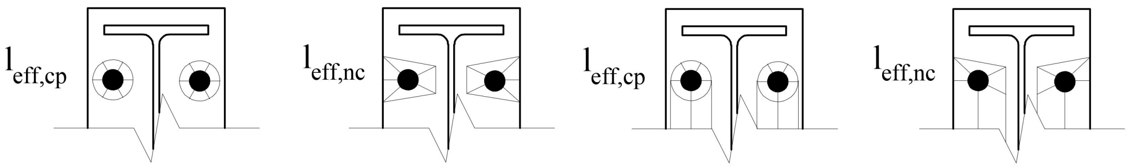

(a) Individual (b) As first row of a group

Figure 4.10: Effective lengths for bolt row 2

- Individual effective lengths

$$l_{eff,cp} = 2\pi m + p \qquad l_{eff,nc} = \alpha m \tag{4.23}$$

-Effective lengths as last bolt row of a group

$$l_{eff,cp} = \pi m + p \qquad l_{eff,nc} = 0.5p + \alpha m - (2m + 0.625e) \tag{4.24}$$

Once again, the resistances are determined for two possible cases, when the bolts are working individually or in a group, as the minimum resistance corresponding to the failure mode of the T-stub from eqs. 6.22, 6.23 and 4.15.

e) Component 5 - Beam flange and web in compression (bfc)

The bending moment applied to the beam leads to the development of compression forces in the proximity of the beam flange and the adjacent part of the web. Due to different lever arms, the concentrated force F_c may differ considerably when compared to the compression force F induced by the same loading at a certain distance from the connection, as depicted in Figure 4.11.

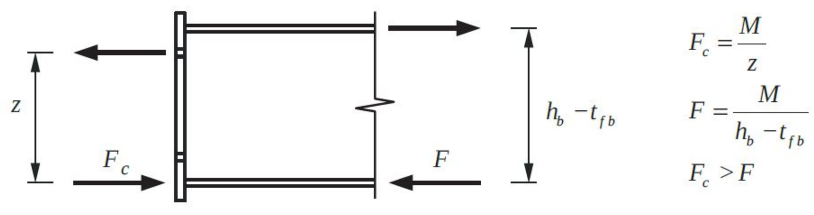

Figure 4.11: Concentrated force F_c and compression force F (Jaspart and Weynand, 2016)

The design compression resistance of the combined beam flange and web is given by the following expression:

$$F_{c,fb,Rd} = \frac{M_{c,Rd}}{h - t_{fb}} \tag{4.25}$$

where h is the depth of the connected beam and $M_{c,Rd}$ is the moment resistance of the beam cross-section.

f) Component 6 - Beam web in tension (bt)

For the beam web in tension, the resistance is estimated with the following expression:

$$F_{t,wb,Rd} = \frac{b_{eff,t,wb}\, t_{wb}\, f_{y,wb}}{\gamma_{M0}} \tag{4.26}$$

The effective width $b_{eff,t,wb}$ is considered to be equal to the equivalent length l_{eff} of the T-stub evaluated for the end-plate in bending component. Therefore, the effective width to compute the resistance of the bolt rows acting individually or as a group is estimated as follows:
- for bolt rows 1 and 2 acting individually

$$b_{eff,t,wb} = \min(l_{eff,cp};\ l_{eff,nc}) \tag{4.27}$$

- for bolt rows 1 and 2 acting as a group

$$b_{eff,t,wb} = \min(\Sigma l_{eff,cp};\ \Sigma l_{eff,nc}) \tag{4.28}$$

4.1.3 Moment resistance

The design moment resistance of a joint ($M_{j,Rd}$ or M_{Rpl}) is associated to the resistance of its weakest basic component (F_{Rd}). Considering the force distribution corresponding to the tensile and compression resistances of the components, the bending capacity of the joint results from the equilibrium condition. In the previous section the analytical expressions proposed in Eurcode 3 for the estimation of resistances of basic active components were comprehensively presented for the components of concern in this study.

The general rules prescribed by Eurocode 3 lead to an estimation of the joint's non-linear response. Serving as a reliable tool for a safe joint design, these rules are, however, insufficient to assess the full mechanical response of a joint. Generally, joint's initial stiffness and its plastic bending resistance are estimated with a reasonable accuracy by applying the component method proposed in Eurocode 3. After its bending capacity is reached, the joint is assumed to exhibit no rotational-stiffness and deforming up to its ultimate deformation capacity, following thus a bilinear model. The most important drawback of this idealisation is not the fact that the ultimate bending capacity of the joint is underestimated, but the impossibility to assess the ductility of a certain joint configuration, since its rotational capacity is evaluated rather qualitative in Eurocode 3. These challenges may be overcome with the extension to the component method developed by Japsart et al. (2019) for the evaluation of the strain-hardening stiffness, ultimate bending capacity and the rotational capacity of a joint.

In this particular case the plastic bending capacity (M_{Rpl}) was estimated relying on the provisions of Eurocode 3 as follows:

$$M_{Rpl} = \Sigma h_r F_{tr,Rd} \tag{4.29}$$

where, h_r is either the distance from the compression center to the r$^{\text{th}}$ bolt row if the connection is bolted or the distance between the mid-section of the beam flanges if the connection is welded. $F_{r,Rd}$ is the minimum resistance of the r$^{\text{th}}$ bolt row for bolted connections, or the minimum resistance of the basic active components for welded joints.

The ultimate bending capacity (M_{Ru}) has been determined in a similar manner by simply substituting the yield strength of steel (f_y) by its ultimate strength (f_u) when computing the resistances of individual active components, as recommended in Japsart et al. (2019).

4.1.4 Rotational stiffness

4.1.4.1 Initial stiffness

The rotational stiffness of a joint relies on the mechanical properties of its basic active components. The initial stiffness ($S_{j,ini}$) is estimated on the basis of the elastic stiffness of the constitutive components. As the elastic response of each component is assumed through an equivalent $F - \Delta$ spring, the expression of the joint elastic stiffness is derived based on the elastic properties of the equivalent springs as follows:

$$S_{j,ini} = \frac{M_{Ed}}{\phi} = \frac{Ez^2}{\sum_i \frac{1}{k_i}} \tag{4.30}$$

where, k_i is the elastic stiffness coefficient of each i$^{\text{th}}$ contributing component, z is the lever arm and E - steel's Young modulus.

In this particular case, under the action of the vertically applied force on the column's head, the joints are subjected mainly to sagging bending moments and shear forces. The activated components for the two categories of joints addressed in this paper are specified in Table 4.1. For the specimens with bolted connections (RJ, EPB, CFB) a mechanical model comprising all the active components is depicted in Figure 4.12.

When subjected to sagging bending moment, the tension zone in the joint is concentrated at the level of the lower beam flange and lower bolt row. Nonetheless, for all bolted joints investigated in this paper, the forces equilibrium was achieved when the bolt row positioned in the proximity of the beam flange in compression was subjected to tension as well. Therefore, the bolt rows were labeled from bottom to the top as "Bolt row 1" and "Bolt row 2", with respect to the tensile force associated to each of them.

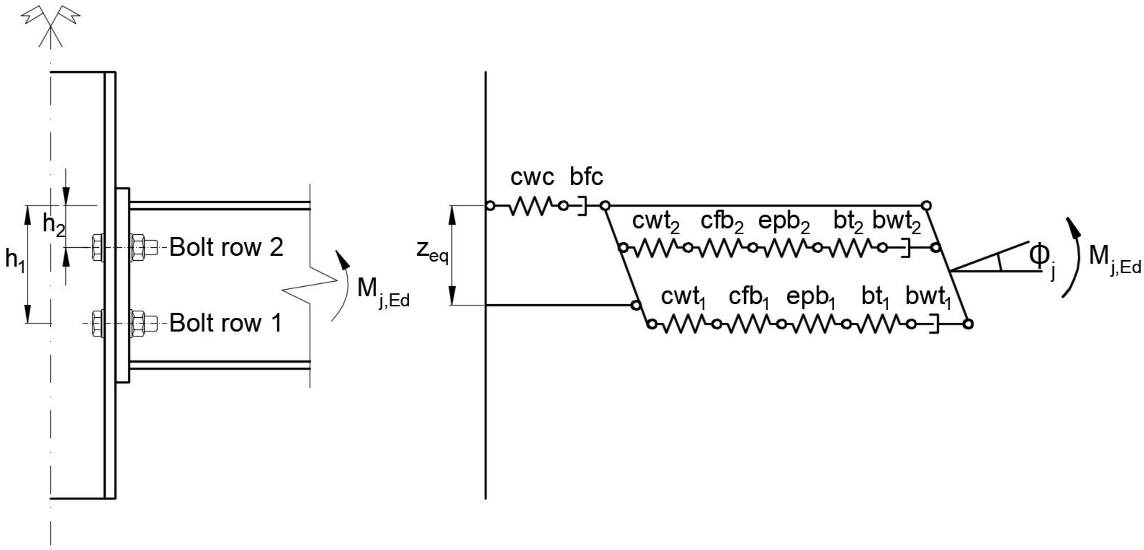

Figure 4.12: Mechanical model for bolted specimens (RJ, EPB and CFB)

A stiffness coefficient k_i is associated to each active components of the joint. However, the deformations of *bfc* and *bwt* components are assumed to be included in the deformations of the beam in bending, hence, their stiffness is disregarded when the overall stiffness of the joint is estimated. For all bolt rows, the deformations are assumed to be proportional to the distance to the centre of compression. Thus, the deformations associated to each bolt row can be expressed through an effective stiffness coefficient (as shown in Figure 4.13) which can be estimated as:

$$k_{eff,r} = \frac{1}{\sum_i \frac{1}{k_{i,r}}} \tag{4.31}$$

where, $k_{i,r}$ are the stiffness coefficients of the components active at a bolt row r.

Subsequently, the effective springs per bolt-row can be replaced by an equivalent spring acting at an equivalent lever arm z_{eq} as depicted in Figure 4.13.

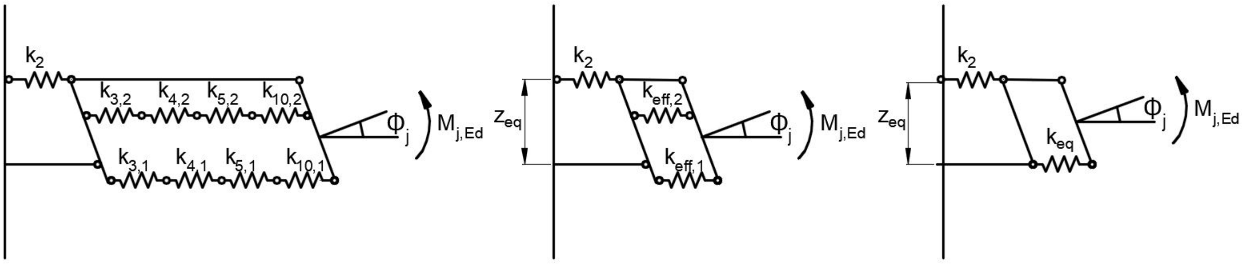

Figure 4.13: Spring model for bolted specimens (RJ, EPB and CFB)

The equivalent lever arm z_{eq} and the equivalent stiffness coefficient k_{eq} are derived from the effective bolt-row characteristics as follows:

$$z_{eq} = \frac{\sum_r k_{eff,r}\, h_r^2}{\sum_r k_{eff,r}\, h_r} \tag{4.32}$$

$$k_{eq} = \frac{\sum_r k_{efff,r}\, h_r}{z_{eq}} \tag{4.33}$$

Knowing the properties of the joint's constitutive components (reference is made to section 4.1.2 of this paper), the individual stiffness coefficients can be readily evaluated with the expressions proposed in Eurocode 3, as listed below.

- Column web in compression (cwc):

$$k_2 = \frac{0.7 b_{eff,c,wc}\, t_{wc}}{d_c} \tag{4.34}$$

where, $b_{eff,c,wc}$ is the effective width and $d_c = d_{wc}$ estimated for the *cwc* component;

- Column web in tension (cwt):

$$k_{3,1} = k_{3,2} = \frac{0.7 b_{eff,t,wc}\, t_{wc}}{d_c} \tag{4.35}$$

where, $b_{eff,t,wc}$ is the effective width of the column web in tension taken as the minimum between the effective lengths l_{eff} (individually or as a part of a group);

- Column flange in bending (cfb):

$$k_{4,1} = k_{4,2} = \frac{0.9 l_{eff}\, t_{fc}^3}{m^3} \tag{4.36}$$

where, the parameter m and the minimum effective length (individually or as a part of a group)- l_{eff} are estimated for the *cfb* component;

- End-plate in bending (epb):

$$k_{5,1} = k_{5,2} = \frac{0.9 l_{eff}\, t_p^3}{m^3} \tag{4.37}$$

where, the parameter m and the minimum effective length (individually or as a part of a group)- l_{eff} are estimated for the *epb* component;

- Bolts in tension (bt):

$$k_{10,1} = k_{10,2} = \frac{1.6 A_s}{L_b} \tag{4.38}$$

where, A_s is the bolt resistance area and L_b is the bolt elongation length.

4.1.4.2 Strain-hardening stiffness

With a view to simplifying the design procedure, in Eurocode 3, the joint is considered to exhibit no rotational stiffness once its plastic resistance is reached. However, this idealisation, even if widely used for its practical meaning, is a very rough estimation of the post-yielding behaviour. The term "strain-hardening stiffness" was adopted for the characterisation of a joint post-plastic behaviour. As presented in section 2.2, Japsart et al. (2019) extended the use of the component method to the evaluation of ductility capacity of steel joints. Within this approach, analytical expressions are proposed for the estimation of post-plastic behaviour of basic components, allowing, as a consequence, to assess the full $M-\phi$ curve of a specific joint. The main differences between this analytical method and the Eurocode 3 approach are illustrated in Figure 4.14.

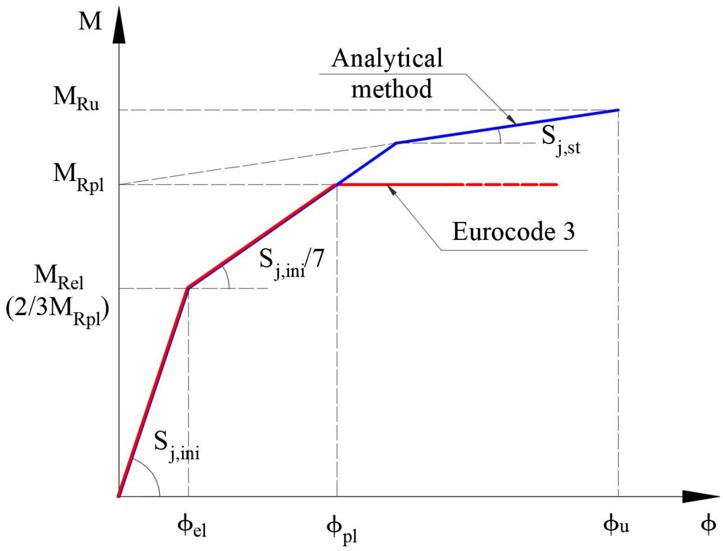

Figure 4.14: Eurocode 3 approach vs. Analytical method

The prediction accuracy relies on the efficient assessment of the strain hardening coefficients k_{st} for all active basic components. The expressions proposed for the estimation of k_{st} were derived from extensive studies of tests results on components (Jaspart, 1991) as listed below.

For column webs in compression/tension(*cwc/cwt*) and column flanges and end plates in bending (*cfb & epb*):

$$k_{st} = \frac{E_{st}}{E} k_i \tag{4.39}$$

For the column web panels in shear (*cws*) :

$$k_{st} = \frac{2(1+\nu)}{3} \frac{E_{st}}{E} k_i \tag{4.40}$$

where, k_{st} is the strain-hardening stiffness coefficient, k_i - the initial stiffness coefficient, E - the modulus of elasticity of steel, E_{st} - the strain-hardening modulus of elasticity and ν is the steel Poisson coefficient.

The assembly procedure is performed taking into account the relative importance of the deign moment resistance of each individual basic component ($M_{Rpl,comp,i}$). The latter is estimated by assuming that temporarily only the i^{th} component is active in the joint. Once evaluated, the component individual moment resistances are compared to the plastic moment resistance of the joint (M_{Rpl}). It is assumed that a certain component will contribute in an elastic way to the strain hardening stiffness ($S_{j,st}$) if its individual moment resistance is considerably higher than M_{Rpl}. Contrarily, when $M_{Rpl,comp,i}$ is comparable to the joint moment resistance, the component will have a greater influence on $S_{j,st}$. Therefore, the strain hardening stiffness is estimated on the basis of components contribution, which, by definition, can be elastic, through an initial stiffness coefficient or plastic, through a strain hardening coefficient. According to Japsart et al. (2019), the basic components are assumed to have an elastic or a plastic contribution by comparing their individual plastic resistance to a reference limit value. This boundary value has been defined after an extended experimental campaign on joints with end-plates as follows:

$$M_{Rpl,limit} = 1.65 M_{Rpl} \tag{4.41}$$

Accordingly, when $M_{Rpl,comp,i} > M_{Rpl,limit}$ the i^{th} component is considered to have an elastic contribution to $S_{j,st}$, hence, its initial stiffness is not affected. When $M_{Rpl,comp,i} < M_{Rpl,limit}$ the component will have a strain hardening contribution and its associated strain-hardening coefficient will be employed in the assembly procedure.

Derived from this classification, the strain hardening stiffness of a joint may be estimated as:

$$S_{j,st} = \frac{Ez^2}{\sum \frac{1}{k^*}} \tag{4.42}$$

where:

$$\sum \frac{1}{k^*} = \sum_m \left(\frac{1}{k_{i,m}}\right)_{M_{Rpl,comp,i} > M_{Rpl,limit}} + \sum_k \left(\frac{1}{k_{st,k}}\right)_{M_{Rpl,comp,k} \leq M_{Rpl,limit}} \tag{4.43}$$

If to refer to Figure 4.14, the ultimate rotational capacity ϕ_u, which, as a matter of fact, is impossible to be assessed when relying on the guidelines of Eurocode 3, can be estimated easily on the basis of M_{Ru}, $M_{R,pl}$ and $S_{j,st}$ from eq. 4.44.

$$\phi_u = \frac{M_{Ru} - M_{Rpl}}{S_{j,st}} \tag{4.44}$$

Subsequently, the plastic rotational capacity ϕ_{pl} yields:

$$\phi_{pl} = \frac{M_{Rpl} + 2/3 M_{Rpl}}{S_{j,ini}/7} - \frac{2/3 M_{Rpl}}{S_{j,ini}} \tag{4.45}$$

4.1.5 Validation of the analytical method

The theoretical aspects presented in the previous sections concern the characterisation of steel joint response through the component method. In this section, the analytical approach is validated against experimental data collected throughout physical tests performed under quasi-static loading regime. In section 3.5.1 the behaviour of test specimens is expressed in terms of $F - \Delta$ and $M - \phi$ curves. The latter are used in this section to validate the applicability of the component method on different joint configurations.

In order to assess accurately the behavior of joints under static loading conditions, the actual material properties reported in section 3.4 were employed when the analytical formulae of the component method were applied. As the objective of this approach is to replicate as close as possible the real behaviour of joints, a special attention has been paid at the dimensions of the members and components of the specimen. Therefore, the actual dimensions measured during the tests have been used for the analytical prediction. In (Hoffmann et al., 2016) the actual dimensions of the profiles and plates used in the manufacturing of physical specimens are available. For the sake of brevity, these dimensions were not explicitly reported in the main body of this thesis. However, because they proved to play a significant role when a high precision is sought, the reader may find this data in the appendices of this paper.

In Figure 4.15 the behaviour of the RJ specimen assessed through the analytical procedure is compared to the one observed in the experimental test. Considering the rather low complexity of the connection, a very good agreement between the analytical prediction and the real $M - \phi$ curve is reported. The component method proved to be reliable for the estimation of initial and post-plastic stiffness of the joint. Additionally, there is observed a very accurate prediction for the plastic and ultimate rotation capacities of the joint.

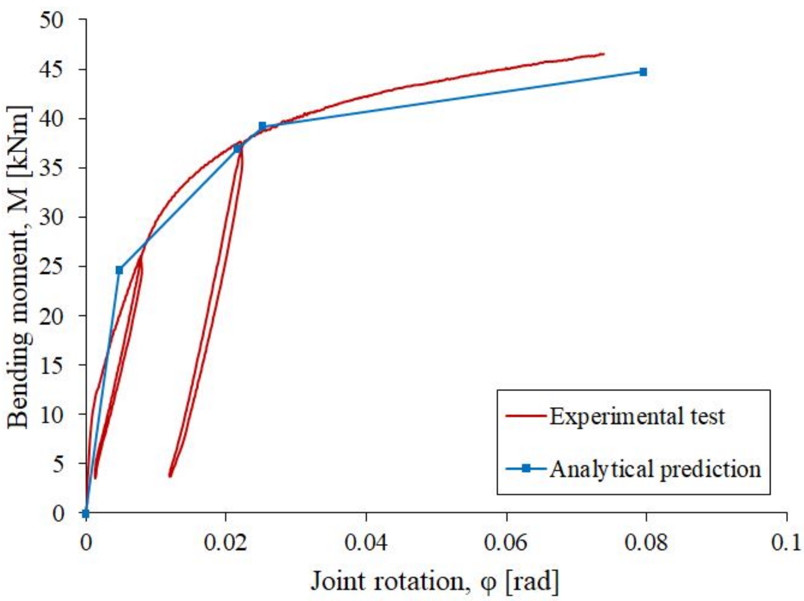

Figure 4.15: RJ: Test vs. analytical approach

Even though from the experimental data it is difficult to extract precisely the elastic and plastic bending resistances, judging on how the analytical model matches the actual $M-\phi$ curve, the difference between the predicted values and the actual ones is not significant. Having all these validation criteria fulfilled, the analytical method is considered to predict with high accuracy the full response of the RJ specimen.

In Table 4.2 a survey of the component method application on the RJ specimen is provided. It is noticeable that the analytical prediction for ultimate bending resistance is not significantly different when compared to what has been reported in the physical test results. A maximum bending moment of 47.5 kNm was reached during the test, whereas the analytical approach leads to a value of 44.75 kNm, thus the prediction error is estimated to be of approx. 7%.

	Active components										
	cfb		cwt		epb		bwt		bt	cwc	bfc
	row 1	row 2	row 1	row 2	row 1	row 2	row 1	row 2			
FR_{pl} [kN]	225.7	191	382.9	222	264.7	200.3	368.8	199.5	152.6	450.4	429.5
F_{Ru} [kN]	274.8	226.3	480.3	279.7	336.5	245.5	461.7	249.8	169.6	562	537.7
k_i [mm]	11	11	5.5	5.5	11.6	11.6	∞	∞	5.6	8.1	∞
k_{st} [mm]	0.22	0.22	0.109	0.109	0.233	0.233	∞	∞	0.113	0.16	∞
M_{Rpl} [kNm]	36.98										
Plastic Failue Mode	Bolt row 1: Column flange in bending Bolt row 2: Column flange in bending - Mode 2										
M_{Ru} [kNm]	44.75										
Ultimate Failure Mode	Bolt row 1: Column flange in bending Bolt row 2: Column flange in bending - Mode 2										
$S_{j,ini}$ [kNm/rad]	5107.2										
$S_{j,st}$ [kNm/rad]	102.14										

Table 4.2: RJ - Resistance and stiffness estimation

The analytical prediction for the behaviour of EPB specimen is provided in Figure 4.16. One may perceive the obvious difference between the results as a rough error emerged from the analytical model. However, this specific case does not reveal anything else than the limitations of the assumptions made in the analytical approach. More specifically, the source of the underestimation of the ultimate bending capacity may be attributed to the analytical formulae developed to characterise the behaviour of *epb* component, as in this case this is the failing component that governs the overall response of the joint. As reported in Table 4.3, the main failure modes are associated to the failure in bending of the end-plate by Mode 1 and Mode 2. The accuracy of the analytical formulae developed for the equivalent T-stub element, on which the characterisation of *epb* component relies, tends to be negatively affected when the model is applied to thin plates. Failure modes 1 and 2 are associated to substantial development of yielding patterns into the flange of the equivalent T-stub. In this particular case, the end-plate represents the flange of the

T-stub element, and as it is only 8 mm thick, it can be classified as a thin plate, thus justifying the discrepancies between the actual and predicted bending capacities.

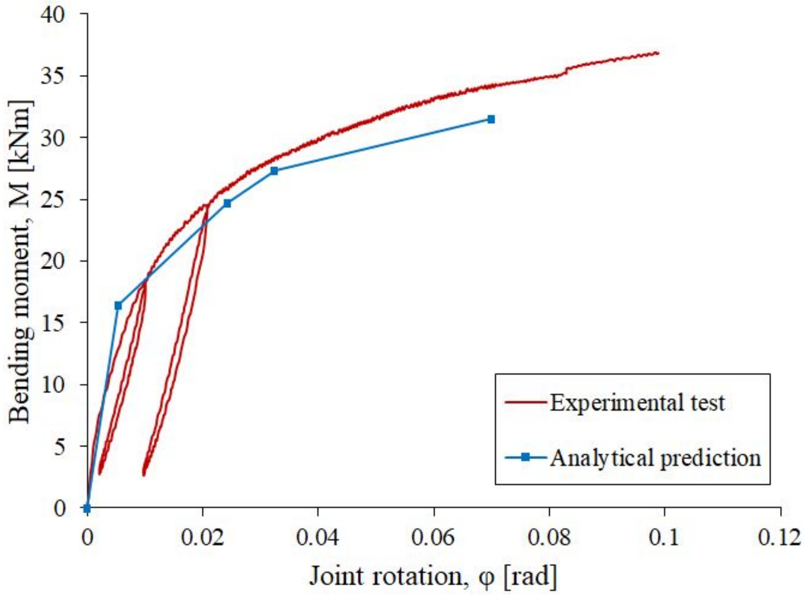

Figure 4.16: EPB: Test vs. analytical approach

Despite the significant underestimation of the ultimate resistance capacity, the analytical method can be still viewed as a reliable alternative when referring to initial stiffness and plastic bending resistance estimation. In Table 4.3 are provided the main characteristics of the EPB specimen estimated through the component method.

	Active components										
	cfb		cwt		epb		bwt		bt	cwc	bfc
	row 1	row 2	row 1	row 2	row 1	row 2	row 1	row 2			
FR_{pl} [kN]	225.7	191.1	384.6	224	164.5	103.1	368.8	199.5	152.6	402.4	429.5
F_{Ru} [kN]	274.8	226.3	482.4	281.1	196.4	169.7	461.7	249.8	169.6	466.9	537.7
k_i [mm]	11	11	5.5	5.5	1.8	1.8	∞	∞	6.67	7.7	∞
k_{st} [mm]	0.22	0.22	5.5	5.5	0.036	0.036	∞	∞	6.67	7.7	∞
M_{Rpl} [kNm]	24.78										
Plastic Failue Mode	Bolt row 1: End-plate in bending Bolt row 2: End-plate in bending - Mode 1										
M_{Ru} [kNm]	31.56										
Ultimate Failure Mode	Bolt row 1: End-plate in bending Bolt row 2: End-plate in bending - Mode 2										
$S_{j,ini}$ [kNm/rad]	3063.7										
$S_{j,st}$ [kNm/rad]	111.25										

Table 4.3: EPB - Resistance and stiffness estimation

Unlike the previous case, the analytical prediction of the $M - \phi$ curve for the CFB specimen seems to be in a remarkable agreement with the one experimentally assessed. An undeniable fulfillment of all validation criteria is depicted in Figure 4.17.

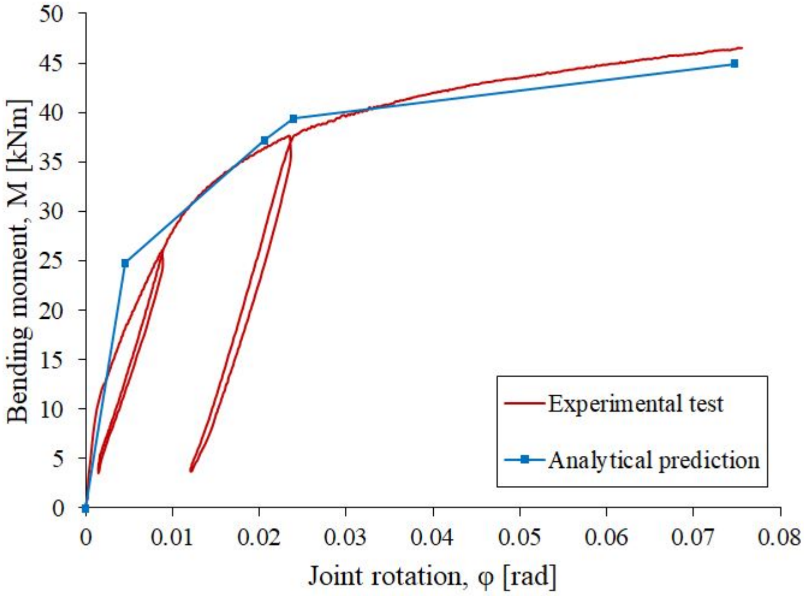

Figure 4.17: CFB: Test vs. analytical approach

The component method provides very accurate estimations for the plastic and ultimate bending capacity, despite the fact that the failure modes reported in Table 4.4 are similar to the ones observed on the EPB specimen.

	Active components										
	cfb		cwt		epb		bwt		bt	cwc	bfc
	row 1	row 2	row 1	row 2	row 1	row 2	row 1	row 2			
FR_{pl} [kN]	225.7	191.1	384.6	224	305.2	226	368.8	199.5	152.6	431.6	674.6
F_{Ru} [kN]	274.8	226.3	482.4	281.1	339.1	339.1	461.7	249.8	169.6	499.6	844.7
k_i [mm]	11	11	5.5	5.5	19.6	19.6	-	-	5.3	8.6	-
k_{st} [mm]	0.22	0.22	0.11	0.11	0.393	0.393	-	-	0.106	0.17	-
M_{Rpl} [kNm]	37.19										
Plastic Failue Mode	Bolt row 1: Column flange in bending Bolt row 2: Column flange in bending - Mode 2										
M_{Ru} [kNm]	44.93										
Ultimate Failure Mode	Bolt row 1: End-plate in bending Bolt row 2: End-plate in bending - Mode 2										
$S_{j,ini}$ [kNm/rad]	5407.3										
$S_{j,st}$ [kNm/rad]	108.15										

Table 4.4: CFB - Resistance and stiffness estimation

Reference is made once again to the T-stub model, as the ultimate failure mode is associated to yielding and high plasticity development in the end-plate. Nevertheless, in this case, the end-plate is 18 mm thick, hence is in the usual thickness ranges for which the T-stub model have been calibrated. The results are confirming what was previously stated on the reliability of the T-stub model. The conclusions to be drawn are concerning the limitations and the applicability of the T-stub model for thin plates.

The application of the component method to the specimens with welded connections did not require any substantial computational effort, mostly due to the simple joint configurations. Since for these specimens generally one or two components were activated, the results will be reported only in terms of overall plastic bending resistance and initial stiffness (if there is any).

Figure 4.18 illustrates the comparison between the analytical prediction and the actual behaviour of the BFC specimen. As a reminder, this specimen consisted of a welded connection between two beams and a fully stiffened column. Therefore, the only active component that can be identified is the beam flange in compression. Indeed, in the design phase of this specimen, the main objective was to create a joint for which the failure component would be the *bfc* .

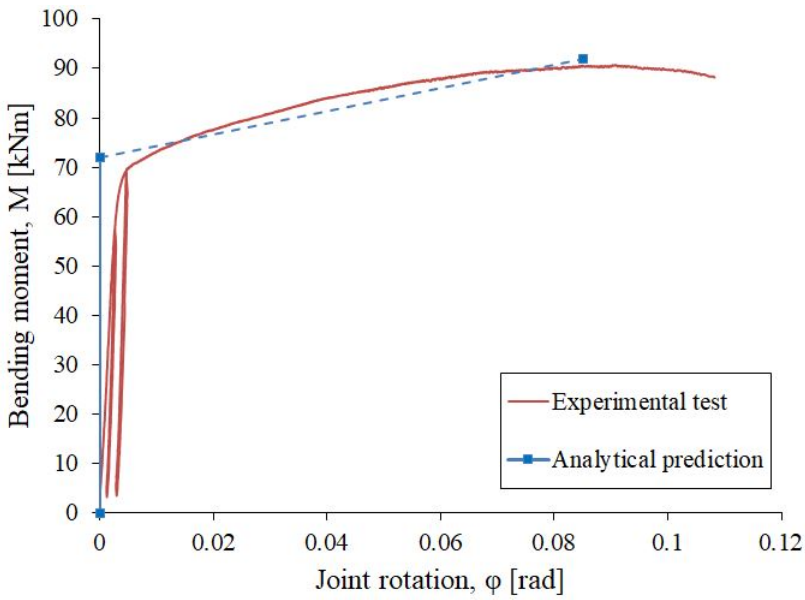

Figure 4.18: BFC: Test vs. analytical approach

According to Eurocode 3, the beam flange in compression component is assumed to have an infinite initial stiffness. The bending resistance of this component is associated entirely to the beam resistance capacity. Accordingly, the bending capacity of the joint becomes directly a function of beam's characteristics. When a beam of class 1 or 2 cross-section is welded to a stiffened column, the ultimate bending capacity will overpass the plastic one, as for these cross-section classes it is assumed that the plastic resistance can be reached without the occurrence of buckling phenomena and further plasticity can develop. This situation have been encountered for the BFC specimen, for which the IPE 180 profile of the beam is a class 2 cross-section, thus allowing to account for the plastic resistance of the section. A plastic bending capacity of $M_{Rpl} = 72$ kNm have been estimated in this case, whilst the ultimate resistance, considering the ultimate strength of the material, is $M_{Ru} = 91.9$ kNm. Although the values for the bending resistances are in a good agreement with the ones reported from the test, the full behaviour of the joint is of great complexity in this case, because it depends entirely on the response of the beam. The rotation capacity of the joint becomes a complex matter that will not be addressed in this study. However, for the sake of completeness, in Figure 4.18 an "expected" post-plastic behaviour of the joint is represented with the dashed blue line. An arbitrary value for the ultimate rotation ϕ_u which is in line with the expectations has been chosen.

Due to complexity related to the buckling phenomena, the analytical prediction for CWC specimen is very conservative, when compared to the physical test results. When assessing the capacity of the joint following closely the approach proposed by Eurocode 3, represented in Figure 4.19 with a blue line, the "plastic" bending resistance of the joint is greatly underestimated. Since the failure of the joint in this case is associated to the buckling of the column web, the plastic bending resistance stands for the ultimate bending resistance as well. After reaching its buckling capacity the joint is assumed to not exhibit any resistance, thus the ultimate rotation capacity is reached when buckling occurs.

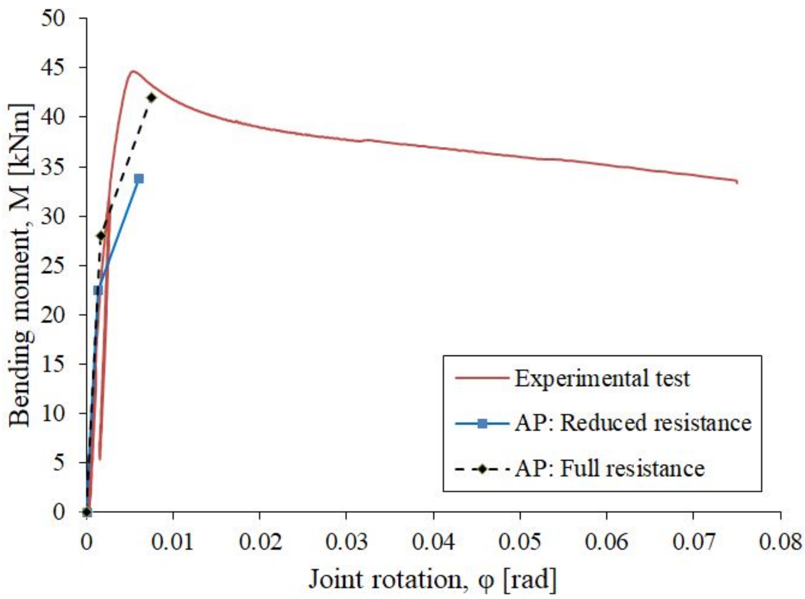

Figure 4.19: CWC: Test vs. analytical approach

It is worth noting that in Eurocode 3, the analytical formulae adopted for the characterization of *cwc* component tend to provide very conservative results, as they imply the use of maximum expected initial imperfections. The latter are leading to great buckling reduction factors (ρ) and consequently to reduced resistance capacities. In Figure 4.19, with a black dashed line is represented the behaviour of the joint considering the buckling reduction factor $\rho = 1$. It is easily noticeable that the joint behaviour is closer to reality in this case, highlighting the influence of great initial imperfections that are considered in Eurocode 3.

4.2 Finite element model

Physical tests performed on full-scale joints represent the most reliable source of information when the behaviour of joints is investigated. However, such experiments are most of the time economically inefficient and challenging to perform in a controlled manner due to the limitations of the specific instrumentation. Moreover, through an experimental test it is difficult to capture and investigate all parameters of concern, such as the energy dissipation, stress distribution or strain rate effects. Numerical simulations are usually used to overcome such challenges. These models can be used as an alternative inexpensive and robust tool, that allows for the investigation of local effects that are otherwise difficult to be estimated through physical tests. Furthermore, using the numerical simulations, one can generate extensive parametric studies, allowing for the investigation of a specific parameter influence on the overall response of the joint in an economically efficient manner.

Nonetheless, a reliable numerical simulation implies a beforehand validation of the model. Generally, when the joint behaviour is investigated using FE solutions, the model is considered to be validated when it is able to predict accurately the global and local response of the joint, including the failure mode experimentally observed.

In order to validate a numerical model that would be used subsequently for the investigation of strain rate effects under dynamic loads, FE models for all five specimens were developed using the commercial FE software Abaqus 2016. The main goal is to validate the numerical models against the results of the physical tests performed under quasi-static loading conditions and to prove the reliability of such a tool for further investigations.

In FE simulations an incremental procedure is used generally to solve the non-linear response of a system. In Abaqus, for static analyses, the convergence of the solution is met by using the iterative Newton-Raphson method for solving the non-linear equilibrium equations. For the applications implying transient dynamic situations, the Newton-Raphson method is replaced by two different solvers: implicit and explicit. In this particular case, the quasi-static tests on the beams-column assembly were simulated as a static analysis using Abaqus/Standard.

4.2.1 Geometry and discretisation

By exploiting the symmetry, only $1/4^{th}$ of the physical specimen has been modelled, allowing for the reduction of the overall computational effort. Solid elements were used for all constitutive elements of the assembly. The parts were modelled using the actual geometrical properties of the profiles provided in detail in (Hoffmann et al., 2016). A detailed view of one of the FE models (RJ specimen) is provided in Figure 4.20.

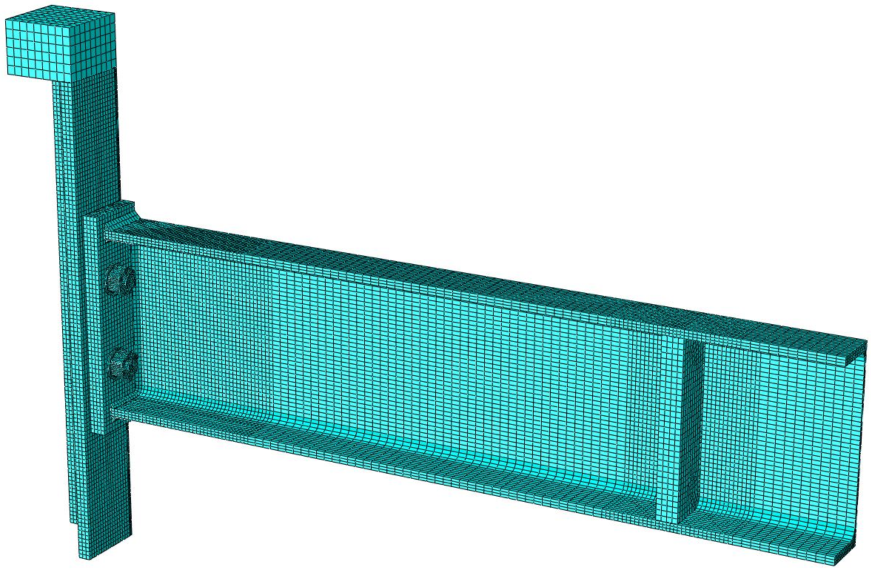

Figure 4.20: FE model of the RJ specimen

The welds were modelled as triangular parts and the bolts were modelled as having a smooth shank, thus not including in the model the threads. The threaded portion of the bolt was modelled using a diameter of 14.1 mm, that would simulate the resistant area of the bolt. The nuts and the washers used for the real assembly were explicitly modelled using the nominal geometrical properties.

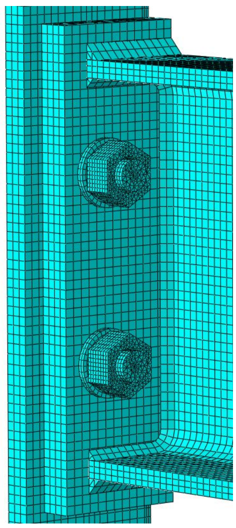

(a) Mesh density

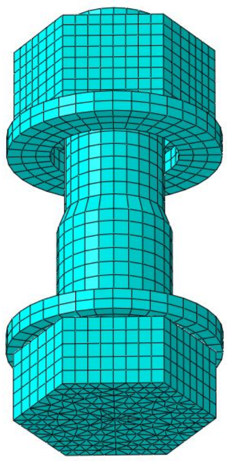

(b) Bolt detailed view

Figure 4.21: Specific parts of the FE model

Figure 4.21a depicts the mesh density of the model. A more dense mesh was assigned to the regions were local effects are more likely to occur, thus, the end-plate and the region in the immediate proximity of the connection has been discretised with more reduced elements. A coarser mesh has been applied to the regions corresponding to the beam's midspan and to the beam's free end. Generally, a minimum number of 3 elements over the thickness was assigned for all plates of the joint. Mesh seeds of 4 mm were applied to the parts of the model in the regions with high density mesh. Mesh seeds of 2 mm were used for the bolts.

Because the model provided results in a good agreement with the ones obtained through the physical test, the mesh density was considered to be adequate. However, some mesh sensitivity studies were conducted additionally and the results have shown that a mesh refinement would minimally affect the results. Solid C3D8R 8-node linear brick elements with reduced integration were used for the entire model, except for the welds and the profiles' root radius region, where C3D6 wedge elements have been used.

4.2.2 Materials

The non-linear behaviour of the material is included in the FE simulation by specifying a non-linear stress-strain relationship for material hardening. The elasto-plastic behaviour of steel was implemented in the numerical model based on the engineering stress-strain curves previously presented. A modulus of elasticity of 210 GPa was considered for all the materials, even if from the tests performed on coupons the values of the modulus of elasticity were slightly bellow this standard used value.

The engineering stress and strain measured during the coupon tests do not account for the changes in the cross-sectional area of the sample in plastic region. Based on the initial area of the coupon, the engineering stress - strain curves descend after the bearing capacity of the sample is reached as the tensile resistance decreases in-time with the reduction of the cross-section. To overcome this issue, the concept of *true stress - logarithmic plastic strain* curves is introduced, the latter are based on the actual area of the sample and, as opposite to the engineering ones, continues to ascend until the fracture point.

The engineering stress - strain curves are converted into the true stress - logarithmic plastic strain using the following expressions:

$$\sigma_{true} = \sigma_{eng}(1+\varepsilon_{eng}) \tag{4.46}$$

$$\varepsilon_{true} = \ln(1+\varepsilon_{eng}) \tag{4.47}$$

where σ_{eng} and ε_{eng} are the engineering stress and the corresponding engineering strain, respectively.

Subsequently, the true plastic strain is derived by simply extracting the elastic strain from the total true strain:

$$\varepsilon_{pl} = \varepsilon_{true} - \frac{\sigma_{true}}{E} \tag{4.48}$$

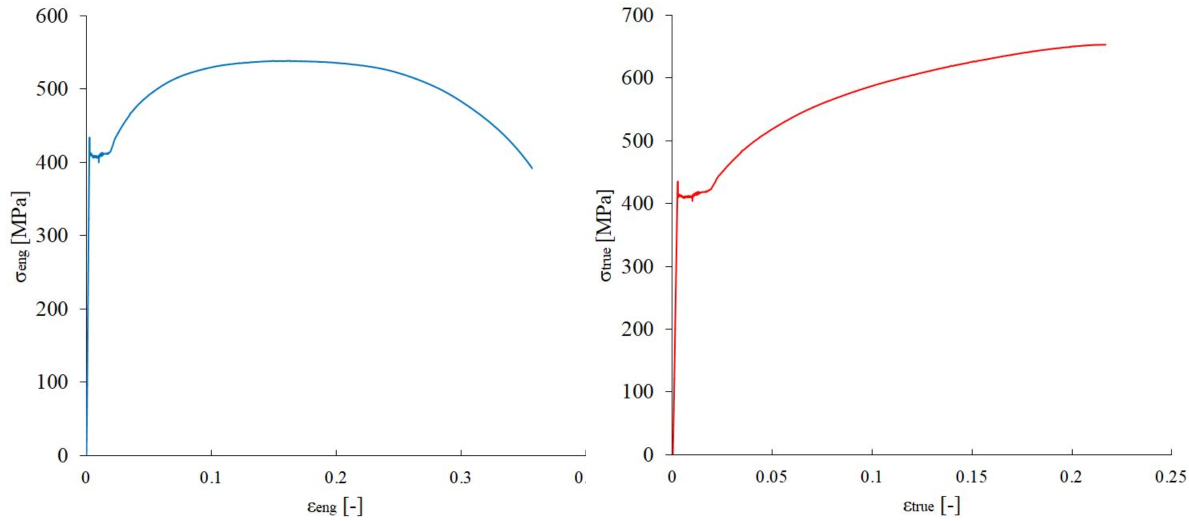

(a) Engineering stress - strain curve

(b) True stress - true strain curve

Figure 4.22: Conversion of engineering stress - strain curve into true stress - true strain

The welds were assigned the same material parameters as the base material of the profiles, as well for the stiffeners. Because no coupon tests were performed on the bolts material, the values for the yield strength and the ultimate strength were considered the ones reported by Hoffmann et al. (2016) (f_y=1020 N/mm^2 and f_u=1080 N/mm^2) for similar 10.9 bolts grade and material behaviour was implemented through a bi-linear model.

It is worthy to mention that the damage evolution and failure criteria were not implemented in the material model, this representing a potential complement in the future work on this topic.

4.2.3 Loading and boundary conditions

The boundary conditions play a crucial role when the reliability of a model is assessed. The physical restrains of the test setup have to be accurately replicated in the numerical model. Aiming at providing the appropriate restrains, the following boundary conditions were applied to the numerical model:

- the beam is simply supported at its end, thus the vertical displacement of the beam at the level of its extremity has been restrained;
- lateral supports were provided at the level of beam's stiffeners, in order to prevent the loss of stability and the lateral torsional buckling of the beam;
- symmetry boundary conditions were applied along the two symmetry planes.

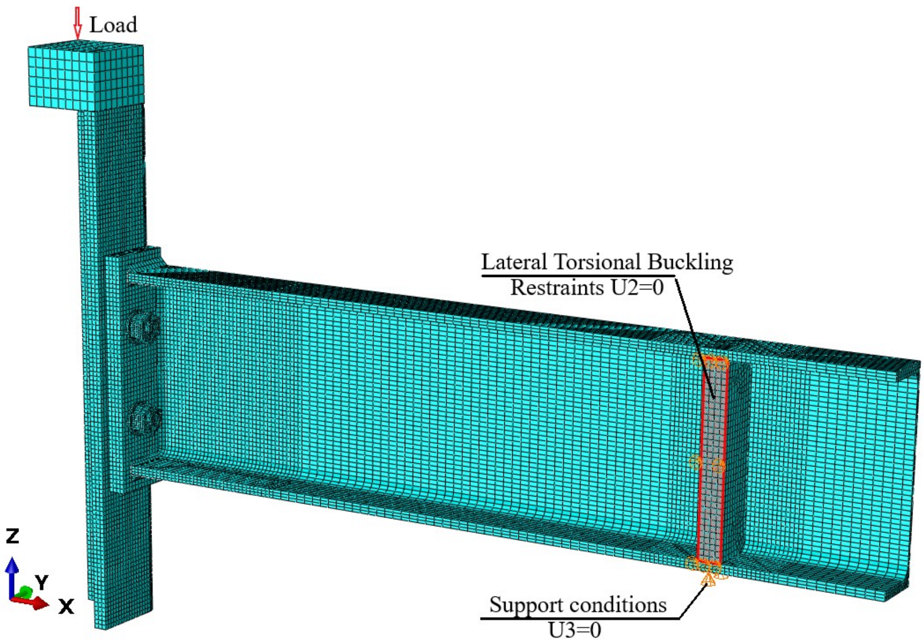

Figure 4.23: Boundary conditions

The vertical monotonic force simulating the force applied by the hydraulic jack has been applied in the numerical model using a displacement control option. The maximum value of the induced displacement was set to the one registered during the physical test and corresponding to the specimen's failure.

Because the bolts were only snug tight, the pre-tensioning of the bolts was not considered in the following simulations.

4.2.4 Interactions and contact

Three different types of interactions between the elements of the system have been defined in the FE model. Tie constraints were used to connect the elements between which no relative displacement is allowed. Therefore, this constrain was used to connect the welds to the beams, the beams to the end-plates, the stiffeners to the beams and to the columns, and the loading plate to the column.

The contact between different parts of the assembly has been modeled through a contact interaction. A surface-to-surface type of contact has been defined for the interaction between several contact pairs: bolt-heads and end-plates, bolt shanks and bolt holes of end-plates and column flanges, nuts and column flanges,and end-plates and column flanges. The normal direction behaviour has been defined using a "Hard contact" property, that does not allow the interpenetration of the surfaces in contact. For the tangential direction a Coulomb friction model with a penalty formulation has been applied. A friction coefficient of 0.3 was adopted for all contact pairs in the model.

4.2.5 FE model validation

As previously stated, the numerical models were considered to be reliable when the global and local response of the joint was accurately captured when compared to the one experimentally observed. In order to validate the models, the response of the specimens was compared in terms of global force-displacement curve and failure mechanisms. For most of the specimens, a generally good agreement has been observed between the two methods. The FE simulations provided generally accurate predictions for the behaviour of different joint configurations under quasi-static loading conditions.

This section provides the comparison between the physical tests and the FE simulations. It can be easily noticeable that for the situations where no buckling phenomena are expected to occur, the FE simulations were able to capture accurately the initial stiffness of the joints and their plastic resistance. Additionally, the expected failure modes have been captured as well, representing a supplementary validation criteria.

4.2.5.1 RJ specimen

The FE model of the RJ specimen captured with a high accuracy the initial rotational stiffness of the joint (note that the initial stiffness in the numerical model follows closely the loading-unloading path). The strain-hardening stiffness of the real specimen proved to be somehow bigger than the one exhibited by the numerical model. However, the difference is not significant and the numerical simulation captures the global failure mode by high plasticity development in the column flange, beam top flange and the end-plate.

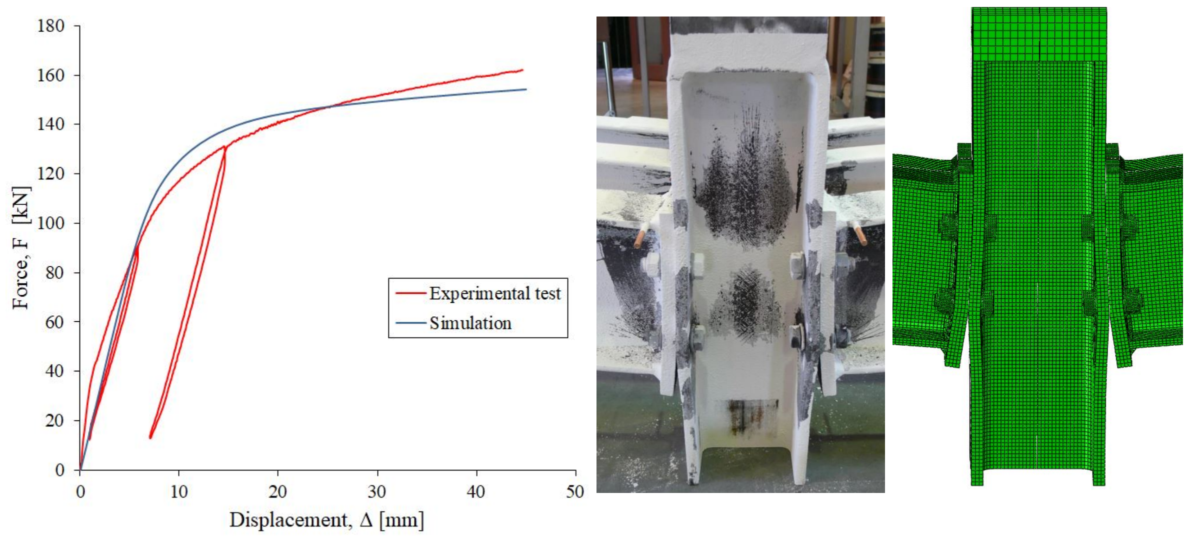

(a) Force-displacement curve (b) Test failure mode (c) FE failure mode

Figure 4.24: RJ specimen: FE simulation vs. Experimental test

Figure 4.24 depicts the validation of the FE model for the RJ configuration. The comparison is made between the physical test and the numerical simulation in terms of global force-displacement curve and failure mode.

4.2.5.2 EPB specimen

The EPB specimen was modelled in Abaqus based on the RJ model, the only modification made being the thickness of the end-plate and the adjustment of the beam's length, respectively. As expected, based on the previous experience, the results provided by the numerical model are in a good agreement with those obtained from the test. The initial rotational stiffness of the joint is captured with high accuracy and the failure mode is associated to the failure of the "end-plate in bending" (*epb*) component at the level of both bolt rows, confirming the reliability of the FE model. The validation of the model is illustrated in the figures bellow by comparing the overall response of the joint obtained through physical and numerical tests.

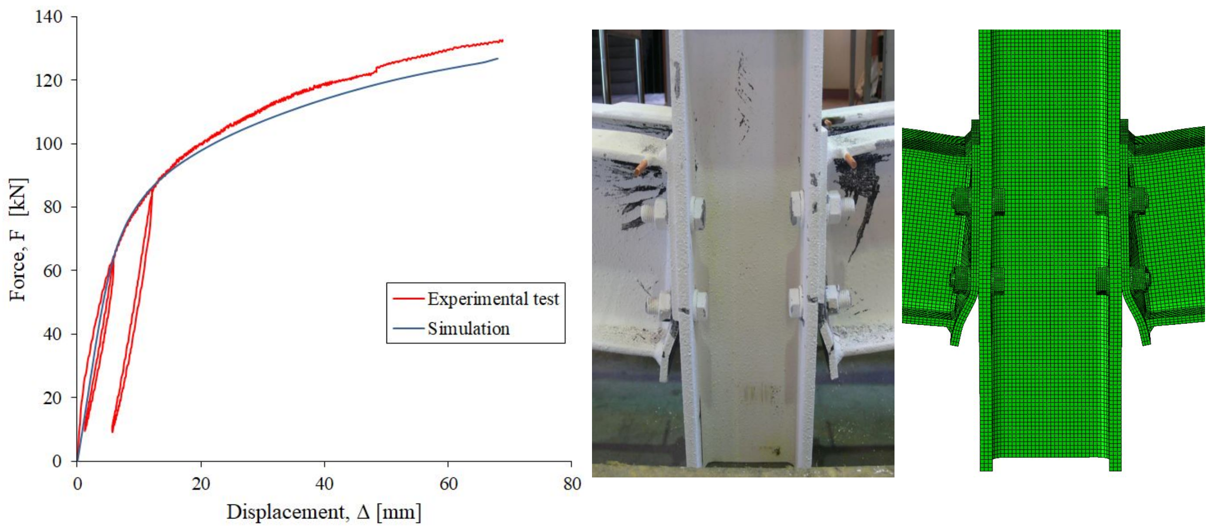

(a) Force-displacement curve (b) Test failure mode (c) FE failure mode

Figure 4.25: EPB specimen: FE simulation vs. Experimental test

4.2.5.3 CFB specimen

For the CFB specimen, once again, modifications have been implemented in the RJ model, in order to achieve the final geometry of the CFB specimen. Therefore, the thickness of the end-plate has been increased from 15 to 18 mm and the beam's length has been adjusted in order to comply with the overall setup limitations. The reliability of the FE simulation is proven for an additional time by observing the agreement between the results in the figure bellow.

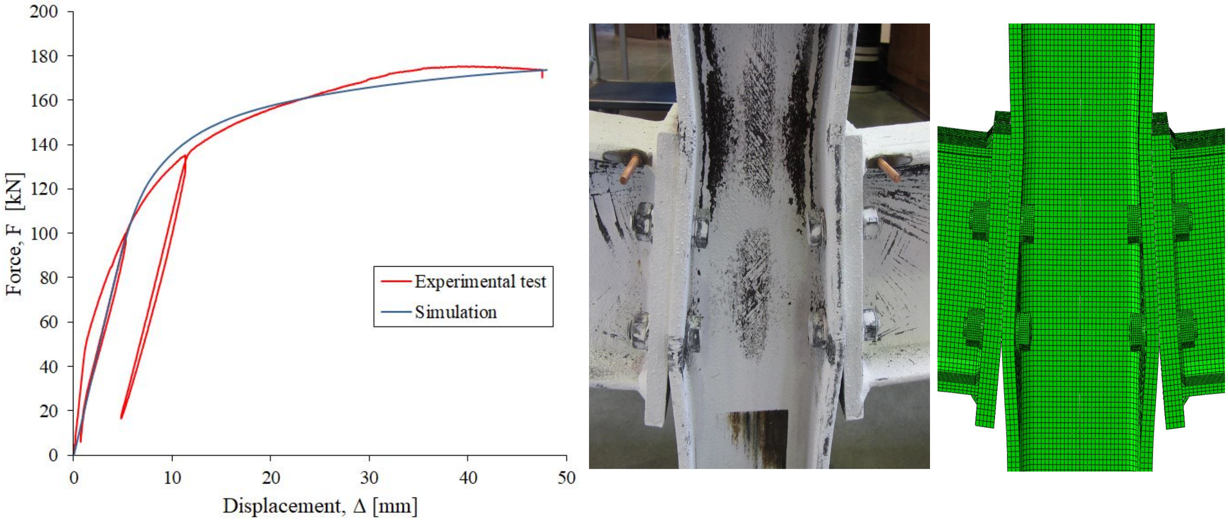

(a) Force-displacement curve (b) Test failure mode (c) FE failure mode

Figure 4.26: CFB specimen: FE simulation vs. Experimental test

4.2.5.4 BFC specimen

Additional modifications were performed on the RJ numerical model in order to achieve the general layout of the BFC specimen. The beam was directly welded to the column's flange and two 12 mm thick stiffeners were added on the column's web. The FE simulation captured the initial rotational stiffness of the joint and it's strain-hardening stiffness as well. The difference between the predicted values of the resistance capacity and the experimentally recorded ones is negligible, a general agreement in the joint's response being achieved and depicted in Figure 4.27.

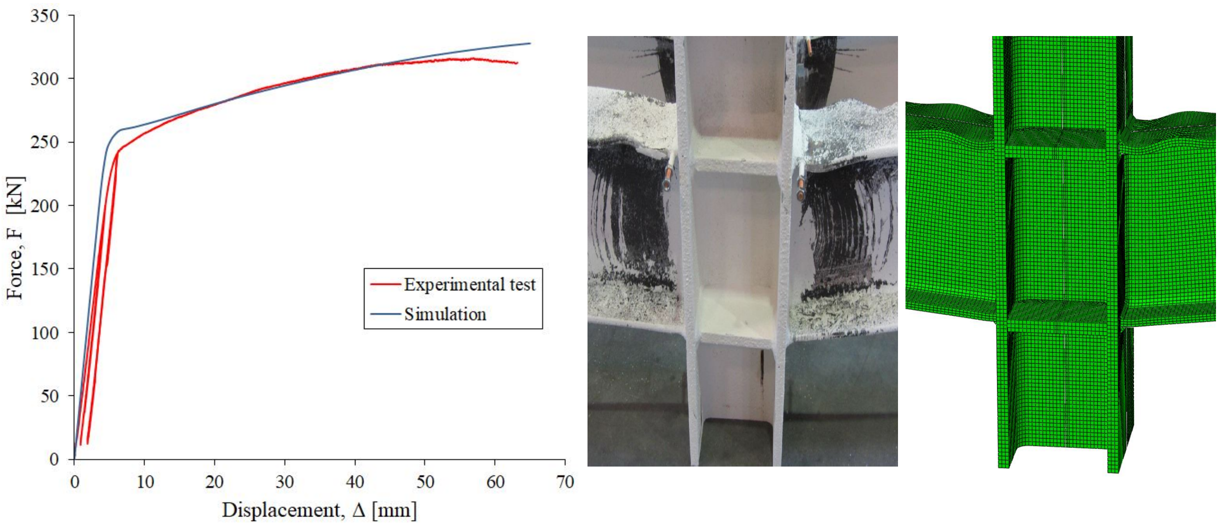

(a) Force-displacement curve (b) Test failure mode (c) FE failure mode

Figure 4.27: BFC specimen: FE simulation vs. Experimental test

4.2.5.5 CWC specimen

Unlike the previous cases, where only $1/4^{th}$ of the physical specimen was modelled, due to the complexity of the buckling related problems, it was decided to model the full assembly for the CWC specimen. In order to induce a certain buckling mode in the FE model, there was required to implement some initial imperfections. Prior to the actual static analysis of the specimen, a Linear Buckling Analysis has been conducted in order to evaluate the main buckling modes and their correspondent eigenvalues. Based on the parameters obtained through the LBA, a post-buckling analysis was carried out. The initial imperfections implemented in the model correspond to approximately 10% of the plates' thicknesses. The monotonic loading has been applied in a displacement control manner similarly to the previous cases. Figure 4.28 depicts the response of the joint assessed through physical and numerical tests.

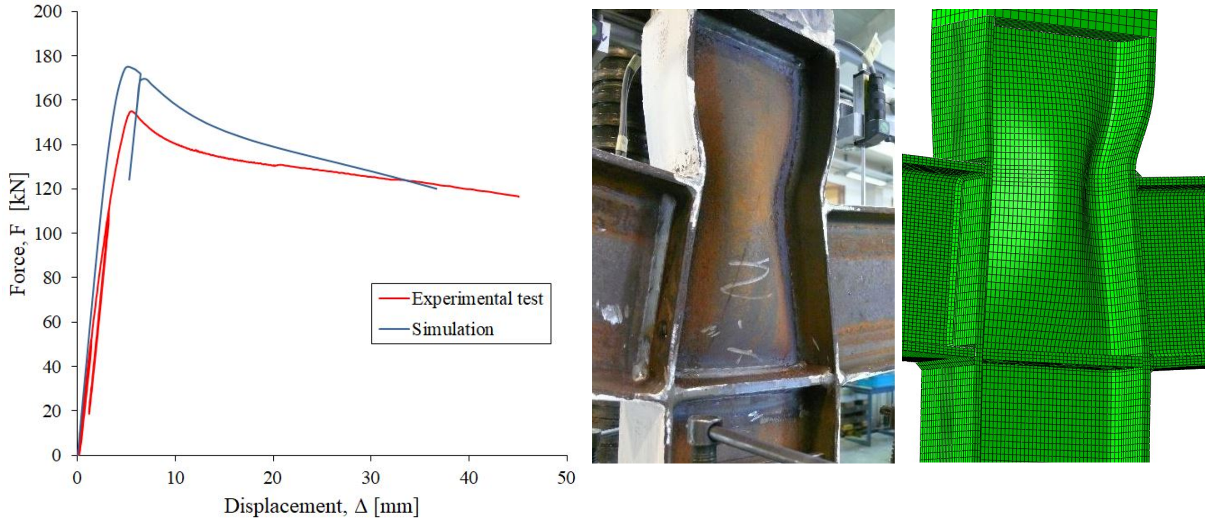

(a) Force-displacement curve (b) Test failure mode (c) FE failure mode

Figure 4.28: CWC specimen: FE simulation vs. Experimental test

The FE simulation captures the initial stiffness of the joint, but slightly overestimates the buckling load. Numerically predicted buckling load is 11.5% higher than the experimentally registered one; this can be related to the uncertainties on real imperfections of the profiles or to the fact that the load is applied with a small eccentricity inducing a "parasite" moment that is decreasing the column's web buckling load. Due to the complexity of the model and the phenomenon involved in the analysis, the analysis crashes after approximately 160 increments. Convergence related problems are causing the break of the analysis before the experimental ultimate vertical displacement of the connection is reached, but the results up to this point are still usable. Moreover, the agreement between the results can be considered as satisfactory as the difference between the buckling load is not significant and the general failure mode has been captured by the numerical model.

5 | Behaviour under dynamic loading

The behaviour of steel joints subjected to static loading conditions has been extensively investigated in the last 50 years. The outcome of the studies allowed the research community to provide reliable and practical tools to assess the resistance and the rotational stiffness of the joints. On the other hand, the response under severe dynamic loads has been studied by a limited number of researchers, generally, a limited amount of information on this topic being available in the scientific literature. Even though a joint may exhibit adequate levels of resistance and ductility under quasi-static loading conditions, it does not necessarily respond satisfactorily under severe dynamic loads. Therefore, the enhancement of knowledge on the behaviour of steel joints subjected to dynamic loads is crucial.

This chapter presents the extension of the experimental campaign to the investigation of joints response under dynamic impact loading scenario. The effects related to the dynamic transient character of the loading are quantified through a graphic method relying on the outcome of the tests under the two loading scenarios (static and dynamic). Additionally, using the experimental results, a 3D finite element model is validated and used to assess the dynamic effects due to various levels of loading rates. Essential aspects concerning the material behaviour under severe impulsive loading are addressed and the modelling assumptions made for the development of the FE model are presented in detail in the following sections.

5.1 Estimation of the impact force

During testing, the impact force applied on the column head can be accurately captured by using high frequency load cells. Unfortunately, the laboratory at the Univerity of Liège is not equipped with a such data acquisition equipment. Theoretically, the average impact force F_{IT} can be estimated according to the impulse-momentum theorem, which is basically the equivalent of the Newton's second law of motion and can be expressed based on the velocity of the impactor as follows:

$$\vec{F_{IT}}\Delta t = m\Delta\vec{v} \quad \Rightarrow \quad \vec{F_{IT}} = m\frac{\vec{v_{imp}} - \vec{v_{reb}}}{\Delta t} \tag{5.1}$$

where, m is the mass of the impactor, v_{imp} is the impact velocity, v_{reb} is the velocity of the impactor at the moment when it rebounds separating from the impacted body and Δt is the time of permanent contact between the two bodies during the impact.

Even though the rebound velocity of the impactor has been recorded during the tests, the moment in time when the mass separation occurs was not explicitly reported. Thus, in this particular case, the use of this theoretical method is constrained by the lack of experimental data.

As an alternative to the impulse-momentum theorem, a graphic approach has been developed and presented by Hoffmann et al. (2016). The basic principle of this method is to predict the applied impact force knowing the stiffness of the impacted specimen and its maximum and permanent displacements during the impact. A reference is made to the static behaviour of the joints, as their stiffness is derived from the results of the static tests. Moreover, the $F-\delta$ curves, reported for the joints behaviour under quasi-static loading conditions, will be employed in the estimation of the maximum impact force through the procedure depicted in Figure 5.1.

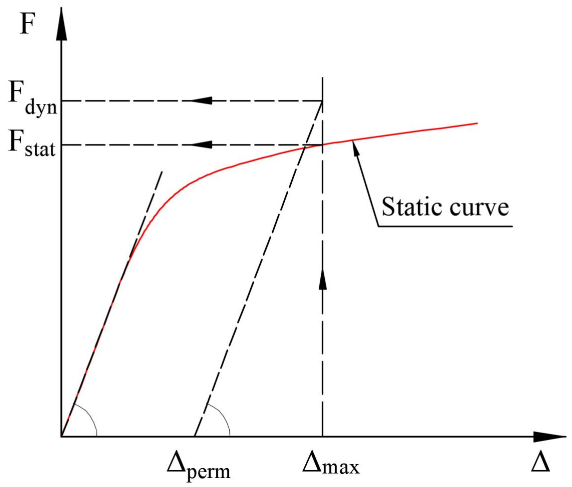

Figure 5.1: Graphic estimation of the impact force

Starting from the plastic permanent deflection δ_{perm}, the maximum impact force is derived by simply drawing a line with the same pitch angle as the initial stiffness $S_{j,ini}$. The intersection point of this line with the vertical line corresponding to the maximum measured displacement δ_{max} represents the value of the applied dynamic force during the test. In Figure 5.1, F_{stat} is defined as the equivalent static load corresponding to a displacement δ_{max}.

The graphic approach may be considered as a rough estimation of the real impact force, however, despite its simplicity, it tends to deliver similar values with the ones yielded from the impulse-momentum theorem. A good agreement between the results obtained through both methods was reported by D'Antimo et al. (2019) and D'Antimo (2020). Additionally, the two methods were compared to numerical simulations, a good agreement between the results being achieved, even though it was reported that the two approaches are slightly underestimating the maximum dynamic force.

The difficulty of predicting accurately the maximum dynamic load associated to the impact could be readily mitigated by the use of FE simulations. The wide range of output options of the FE software allows for the prediction of the applied impact force at each incremental time step of the simulation. This option will be used afterwards when the FE simulations will be employed to replicate the impact tests.

5.2 Strain rate effects - analytical prediction

As a definition, the strain rate $\dot{\varepsilon}$ is the parameter that describes the strain variation of a material per time unit, $d\varepsilon/dt$. Like most ductile materials, it is well known that the strength properties of mild steel are strongly affected by the loading speed. Under elevated strain rates, steel strength is enhanced by its visco-plastic behaviour. Consequently, the increase in strength at the material level leads to secondary effects in the global response of the element subjected to severe dynamic actions. Previous studies (Grimsmo et al., 2015; D'Antimo, 2020) highlighted the effects induced by elevated loading rates to the behaviour of steel elements, enhancing their resistance capacity under impulsive loading conditions.

Generally, in structural engineering the effects related to the strength enhancement caused by the loading rate are expressed by means of Dynamic Increase Factors ($DIFs$). The DIF is, thus, an "overstrength" coefficient that is used in the applications with elevated strain rates. The dynamic strength of a structural member is estimated by enhancing its static strength, simply multiplying it by an appropriate DIF. Two types of DIFs are commonly used by the engineers: force-based and displacement-based DIFs. The first type is expressing the ratio of the dynamic load to the static load of the structural system at the same displacement, while the latter is the ratio of the dynamic to static displacements under the same load. One can identify an additional DIF at the material level expressed in terms of stresses as:

$$DIF = \frac{\sigma_{dyn}}{\sigma_{stat}} \tag{5.2}$$

where, σ_{dyn} is the dynamic strength and σ_{stat} is the strength obtained under static conditions.

Based on the experimental results, the magnitude of the dynamic effects may be straightforwardly estimated using a force-based DIF. The forces corresponding to the static and dynamic responses (F_{stat} and F_{dyn}) can be readily evaluated by applying the procedure presented in the previous section. This allows for the estimation of the strain-rate effects as follows:

$$DIF = \frac{F_{dyn}}{F_{stat}} \tag{5.3}$$

As presented in section 3.5.2, four impact tests were performed on the RJ specimen. Figure 5.2 depicts the response of the joint under static and dynamic loading conditions. It is easily noticeable that, for impacts with higher levels of energy, the joint exhibits enhanced plastic resistance capacities. The DIFs for this specific configuration, reported in Table 5.1, range between 1.31 to 1.34, thus a strength enhancement of more than 30% is achieved when the load application has a strong dynamic character. For the test conducted in the elastic domain, the DIF is not computed, as it has a physical meaning only for post-elastic behaviour.

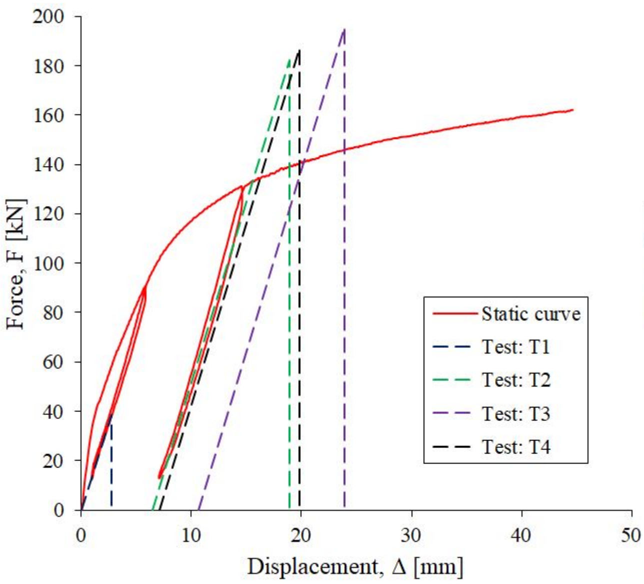

Figure 5.2: RJ - Static vs. impact tests

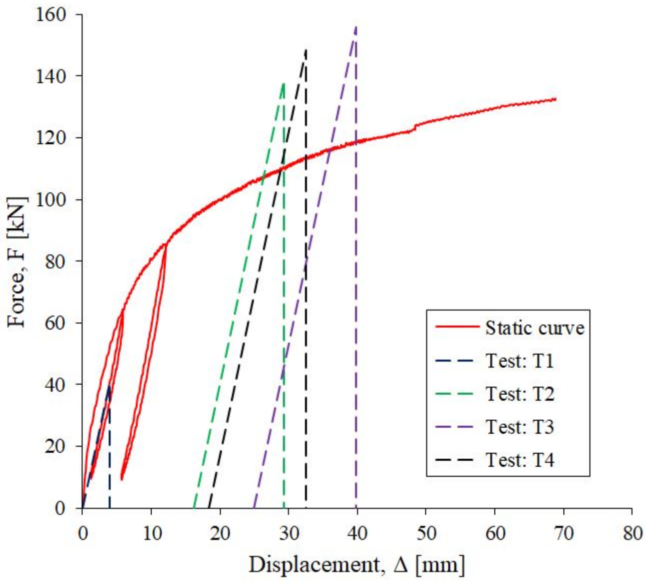

Figure 5.3: EPB - Static vs. impact tests

Test	Δ_{max} [mm]	Δ_{perm} [mm]	F_{stat} [kN]	F_{dyn} [kN]	DIF [-]
T1	2.73	0.1	38.7	38.7	-
T2	18.89	6.5	139	182.1	1.31
T3	23.94	10.64	146	195.5	1.34
T4	19.82	7.1	141	187	1.33

Table 5.1: RJ - DIF estimation

Test	Δ_{max} [mm]	Δ_{perm} [mm]	F_{stat} [kN]	F_{dyn} [kN]	DIF [-]
T1	3.87	0	40.6	40.6	-
T2	29.36	16.16	115	138.6	1.2
T3	39.83	25	118.7	155.7	1.31
T4	32.47	18.33	116.8	148.5	1.27

Table 5.2: EPB - DIF estimation

The graphic estimation of the forces associated to the impact tests performed on the EPB specimen is presented in an illustrative manner in Figure 5.3. The DIFs reported in Table 5.2 highlight the strain rate sensitivity of the end-plate in bending (*epb*) component. The dynamic resistance is enhanced by more than 20% when compared to the static one. For the tests with high levels of plasticity reached in the *epb* component, a general trend is observed with the increase of the DIFs concurrently with the increase of the dynamic load.

The CFB specimen has been subjected to a sequence of four impact tests. As can be observed in Figure 5.4, the joint behaves in an elastic way for the first two tests, as a consequence of the low energy associated to the impact. However, when subjected to greater impact forces, the response becomes significantly different when compared to the static reference. When plasticity develops under impulsive loading, the column flange in bending (*cfb*) component exhibits a post-elastic behaviour strongly influenced by the loading rate. This can be concluded judging on the high values of DIFs reported in Table 5.3 ranging between 1.66 and 1.7 for the plastic impacts. Moreover, from all basic components treated in the framework of this experimental campaign, the response of the *epb* component proved to be the most susceptible to strain rate effects.

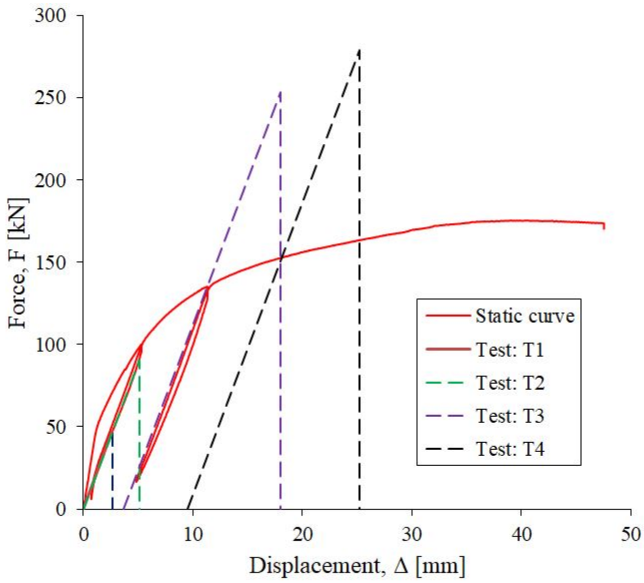

Figure 5.4: CFB - Static vs. impact tests

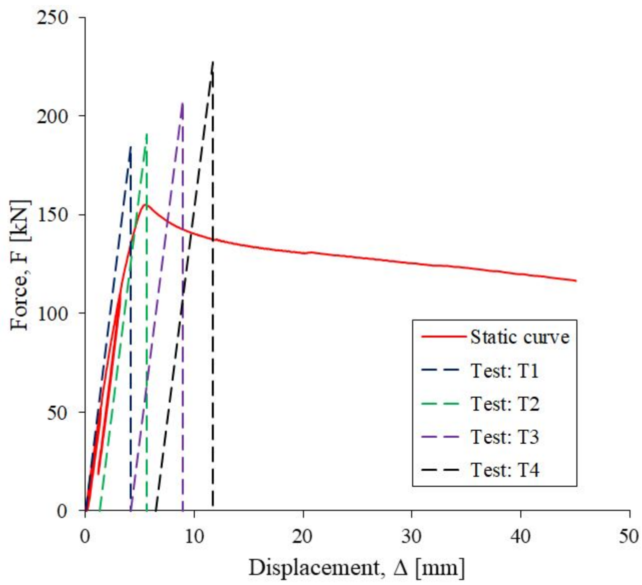

Figure 5.5: CWC - Static vs. impact tests

Test	Δ_{max} [mm]	Δ_{perm} [mm]	F_{stat} [kN]	F_{dyn} [kN]	DIF [-]
T1	2.65	0	46.9	46.9	-
T2	5.13	0	90.7	90.7	-
T3	18	3.7	152	253.1	1.66
T4	25.25	9.5	163.7	278.8	1.7

Table 5.3: CFB - DIF estimation

Test	Δ_{max} [mm]	Δ_{perm} [mm]	F_{stat} [kN]	F_{dyn} [kN]	DIF [-]
T1	4.19	0	133.5	184.4	1.38
T2	5.63	1.3	155.2	190.5	1.23
T3	8.93	4.2	142.8	208.1	1.46
T4	11.66	6.5	137.5	227	1.65

Table 5.4: CWC - DIF estimation

Unlike the static tests, where the buckling of the column web in compression occurred before reaching the plastic resistance, during the impact tests, the CWC specimen has shown greater resistance capacity, mainly due to the fact that no severe buckling was observed. When compared to the static behaviour, the loading rate seems to influence greatly the response of the *cwc* component, the dynamic forces being certainly higher than the static corresponding ones. The discrepancies between the static and dynamic response of the specimen are graphically displayed in Figure 5.5. Once again, significant values for the DIFs are derived from the tests results, reflecting the magnitude of dynamic effects on the *cwc* component's post-elastic response. In Table 5.4, the DIF varies from 1.23 to 1.65, following the general trend observed for the previous specimens, with the DIFs increasing proportionally to the impact force.

The behaviour of beam flange in compression *bfc* component proved to be somehow not affected by the loading rate. Figure 5.6 depicts the outcome of the tests conducted under the two loading scenarios. If for the previous basic components the strain-rate effects were clearly affecting the post-elastic behaviour, in the case of *bfc* component the influence is rather modest to non-existent. The DIFs reported in Table 5.5 vary within a very narrow range concentrated around the value of 1.

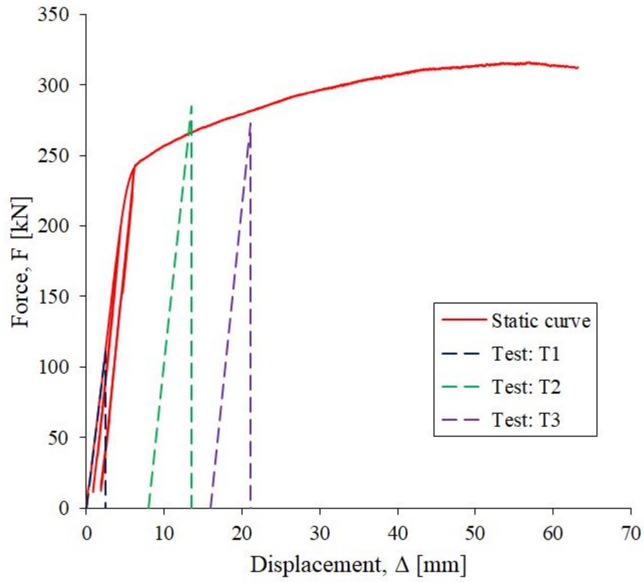

Figure 5.6: BFC - Static vs. impact tests

Test	Δ_{max} [mm]	Δ_{perm} [mm]	F_{stat} [kN]	F_{dyn} [kN]	DIF [-]
T1	2.52	0	131.5	131.5	-
T2	13.46	8	266	285	1.07
T3	21.1	15.86	281.5	273	0.97

Table 5.5: BFC - DIF estimation

Considering the very modest values of the DIFs reported for the BFC specimen, the conclusion that may be drawn is that the behaviour of the *bfc* component is not significantly influenced by the loading rate. This insensitivity to the strain-rate effects can be related to the stiffness associated to this component. Being a very stiff component, with an infinite stiffness when referring to the prescriptions of Eurocode 3, leads to very small strains associated to the deformation of this component, limiting thus the development of effects related to the strain-rate.

5.3 Finite element model

This section provides the main aspects concerning the assumptions made to apply the FE methods in the investigation of steel joints subjected to impact loads. The use of the FE models calibrated for the static tests has been extended to dynamic applications. The accuracy and the reliability of the model has been verified using the physical tests results reported in section 3.5.2. In order to account for the strain rate effects, some specific assumptions have been made for the material behaviour. A material model that accounts for such effects has been previously calibrated by D'Antimo et al. (2019), and employed in current numerical models.

Unlike the simulations for quasi-static loading conditions, the impact simulations have been performed using an explicit solver. The reason behind the switch from Abaqus/Standard to Abaqus/Explicit is related to the computational effort. The analyses conducted with explicit solvers are proved to be more efficient in terms of running time. This enhanced efficiency is mainly stimulated by the procedure used to integrate the equations of motion. The solution for one time step is derived from the kinematic conditions of the previous time increment, thus, the convergence of the solution is met in relatively shorter times when compared to the implicit integration scheme.

As mentioned in the software's documentation: "*Abaqus/Explicit is a special-purpose analysis product that uses an explicit dynamic finite element formulation. It is suitable for modeling brief, transient dynamic events, such as impact and blast problems, and is also very efficient for highly nonlinear problems involving changing contact conditions, such as forming simulations*" (Simulia, 2015).

5.3.1 Model description and modelling assumptions

As presented in section 4.2, the test specimens were numerically modeled in a 3D environment using the commercial finite element software Abaqus 2016. The FE models used for the simulations of quasi-static tests were subjected to several modifications in order to extend their use for dynamic applications. The main features of the FE model are detailed in Figure 5.7.

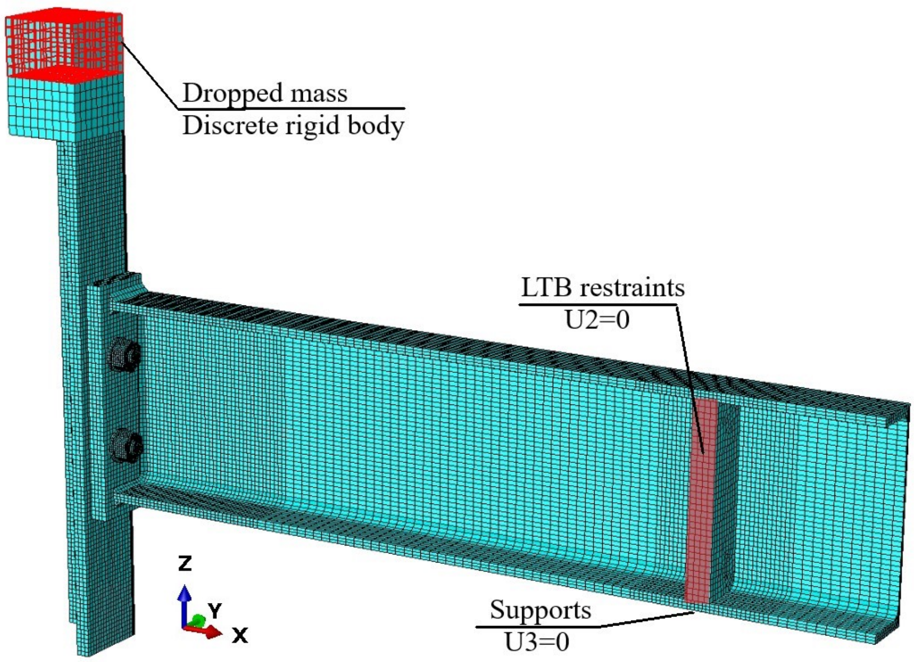

Figure 5.7: FEM detail

As an addition to the models built for the simulations under quasi-static loading conditions, a new part simulating the dropped mass has been modeled as a 3D discrete rigid body. An isotropic inertia with the properties of the dropped mass has been assigned to the discrete rigid body. The choice of modelling the impactor as a discrete rigid element was driven by the fact that the deformations and the stress state of this part are not of much concern to this specific application. A considerable advantage of using a discrete body is related to the computational efficiency. For such a part, only a small computational effort is required for the description of its motion and the evaluation of the concentrated/distributed loads. Moreover, having the inertia properties concentrated in the reference point of the rigid body, its motion is determined only based on the reference point, hence, reducing the overall computational time.

The mesh density used to discretise the models for quasi-static tests has been kept unchanged. The only modification made was the switch from a standard element library to an explicit one, as the impact tests were simulated with an explicit solver. The entire model contained approximately 60 000 elements for the specimens with bolted connections and around 47 000 for the welded ones.

The boundary conditions replicating the actual support conditions were described in section 4.2.3 and were not subjected to any additional modifications. The interaction properties between the different parts of the model have been kept unchanged as well, but an additional one had to be introduced for the contact between the dropped mass and the loading plate. Accordingly, on the contact surface between the two parts was defined a surface to surface contact, with a "Hard contact" definition in the normal direction.

The dropped mass has been initially placed in direct contact with the loading plate, as it can be noticed in Figure 5.7. In order to simulate the impact, the inertia properties of the mass employed in the physical tests were assigned to the 3D discrete rigid body. The corresponding impact speed v_{imp} that has been measured in the experimental tests was set as the initial velocity to the dropped mass in the numerical model.

Aiming at simulating with high accuracy the physical tests, a special attention had to be paid at the eigendynamics of the system. From the impact tests results reported in section 3.5.2 in terms of displacement vs. time curves, it is easily noticeable that after the first impact and the rebound of the mass, the test specimens entered in a free vibration phase. Once entered in this range, the vibration amplitude of the system starts to decrease in time due to the loss of vibration energy. This loss of energy is mainly associated to the internal and external energy dissipation, through friction, viscosity or plasticity. This phenomenon is illustrated in Figure 5.8 for a typical response of the test specimens during the impact tests. For the sake of consistency, the 4^{th} test performed on the RJ specimen has been chosen for this exemplification, as the vibrational characteristics of the system are strongly accentuated for this specific test recording. Even though the time duration of the impact and free vibration phase, respectively, is very short, corresponding to a transient dynamic event, the damping of the free oscillations is still playing an important role when the motion of the specimen is investigated. In Figure 5.8 the damping effects are illustrated by the red dotted line which signifies the signal decay in time.

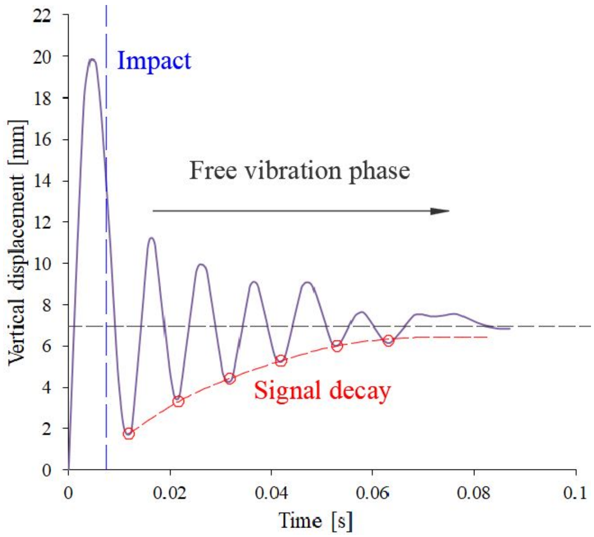

Figure 5.8: Typical vibrations evolution

In structural engineering for dynamic applications, usually, the damping characteristics of a system are denoted by means of damping ratios ξ. Abaqus allows for the consideration of damping through a mass and stiffness proportional damping formulation. Basically, this formulation corresponds to the classical Rayleigh damping model, for which the damping matrix $[C]$ is proportional to the mass and stiffness matrices through the α and β proportionality coefficients as shown in eq. 5.4.

$$[C] = \alpha[M] + \beta[K] \tag{5.4}$$

Once having the proportionality constants α and β, the damping ratio of a certain vibration mode i can be expressed as follows:

$$\xi_i = \frac{1}{2\omega_i}\alpha + \frac{\omega_i}{2}\beta \tag{5.5}$$

where, ω_i is the circular frequency associated to the vibration mode.

The proportionality constants are by definition assessed based on two vibration modes. Consequently, the damping ratio relies on the parameters estimated from two different vibration modes. However, as a simplification of the problematic related to damping phenomena, the analyzed structure comprising of the assembly beams-column can be considered as a generalized single degree of freedom (*1DOF*) system. This assumption allows to characterize the damping of the system through a single proportionality parameter. Therefore, the damping can be defined either as mass proportional, or as stiffness proportional.

In the current case, a mass proportional damping has been incorporated in the FE model. The mass proportionality constant α was introduced at the material level and was estimated form eq. 5.6 as:

$$\alpha = 2\xi_1\omega_1 \tag{5.6}$$

where, ξ_1 is the damping ratio of the first mode of vibration and ω_1 is the natural circular frequency of the specimen.

The natural circular frequency of the system was estimated based on the experimental time-history recordings. As depicted in Figure 5.9, the natural period of vibration T_1 was measured as the time interval between two consecutive vibration peaks. Consequently, the natural circular frequency could be estimated as:

$$\omega_1 = 2\pi T_1 \tag{5.7}$$

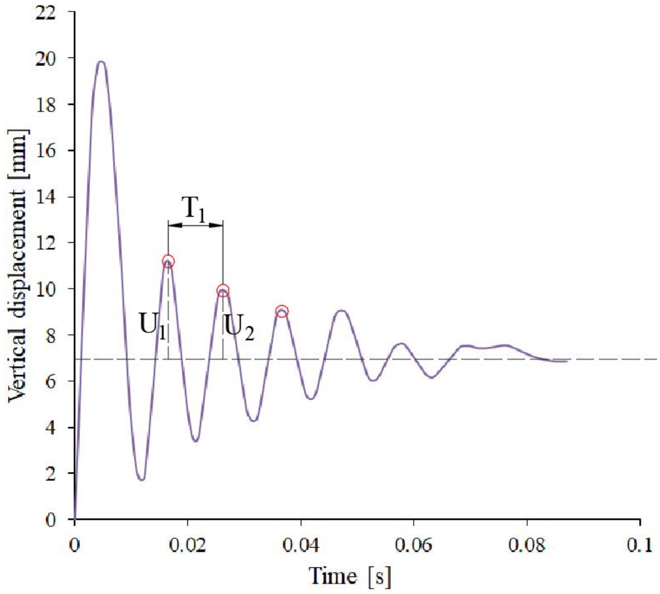

Figure 5.9: Estimation of natural period T_1

The damping ratio was estimated from the time-history recordings based on the logarithmic decrement of the displacement between two consequent amplitude peaks. For low values of damping, one can assume that the natural circular frequency of the undamped system ω_n is very similar to the one of the damped system ω_d and considering that the motion decay follows a decreasing exponential law as:

$$u(t) = \pm A e^{-\xi \omega t} \tag{5.8}$$

it can be assumed that the damping ratio can be expressed as:

$$\xi_1 = \frac{\delta}{2\pi} \tag{5.9}$$

where, δ is the logarithmic decrement estimated from the free vibration phase according to eq. 5.10:

$$\delta = \ln \frac{U_n}{U_{n+1}} \tag{5.10}$$

As an alternative to the procedure descried above, an estimation of the natural circular frequency of the system may be achieved by assuming the specimen as being a simply supported beam with continuous inertia properties. In theory, the natural circular frequency of such a system can be derived from the following expression.

$$\omega_1 = 9.87\sqrt{\frac{EIg}{wL^4}} \tag{5.11}$$

where, E is the elastic modulus of the material, I is the moment of inertia of the beam, w is the self-weight per unit length and g is the gravitational acceleration.

The assumption of having a constant weight distribution on the length of the equivalent simply supported beam requires the distribution of the "concentrated" weight coming from the column. Based on the column cross-sectional dimensions, its total weight is roughly estimated to be around 34 kg/m. The IPE 180 profile has a weight of 18.8 kg/m. The loading plate welded to the column head weights approximately 6.7 kg. Therefore, the total weight distributed on the length of the equivalent beam will be:

$$w_{eq} = 0.188 + \frac{0.34 \cdot 0.46}{1.3} + \frac{0.067}{1.3} = 0.36 \text{ kN/m} \tag{5.12}$$

Accordingly, if to consider the moment of inertia corresponding to an IPE 180 profile, the natural circular frequency yields:

$$\omega_1 = 9.87\sqrt{\frac{2.1 \cdot 10^5 \cdot 1.317 \cdot 10^7 \cdot 9.81 \cdot 10^3}{0.36 \cdot 1300^4}} = 1603.3 \text{ rad/s} \tag{5.13}$$

this value corresponding to a natural frequency $f_1 = 255.1$ Hz and a natural period of vibration $T_1 = 3.9$ ms.

The representative parameters used for the estimation of the mass proportionality constant α for all the test specimens are summarized in Table 5.6.

Specimen	T_1 [ms]	f_1 [Hz]	ω_1 [rad/s]	ξ_1 [%]	α
RJ	9.5	105	659.7	1.9	25.07
EPB	9.8	102	641.1	0.98	12.57
CFB	10.1	99	622	2.4	29.86
BFC*	4.9	200.7	1261	5	126.1
CWC	5	200	1256	4.7	118.06

Table 5.6: Mass proportionality constant estimation

*Note: In order to assess the eigendynamics of the BFC specimen, a modal analysis has been conducted in Abaqus, as the test time-history recordings of this specimen were not accurate for the free vibration phase.

It is noticeable that for the specimens with welded connections (BFC and CWC) the natural circular frequency is similar to the value computed analytically in eq. 5.13, even though the analytical method is a very rough estimation in this case. The bolted specimens (RJ, EPB and CFB) are less stiff when compared to the welded ones, mainly due to the fastening method and the possibility to develop small relative displacements between the members of the system. As a consequence, a higher natural period of vibration is exhibited by the specimens. It is worthy to mention that the estimated values for the damping ratios ξ_1 are not exceeding the threshold value of 5%, which is frequently used in structural engineering for seismic design applications.

5.3.2 Material modelling at high strain rates

As previously mentioned, the loading rate may have significant effects on the material post-elastic behaviour. The strain rate sensitivity may vary from material to material function of the latter's crystallographic structure, chemical composition or even thermal conditions. Although, the steel is a well-known strain rate sensitive material and during the 20$^{\text{th}}$ century numerous studies were conducted around the definition of its rate sensitivity law. However, in structural engineering, the use of such formulations is rather limited do to their complexity.

Reference is made once again to the DIF, when a simplified way to account for the strain rate effects is sought. The high strain rate enhancement in the material strength is, thus, defined as the ratio between its dynamic strength, σ_{dyn} to the strength obtained under static conditions, σ_{stat}:

$$DIF = \frac{\sigma_{dyn}}{\sigma_{stat}} \tag{5.14}$$

When FE solutions are employed in the investigation of structural elements subjected to transient dynamic events, the accurate definition of the material behaviour becomes a crucial concern. Various empirical models can be used to represent the material behaviour for a wide range of strain rates. Among the most used constitutive models for metallic materials which account for the strain rate sensitivity are the Johnson-Cook model (Johnson and Cook, 1983) and Cowper-Symonds formulation (Cowper and Symonds, 1957). The latter is a widely used rate-dependent formulation expressed as a power law as follows:

$$\sigma_{dyn} = \sigma_{stat}\left[1 + \left(\frac{\dot{\varepsilon}_p}{D}\right)^{\frac{1}{q}}\right] \tag{5.15}$$

where, $\dot{\varepsilon}_p$ is the plastic strain rate, D is the viscosity parameter and q is the strain rate hardening parameter.

From eq. 5.14, the expression for the Cowper-Symonds material law can be simply rewritten as:

$$\sigma_{dyn} = \sigma_{stat} DIF \tag{5.16}$$

$$\text{where,} \qquad DIF = 1 + \left(\frac{\dot{\varepsilon}_p}{D}\right)^{\frac{1}{q}} \tag{5.17}$$

Abaqus allows for the implementation of Cowper-Symonds constitutive law by defining a power law as eq. 5.17. Therefore, its application requires the knowledge of specific material parameters, which, unfortunately, can be estimated only on the basis of experimental data. Due to the fact that dynamic tests on the coupons extracted from the test specimens were not conducted, the material parameters were taken from available literature sources.

D'Antimo et al. (2019) calibrated the material parameters D and q for steel with similar material properties. Through a nonlinear least-squares method, the parameters were calibrated for a series of 18 tensile tests on S355 steel coupons. The deformation rate applied in the tensile coupon tests ranged between $\dot{\varepsilon} = 0.001$ 1/s (considered as the static reference strain rate) and $\dot{\varepsilon} = 5$ 1/s. Through the calibration against test results, the values $q = 6.17$ and $D = 8480$ 1/s were set for the Cowper-Symonds formulation. A general good agreement between the experimental and numerical results was reported, confirming the applicability of these parameters in FE simulations.

5.3.3 FE results and discussion

The investigation of the dynamic response of steel joints has been carried out on three FE models, one for a bolted connection (RJ) and two for welded connections (CWC and BFC) respectively. The results obtained through the FE simulations were compared to the ones of physical impact tests in terms of displacement - time curves. A general trend of overestimating the actual periods of vibrations is observed. However, for the welded connections it seems that the numerical simulations predicted with a good accuracy the values for maximum and residual permanent displacements.

The comparison between the real specimen response and the one assessed from the FE simulations is depicted in Figures 5.10 and 5.11 for the specimens with welded connections. The simulations conducted on the impact tests for the BFC specimen provided generally accurate values for the maximum and permanent displacements, the overall behaviour being similar to the experimental one. Some differences are observed in terms of periods of vibration, which are slightly overestimated in the simulations for both types of tests: elastic and inelastic impacts.

The simulations on the CWC specimen were able to capture with a very good accuracy the response of the joint during and after the impact. As presented in Figure 5.11, a good agreement is met for the characteristic displacements of the joint and for the periods of vibration as well. The assumptions made on the damping characteristics of the system are confirmed by the agreement between the signal decay for the free vibration phase for all the tests simulated. Further investigations conducted on the levels of impact forces could deliver more comparison criteria for the validation of the model. However, as a preliminary conclusion, the numerical model proved to be an accurate tool for the estimation of the overall behaviour of the specimen tested under impact for its elastic and inelastic response.

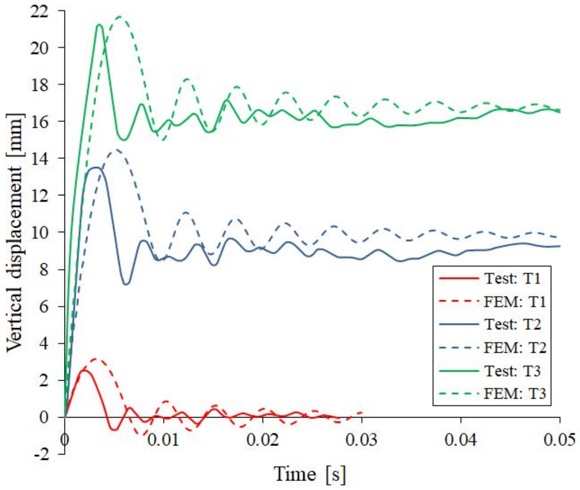

Figure 5.10: BFC specimen - Tests vs. FEM

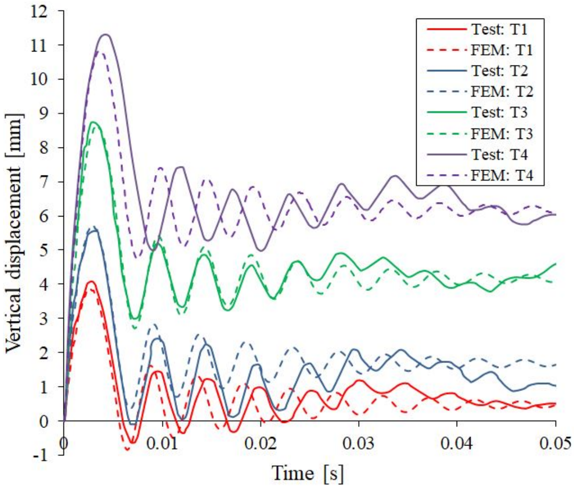

Figure 5.11: CWC specimen - Tests vs. FEM

Unlike the welded specimens, for the bolted joints the accurate simulation of the real behaviour proved to be much more complex. The FE model developed for the RJ specimen provides very different results when compared to the experimental ones. The discrepancies between the periods of vibration are very conspicuous in this particular case. The author has tried multiple modelling approaches in order to bring the results in line with the expectations. However, it seems that although the model provided very accurate results for quasi-static simulations, the extension of its applicability to dynamic loading scenarios requires further investigations. In Figures 5.12a and 5.12b the comparison in terms of displacement-time curves is displayed. It is easily noticeable that the results delivered by the numerical simulations are not much reliable for both terms of comparison: displacements and periods of vibration.

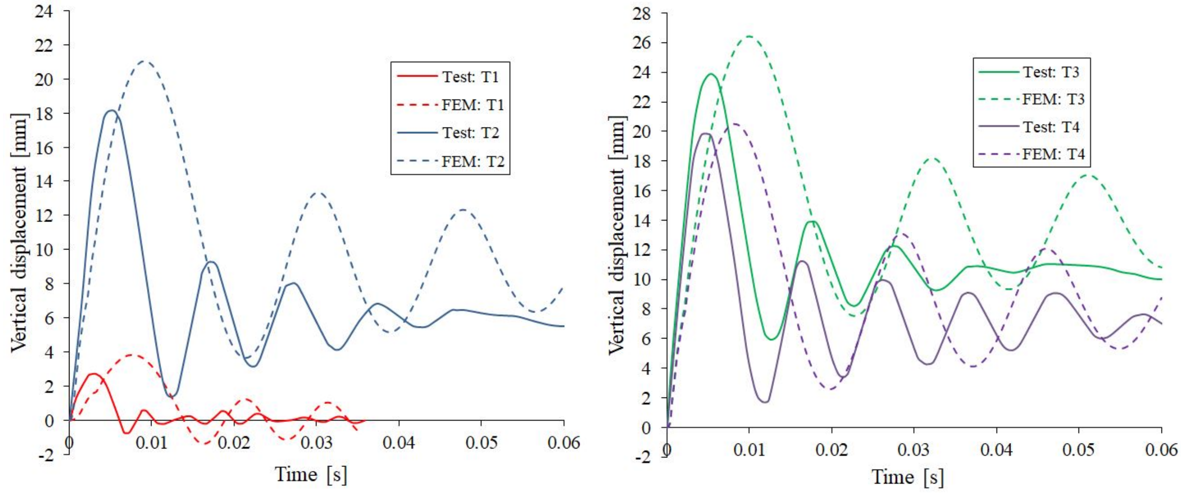

(a) Tests T1&T2

(b) Tests T3&T4

Figure 5.12: RJ specimen - Tests vs. FEM

For the sake of completeness, the results obtained using the FE solutions have been confronted to the ones assessed from the experimental data in terms of impact forces. The impact force estimated on the basis of experimental recordings are presented in detail in section 5.2 where a graphic approach was employed. A comparison between the forces graphically estimated and the ones assessed through FE simulations is presented hereinafter.

The impact forces numerically assessed were extracted from the FEM results as the reaction forces at the level of the supports. Due to the dynamic nature of the loading conditions and the vibrations of the system, the evolution in time of the reaction forces is a signal with a high noise content. In order to mitigate the noise effects, the signal was filtered through a zero-phase digital filtering procedure. The so filtered signal served as a reference for the estimation of the maximum impact force arisen during the impact F_{max}. The procedure used to asses the maximum impact force from the FE results is graphically illustrated in Figures 5.13a - 5.13c for the impact tests conducted on the BFC specimen.

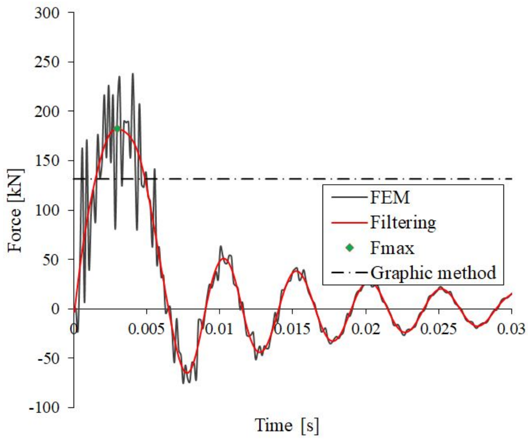

(a) Test T1

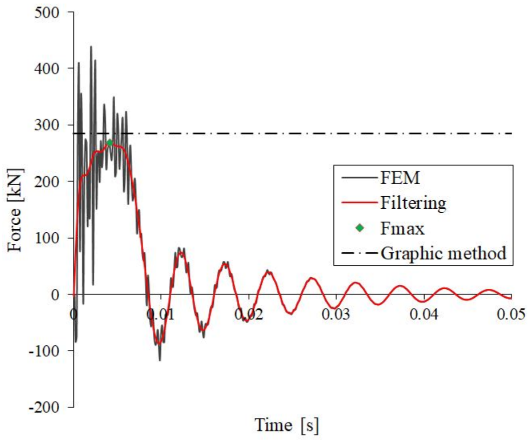

(b) Test T2

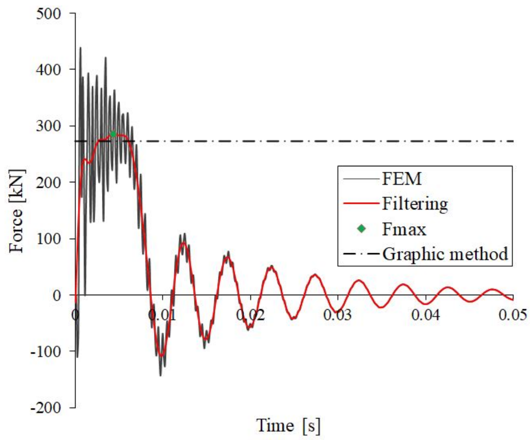

(c) Test T3

Figure 5.13: BFC - FE impact force estimation

For the inelastic impacts, i.e. tests T2 and T3, the forces estimated through the graphic method are very close to the ones predicted by the numerical simulations, even though slightly overestimated. On the contrary, for tests conducted in the elastic range the graphic method seems to underestimate the maximum impact force. The comparison between FE simulations and the graphical method is provided in Table 5.7. It is noticeably that when comparing the DIFs estimated using the two approaches, the values are similar for the inelastic impacts. Surprisingly, the FE simulation tends to overestimate significantly the maximum force for the elastic impact, leading thus to an unjustified value for the DIF.

Test	$\Delta_{max,exp}$ [mm]	$\Delta_{perm,exp}$ [mm]	F_{stat} [kN]	$F_{dyn,GR}$ [kN]	$F_{dyn,FEM}$ [kN]	DIF_{GR} [-]	DIF_{FEM} [-]
T1	2.52	0	131.5	131.5	182.3	-	1.38
T2	13.46	8	266	285	268.9	1.07	1.01
T3	21.1	15.86	281.5	273	286.1	0.97	1.01

Table 5.7: BFC - Impact force and DIF estimation

Similarly, the maximum impact force was estimated for the CWC specimen and reported in Figures 5.14a - 5.14d. A good agreement between the graphical method and the FEM solutions is achieved in this specific case for all the range of performed tests.

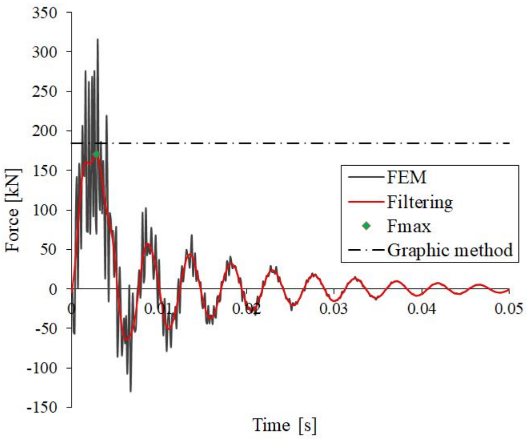

(a) Test T1

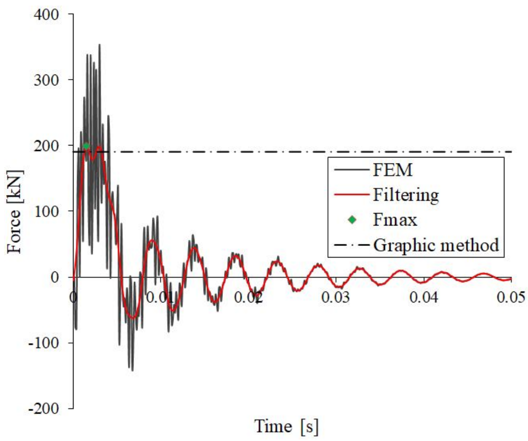

(b) Test T2

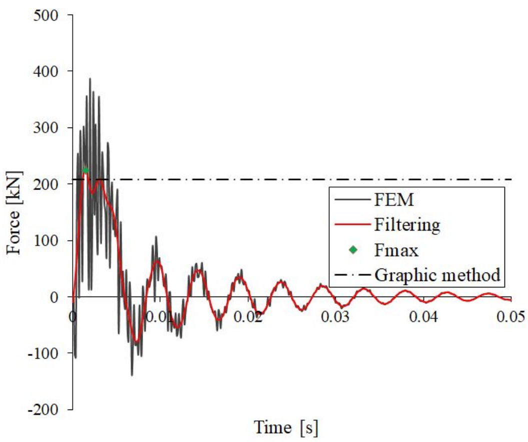

(c) Test T3

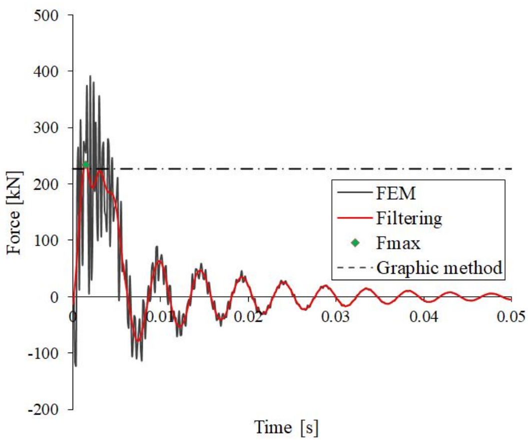

(d) Test T4

Figure 5.14: CWC - FE impact force estimation

A brief survey of the results collected from the two computational approaches is reported in Table 5.8. The FE model proved to be the most reliable in the prediction of the *cwc* component behaviour when subjected to impulsive loading. Generally, the difference between the maximum impact forces predicted using the two method did not exceed 8%.

Test	$\Delta_{max,exp}$ [mm]	$\Delta_{perm,exp}$ [mm]	F_{stat} [kN]	$F_{dyn,GR}$ [kN]	$F_{dyn,FEM}$ [kN]	DIF_{GR} [-]	DIF_{FEM} [-]
T1	4.19	0	133.5	184.4	170.3	1.38	1.28
T2	5.63	1.3	155.2	190.5	199.8	1.23	1.28
T3	8.93	4.2	142.8	208.1	224.5	1.46	1.57
T4	11.66	6.5	137.5	227	234.3	1.65	1.70

Table 5.8: CWC - Impact force and DIF estimation

Although the FE model of the bolted connection proved to be not accurate for transient dynamic events, for the sake of completeness, the procedure described above was performed for the RJ specimen as well and the estimation of maximum impact forces is depicted in Figures 5.15a - 5.15d.

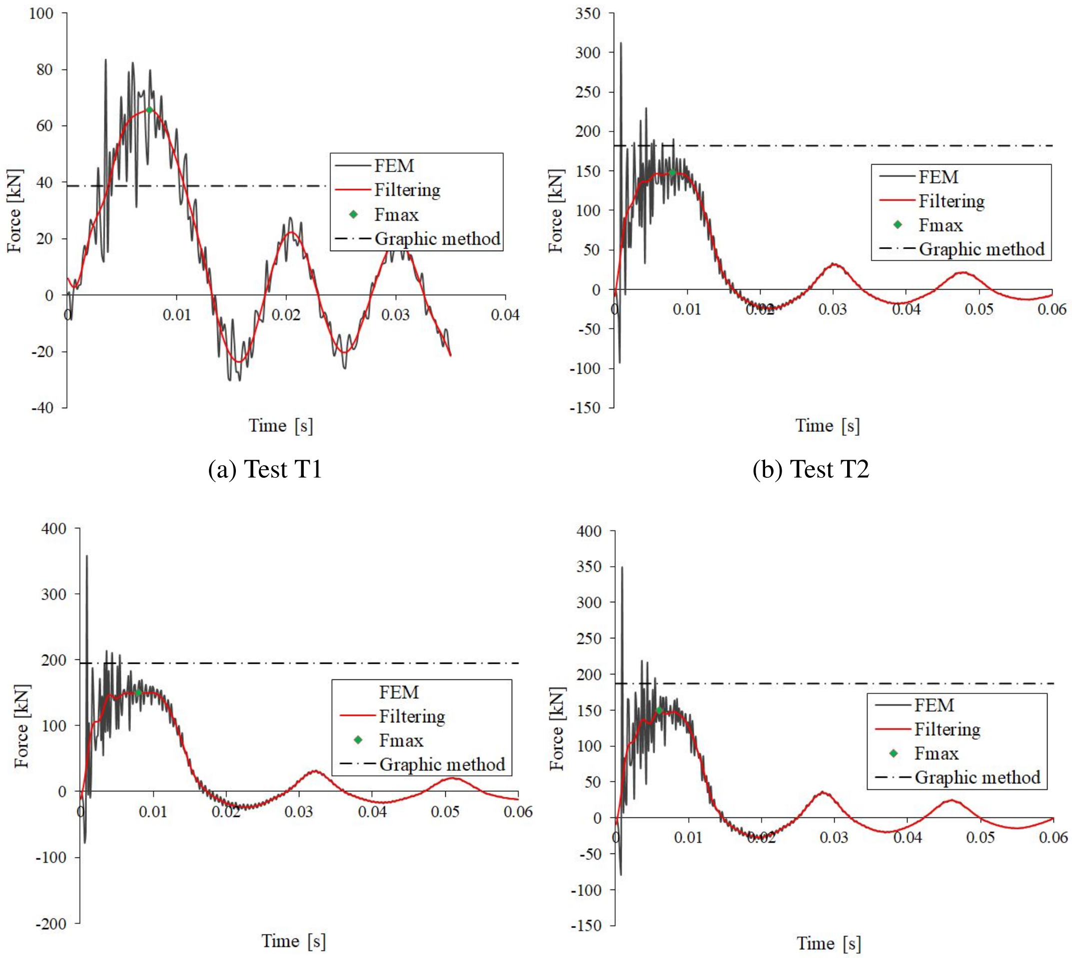

(a) Test T1

(b) Test T2

(c) Test T3

(d) Test T4

Figure 5.15: RJ - FE impact force estimation

Once again, considering the undeniable differences between the two methods, the reliability of the FE model becomes disputable. In Table 5.9 a summary of the outcome concerning the RJ specimen is provided. Despite the fact that the simulations under quasi-static loading were able to predict accurately the overall behaviour of the joint and even the failure mode, in the case of dynamic simulations the results are deviating significantly from what would be expected.

Test	$\Delta_{max,exp}$ [mm]	$\Delta_{perm,exp}$ [mm]	F_{stat} [kN]	$F_{dyn,GR}$ [kN]	$F_{dyn,FEM}$ [kN]	DIF_{GR} [-]	DIF_{FEM} [-]
T1	2.73	0.1	38.7	38.7	65.6	-	1.69
T2	18.89	6.5	139	182.1	148.6	1.31	1.07
T3	23.94	10.64	146	195.5	150.6	1.34	1.03
T4	19.82	7.1	141	187	150	1.33	1.06

Table 5.9: RJ - Impact force and DIF estimation

As a concluding remark, the FE models proved to be a reliable tool when the behaviour of welded steel joints under quasi-static and dynamic loading is investigated. The graphic method used for the estimation of the impact force on the basis of experimental data can be used as an efficient alternative method, as the results reported in this paper and additionally in open scientific literature sources (D'Antimo et al., 2019; D'Antimo, 2020) are, in most of the cases, close to reality. In the case of bolted connections, the extension of applicability of the FE models from quasi-static to impact loading conditions requires further investigations on the eigendynamics and the inertia properties of the system, as the period of vibration is dependent on the system's mass and stiffness.

6 | Conclusions and recommendations

The main objective of this study was to investigate the response of steel joints subjected to dynamic impact loading. The loading rate can influence significantly the behaviour of a joint, as the steel's mechanical properties are highly sensitive to the load application speed. This thesis aims at highlighting the strain rate effects on the performance of specific joint components. Three different approaches were employed for the achievement of these objectives: experimental, analytical and numerical.

The results gathered from experimental campaigns conducted in the framework of the research project RobustImpact served as the reference database in this study. Consequently, the data available for five beam-to-column joint configurations was used to investigate the behaviour of such connections under quasi-static and impact loading conditions. To characterise the response of steel joints subjected to various types of loads, analytical methods have been explored, with a view to validating their applicability. Finite element models incorporating material constitutive laws which account for the rate sensitivity were developed and validated against experimental data.

As a result of this deep investigation on the performance of steel joints subjected to various loading conditions, the following conclusions were drawn:

1. The Component Method can be regarded as a reliable analytical method for the assessment of steel joints behavior under quasi-static loading conditions. Generally, when used in conjunction with the approach proposed by Japsart et al. (2019), it is able to estimate accurately the full non-linear response of a joint. The analytical formulae proved to be somehow inaccurate when the equivalent T-stub model is applied to components with thin plates, underestimating considerably the ultimate bending capacity of the joint. Further investigation is required for the enhancement of the T-stub model applicability for components with thin plates.

2. The FE models are able to replicate accurately the overall behaviour of steel joints under quasi-static loading. A good agreement between the tests results and the numerical predictions was achieved for all of the test specimens, the FE solutions allowing for the assessment of the joint performance with high accuracy and relatively low computational cost. Even complex buckling phenomena can be simulated with reasonable accuracy if the initial imperfections are thoroughly considered.

3. In most of the cases, the effects related to the load's dynamic nature affect substantially the overall behaviour of a joint. The strain rate effects are most likely to develop in the joint components which exhibit high plasticity levels when subjected to dynamic transient

events. A very low to imperceptible strain rate sensitivity is observed for very stiff basic components, such as the beam flange in compression.

4. The graphic approach used for the estimation of maximum forces associated to the impact seems to provide reasonable results and can be used as a reliable alternative to the impulse-momentum theorem, when the initial stiffness of the joint and its full static behaviour are known.

5. Dynamic Increase Factors can be successfully used to quantify the effects related to high loading rates in engineering applications. The practical advantage is the simplicity behind the concept, as the *DIF* can be basically considered as an "overstrength" coefficient.

6. The use of FE solutions in the study of steel members subjected to transient dynamic events implies an accurate description of the material behaviour under such loading conditions. The constitutive laws should incorporate the rate sensitivity of the material and the material constants have to be properly calibrated against tests results on material with the same (or similar) characteristics.

7. When properly calibrated, the Cowper-Symonds material model allows for the assessment of strain rate effects on the overall behaviour of steel joints. Therefore, it can be widely used in dynamic FE simulations as a reliable material model.

8. The applicability of FE models for the study of bolted connections subjected to high loading rates requires further investigation on the eigendynamics and inertia properties of simulated assemblies. A general trend of overestimating the period of vibration for bolted specimens was observed during this study, further improvements of the modelling procedure are required to enhance the prediction accuracy.

Bibliography

Arup. Review of international research on structural robustness and disproportionate collapse. *Deparment for Communities and Local Government*, 2011.

G. R. Cowper and P. S. Symonds. Strain hardening and strain-rate effects in the impact loading of cantilever beams. *Tech. rep., Brown University Division of Applied Mathematics*, 1957.

M. D'Antimo. *Impact characterization of innovative seismically designed connections for robustness application*. PhD thesis, 2020.

M. D'Antimo, M. Latour, G. Rizzanob, and J.F. Demonceaua. Experimental and numerical assessment of steel beams under impact loadings. *J. Constr. Steel Res.*, 158(4):230–247, 2019.

Department of Defence DOD. *Structures to resist the effects of accidental explosions: Unified Facilities Criteria (UFC 3-340-02)*. 2008.

Brussels: European Committee for Standardization EC1. *Eurocode 1: Actions on structures. Part 1-7, General actions - 495 Accidental actions*. 2006.

Brussels: European Committee for Standardization EC3. *Eurocode 3: Design of steel structures Part 1-8: Design of joints*. 2005.

Brussels: European Committee for Standardization EC8. *Design of structures for earthquake resistance - Part 1 : General rules, seismic actions and rules for buildings* . 2004.

E. L. Grimsmo, A. H. Clausen, A. Aalberg, and M. Langseth. Beam-to-column joints subjected to impact loading. *Nord. steel Constr. Conf.*, 2015.

E. L. Grimsmo, A. H. Clausen, A. Aalberg, and M. Langseth. A numerical study of beam-to-column joints subjected to impact. *Eng. Struct.*, 120:103–115, 2016.

Nadine Hoffmann, Ulrike Kuhlmann, Clara Huvelle, Jean-François Demonceau, Jean-Pierre Jaspart, Nadia Baldassino, Fabio Freddi, Riccardo Zandonini, Benno Hoffmeister, Jonas Korndörfer, and Carles Colomer Segura. *Deliverable D.4.1: Design report of the specimens for all the experimental analyses*. 2014.

Nadine Hoffmann, Ulrike Kuhlmann, Hélène Vanvinckenroye, Lihong Zhang, Jean-François Demonceau, Jean-Pierre Jaspart, Nadia Baldassino, Alessandro Banterla, Stefano Girardi, Marco Graziadei, Giacomo Roverso, Riccardo Zandonini, Benno Hoffmeister Jonas Korndörfer, and Carles Colomer Segura. *Deliverable D.5a: Detailed results of the experimental tests* . 2016.

J.-P. Japsart, A. Corman, and J.-F. Demonceau. *Ductility assessment of structural steel and composite joints*. 2019.

J.-P. Jaspart. *Etude de la semi-rigidité des noeuds poutre-colonne et son influence sur la resistance des ossatures en acier*. PhD thesis, 1991.

J.-P. Jaspart and K. Weynand. *Design of Joints in Steel and Composite Structures: Eurocode 3: Design of Steel Structures Part 1-8: Design of Joints / Eurocode 4: Design of Composite Steel and Concrete Structures*. 2016.

G.R. Johnson and W.H. Cook. A constitutive model and data for metals subjected to large strains, high strain rates and high temperatures. *Proceedings of the 7th International Symposium on Ballistics, The Hague, The Netherlands*, pages 541–547, 1983.

T. McAllister. *World Trade Center building performance study: data collection, 489 preliminary observations and recommendations*. 2002.

T. Sabuwala, D. Linzell, and T. Krauthammer. Finite element analysis of steel beam to column connections subjected to blast loads. *Int J Impact Eng*, 31:861–876, 2005.

A. Santiago, L. Simões da Silva, and P. Vila Real. Experimental investigation of the behaviour of a steel sub-frame under a natural fire. *International Journal of Steel and Composite Structures*, pages 243–264, 2008.

Simulia. *Getting Started with Abaqus: Interactive Edition*. 2015.

J.D. Swanson and R Leon. *Advanced finite element modeling of bolted T-stub connection components*. 2002.

G. Xu and B.R. Ellingwood. Disproportionate collapse performance of partially restrained steel frames with bolted T-stub connections. *International Journal of Steel and Composite Structures, Engineering Structures*, 33:32–43, 2011.

H. C. Yim and T. Krauthammer. Load impulse characterization for steel connection. *International Journal of Impact Engineering*, 36:737–745, 2009.

P. Zoetemeijer. *A design method for the tension side of statically-loaded, bolted beam-to-column joints*. 1974.

Appendices

Appendix A - Actual geometrical properties

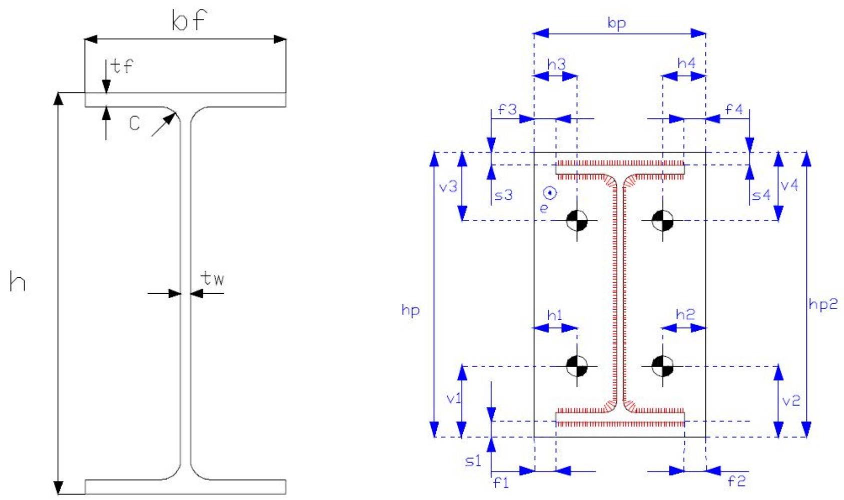

Figure A1: Measured geometrical parameters (Hoffmann et al., 2016)

[mm]	Values	b_f	h	C	t_f	t_w
IPE180	Actual	95,18	179,76	9,50	7,81	5,29
	Nominal	91	180	9	8	5,3
HEB140	Actual	140,91	137,99	12,25	12,02	6,27
	Nominal	140	140	12	12	7

Figure A2: Main actual geometrical properties of the profiles (Hoffmann et al., 2016)

mm	Values	hp	bp	e	v1	v2	v3	v4	s1	s2	s3	s4	h1	h2	h3	h4	f1	f2	f3	f4
RJ	Actual	208,72	119,09	15,08	64,33	63,97	63,55	63,10	15,60	13,50	14,60	14,70	22,41	20,64	22,56	20,99	12,10	12,60	14,20	12,40
	Nominal	210,00	120,00	15,00	64,00	64,00	64,00	64,00	15,00	15,00	15,00	15,00	22,00	22,00	22,00	22,00	14,50	14,50	14,50	14,50
EPB	Actual	204,40	119,68	8,13	63,85	64,27	64,30	63,45	13,50	15,20	15,00	14,70	22,31	21,87	22,30	22,56	18,90	13,40	13,10	13,50
	Nominal	210,00	120,00	8,00	64,00	64,00	64,00	64,00	15,00	15,00	15,00	15,00	22,00	22,00	22,00	22,00	14,50	14,50	14,50	14,50
CFB	Actual	219,65	120,07	17,95	68,13	68,30	67,53	68,55	21,05	20,00	11,10	11,10	21,42	21,12	21,53	20,87	11,30	12,80	14,05	14,40
	Nominal	220,00	120,00	18,00	69,00	69,00	69,00	69,00	20,00	20,00	14,00	14,00	22,00	22,00	22,00	22,00	14,50	14,50	14,50	14,50

Figure A3: Main actual geometrical properties of the end-plates (Hoffmann et al., 2016)

Appendix B - Component method - RJ specimen

Determination of the component properties

a) Component 1 - Column web in compression

The resistance of the unstiffened column web subjected to transverse compression is determined from the following expression:

$$F_{c,wc,Rd} = \frac{\omega k_{wc}\, b_{eff,c,wc}\, t_{wc}\, f_{y,wc}}{\gamma_{M0}} \quad \text{but} \quad F_{c,wc,Rd} \leq \frac{\omega k_{wc}\, \rho\, b_{eff,c,wc}\, t_{wc}\, f_{y,wc}}{\gamma_{M1}} \tag{6.1}$$

Because the transformation parameter for a double-sided symmetrically loaded joint is $\beta = 0$, the reduction factor ω in equation 4.1 can be takes as $\omega = 1$. In most of the cases, the maximum longitudinal compressive stress $\sigma_{com,Ed}$ due to axial force and bending moment in the column web is $\sigma_{com,Ed} \leq 0.7 f_{y,wc}$ and the reduction factor k_{wc} can be taken as to 1.0. The resistance in compression of the column web is limited by local buckling through a reduction factor (ρ) which accounts for potential buckling occurrence. This factor is evaluated based on the slenderness of the column web ($\bar{\lambda}_p$) as follows:

$$\rho = \begin{cases} 1.0 & \text{if} \quad \bar{\lambda}_p \leq 0.72 \\ (\bar{\lambda}_p - 0.2)/\bar{\lambda}_p^2 & \text{if} \quad \bar{\lambda}_p > 0.72 \end{cases} \tag{6.2}$$

The slenderness of the web is estimated as:

$$\bar{\lambda}_p = 0.932\sqrt{\frac{b_{eff,c,wc}\, d_{wc}\, f_{y,wc}}{E t_{wc}^2}} \tag{6.3}$$

where:

$$d_{wc} = h_c - 2(t_{fc} + s) = 138 - 2(12 + 12.25) = 89.5 \text{ mm} \tag{6.4}$$

The resistance to compression of the column web depends on the dispersion length ($b_{eff,c,wc}$) of the compression force through the end-plate and column flange. The area of the web providing resistance to compression is given by the effective width ($b_{eff,c,wc}$) illustrated in Figure B1.

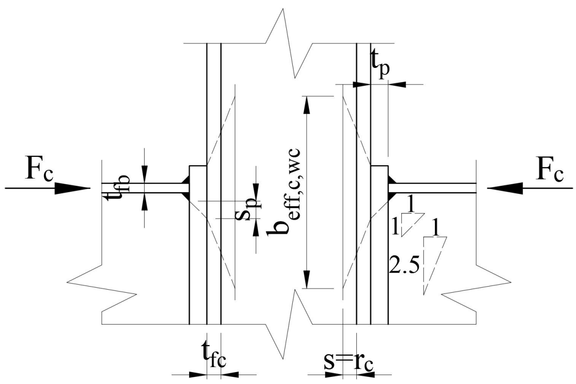

Figure B1: Force dispersion for column web in compression

According to Figure 4.1, the effective width of the column web in compression is yields:

$$\begin{aligned} b_{eff,c,wc} &= t_{fb} + 2\sqrt{2}a_p + 5(t_{fc} + s) + s_p \\ &= 7.8 + 2\sqrt{2}\cdot 5 + 5(12 + 12.25) + 15.08 + \frac{208.7 - 179.8}{2} - \sqrt{2}\cdot 5 \\ &= 165.7 \text{ mm} \end{aligned} \tag{6.5}$$

where, s_p is the length obtained by dispersion at 45° through the end-plate. In this particular case, because the length of the end-plate bellow the flange is less than $2t_p$, s_p was considered as one end-plate thickness - t_p=15.08 mm.

$$\Rightarrow \bar{\lambda}_p = 0.932\sqrt{\frac{165.7\cdot 89.5\cdot 433.7}{210000\cdot 7^2}} = 0.822$$

And the reduction factor ρ yields:

$$\rho = \frac{(\bar{\lambda}_p - 0.2)}{\lambda_p^2} = \frac{0.822 - 0.2}{0.822^2} = 0.92 \tag{6.6}$$

As $\rho < 1$, the plastic resistance in compression will be limited by the local buckling of the column web.

$$F_{Rpl,cwc} = \frac{1.0\cdot 0.92\cdot 165.7\cdot 6.27\cdot 433.7}{1.0\cdot 1000} = 414.5 \text{ kN} \tag{6.7}$$

*Note:

If to consider the reduction factor ρ as recommended in EC3, the *cwc* will govern the failure of the joint. However, as discussed in the body of this thesis, the initial imperfection considered in Eurocode 3 are overestimated, leading to very conservative results for the resistance of this component. Since in the physical test the *cwc* component did not exhibit any evidence of buckling occurrence, it is reasonable to assume that the reduction coefficient $\rho = 1$.

Therefore, the plastic and the ultimate resistances for this component may be estimated as follows:

$$F_{Rpl,cwc} = \frac{1.0\cdot 1.0\cdot 165.7\cdot 6.27\cdot 433.7}{1.0\cdot 1000} = 450.4 \text{ kN} \tag{6.8}$$

$$F_{Ru,cwc} = \frac{1.0\cdot 1.0\cdot 165.7\cdot 6.27\cdot 544}{1.0\cdot 1000} = 565 \text{ kN} \tag{6.9}$$

b) Component 2 - Column web in tension

The resistance of an unstiffened column web subjected to transverse tension is determined according to eq. 6.10.

$$F_{t,wc,Rd} = \frac{\omega\, b_{eff,t,wc}\, t_{wc}\, f_{y,wc}}{\gamma_{M0}} \tag{6.10}$$

Once again, the reduction factor ω which accounts for the interaction with shear in the column web panel will be taken as 1.0. For bolted connections, the effective width $b_{eff,t,wc}$ of column web in tension is evaluated based on the equivalent T-stub for the column flange. The effective length l_{eff} of the equivalent T-stub is estimated for each bolt rows acting individually or in a combination with the other bolt row. Having two bolt rows on the elevation of the connection implies the computation of l_{eff} for the following cases:

- Individual bolt rows 1 and 2

- Group involving bolt rows 1 and 2

The use of the equivalent T-stub model requires the estimation of several geometrical parameters that allow to evaluate its equivalent length. Relying on Figure B2 the geometrical parameters are estimated as follows:

$$\begin{aligned} m &= \frac{p_2}{2} - \frac{t_{wc}}{2} - 0.8r_c = \frac{76}{2} - \frac{6.27}{2} - 0.8 \cdot 12.25 = 25.1 \text{ mm} \\ e &= \frac{b_c}{2} - \frac{p_2}{2} = \frac{140.9}{2} - \frac{76}{2} = 32.45 \text{ mm} \\ e_{min} &= \min(e;\ e_2) = \min(32.45;\ 22) = 22 \text{ mm} \end{aligned} \tag{6.11}$$

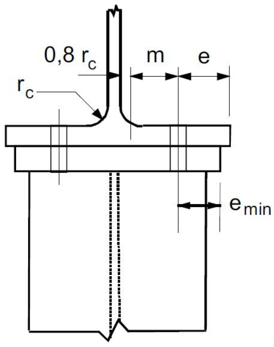

Figure B2: Geometrical parameters for the equivalent T-stub EC3 (2005)

Bolt row 1

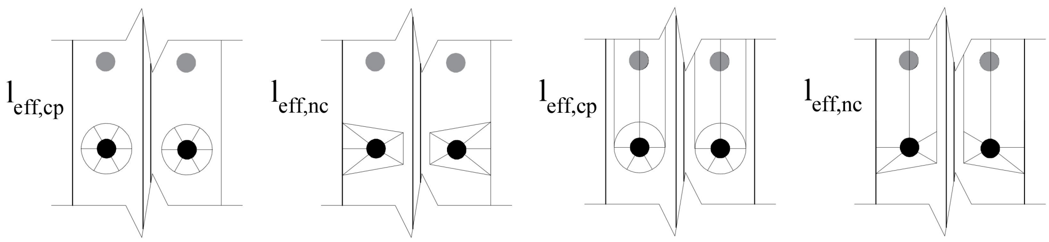

(a) Individual (b) As first row of a group

Figure B3: Effective lengths for bolt row 1

- Individual effective lengths

$$\begin{aligned} l_{eff,cp} &= 2\pi m = 2\pi \cdot 25.1 = 157.5 \text{ mm} \\ l_{eff,nc} &= 4m + 1.25e = 4 \cdot 25.1 + 1.25 \cdot 22 = 140.82 \text{ mm} \end{aligned} \tag{6.12}$$

-Effective lengths as first bolt row of a group

In this case, for bolt row 1 combined with row 2, both bolt rows are considered as "end bolt rows" and the effective lengths for the unstiffened column flange should be taken as the minimum value as follows:

$$l_{eff,cp} = \min(\pi m + p;\ 2e_1 + p) \tag{6.13}$$

$$l_{eff,nc} = \min(2m + 0.625e + 0.5p;\ e_1 + 0.5p) \tag{6.14}$$

However, e_1 is large in the case of the column flange, thus the second term which includes e_1 will not be critical, the final values for the effective lengths being:

$$\begin{aligned} l_{eff,cp} &= \pi m + p = \pi \cdot 25.1 + 82 = 160.74 \text{ mm} \\ l_{eff,nc} &= 2m + 0.625e + 0.5p = 2 \cdot 25.1 + 0.625 \cdot 32.45 + 0.5 \cdot 82 = 111.41 \text{ mm} \end{aligned} \tag{6.15}$$

Bolt row 2

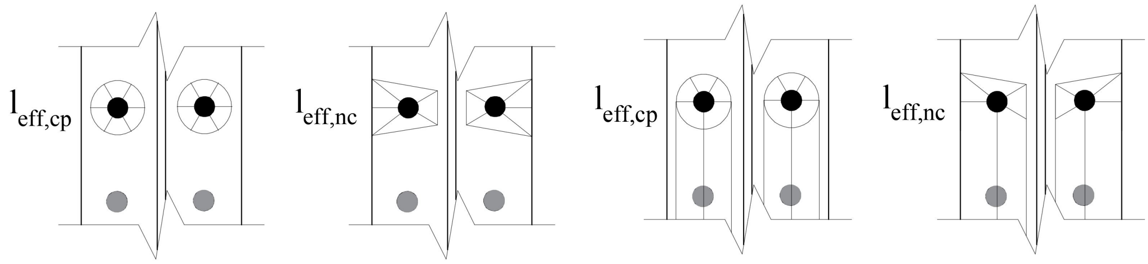

(a) Individual (b) As first row of a group

Figure B4: Effective lengths for bolt row 2

- Individual effective lengths

$$\begin{aligned} l_{eff,cp} &= 2\pi m = 2\pi \cdot 25.1 = 160.74 \text{ mm} \\ l_{eff,nc} &= 4m + 1.25e = 4 \cdot 25.1 + 1.25 \cdot 22 = 140.82 \text{ mm} \end{aligned} \tag{6.16}$$

- Effective lengths as last bolt row of a group

$$\begin{aligned} l_{eff,cp} &= \pi m + p = \pi \cdot 25.1 + 82 = 160.74 \text{ mm} \\ l_{eff,nc} &= 2m + 0.625e + 0.5p = 2 \cdot 25.1 + 0.625 \cdot 32 + 0.5 \cdot 82 = 111.41 \text{ mm} \end{aligned} \tag{6.17}$$

The resistance of each individual row is computed taking the effective width $b_{eff,t,wc}$ as the minimum value between $l_{eff,cp}$ and $l_{eff,nc}$, thus $b_{eff,t,wc} = 140.82$ mm.

The plastic resistance for bolt row 1 and 2 are identical:

$$F^{I}_{Rpl,cwt} = \frac{1.0 \cdot 140.82 \cdot 6.27 \cdot 433.7}{1.0 \cdot 1000} = 382.89 \text{ kN} \tag{6.18}$$

The effective length for the group composed of bolt rows 1 and 2 is:

$$b_{eff,t,wc} = 111.41 + 111.41 = 222.82 \text{ mm}$$

and the corresponding group plastic resistance yields:

$$F^{Gr}_{Rpl,cwt} = \frac{1.0 \cdot 222.82 \cdot 6.27 \cdot 433.7}{1.0 \cdot 1000} = 605.85 \text{ kN} \tag{6.19}$$

The ultimate resistance for bolt row 1 and 2 is:

$$F^{I}_{Ru,cwt} = \frac{1.0 \cdot 140.82 \cdot 6.27 \cdot 544}{1.0 \cdot 1000} = 480.3 \text{ kN} \tag{6.20}$$

and the corresponding group ultimate resistance yields:

$$F^{Gr}_{Ru,cwt} = \frac{1.0 \cdot 222.82 \cdot 6.27 \cdot 544}{1.0 \cdot 1000} = 760 \text{ kN} \tag{6.21}$$

c) Component 3 - Column flange in bending

The resistance and the failure mode of an unstiffened column flange in bending are evaluated using the equivalent T-stub model for both - individual and group bolt rows. Associated resistances are calculated for three possible failure modes and the overall resistance is taken as the minimum of the three. In the figure below, the possible failure modes of the equivalent T-stub are illustrated. Failure mode 1 corresponds to the complete yielding of the column flange. Failure mode 2 is associated to a combined failure of the bolts and yielding in the flange whereas the 3rd mode is totally associated to the bolt fracture.

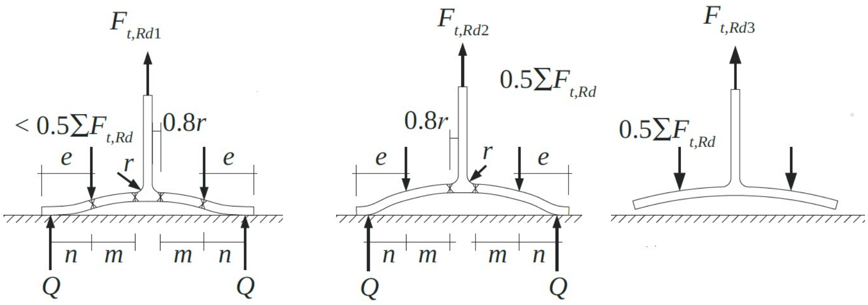

(a) Failure mode 1 (b) Failure mode 2 (c) Failure mode 3

Figure B5: Equivalent T-stub failure modes Jaspart and Weynand (2016)

EN 1993-1-8 provides the analytical formulae for the evaluation of the resistance for each of the three failure modes as follows:

- for Mode 1 (alternative method)

$$F_{t,1,Rd} = \frac{(8n - 2e_w)M_{pl,1,Rd}}{2nm - e_w(m+n)} \tag{6.22}$$

- for Mode 2

$$F_{t,2,Rd} = \frac{2M_{pl,2,Rd} + n\Sigma F_{t,Rd}}{m+n} \tag{6.23}$$

- for Mode 3

$$F_{t,3,Rd} = \Sigma F_{t,Rd} \tag{6.24}$$

where:

$$M_{pl,1,Rd} = \frac{0.25\Sigma l_{eff,1}\, t_f^2\, f_y}{\gamma_{M0}} \quad \text{and} \quad M_{pl,2,Rd} = \frac{0.25\Sigma l_{eff,2}\, t_f^2\, f_y}{\gamma_{M0}} \tag{6.25}$$

Figure B6 depicts the geometrical parameters from eq. 6.22 and 6.23. Previously estimated parameter m will remain unchanged, while e_w and n are determined as follows:

$$n = \min(e_{min};\ 1.25m) = \min(22;\ 1.25 \cdot 25.1) = 22 \text{ mm} \tag{6.26}$$

$$e_w = \frac{d_w}{4} = \frac{30}{4} = 7.5 \text{ mm} \tag{6.27}$$

where, d_w is the diameter of the washer.

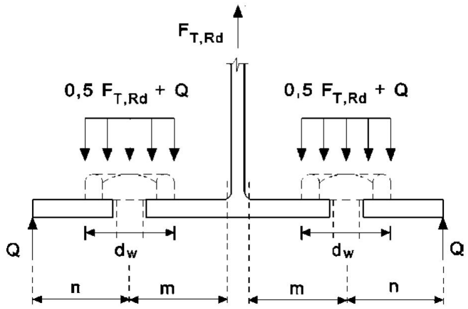

Figure B6: Geometrical parameters for the equivalent T-stub EC3 (2005)

For mode 2 and 3, the resistance of the bolts influences the value of the overall resistance of the T-stub. The resistance of a bolt in tension is evaluated as:

$$F_{t,Rd} = \frac{0.9 f_{ub} A_s}{\gamma_{M2}} = \frac{0.9 \cdot 1080 \cdot 157}{1.0} = 152.6 \text{ kN} \tag{6.28}$$

The effective lengths $l_{eff,1}$ and $l_{eff,2}$ correspond to the first two failure modes and are derived from the values previously determined (see previous section):

$$l_{eff,1} = \min(l_{eff,cp};\, l_{eff,nc}) \qquad \text{and} \qquad l_{eff,2} = l_{eff,nc} \tag{6.29}$$

The plastic resistances are determined once more for two possible cases when the bolts are working individually or in a group.

Individual resistances of bolt rows 1 and 2

Mode 1

$$M^{I}_{pl,1,Rd} = \frac{0.25 \cdot 140.82 \cdot 12^2 \cdot 385.3}{1.0 \cdot 1000} = 1953.3 \text{ kNmm} \tag{6.30}$$

$$\Rightarrow F^{I}_{t,1,Rpl} = \frac{(8 \cdot 22 - 2 \cdot 7.5) \cdot 1953.3}{2 \cdot 22 \cdot 25.1 - 7.5(25.1 + 22)} = 419.4 \text{ kN} \tag{6.31}$$

Mode 2

$$M^{I}_{pl,2,Rpl} = \frac{0.25 \cdot 140.82 \cdot 12^2 \cdot 385.3}{1.0 \cdot 1000} = 1953.3 \text{ kNmm} \tag{6.32}$$

$$\Rightarrow F^{I}_{t,2,Rpl} = \frac{2 \cdot 1953.3 + 22 \cdot 2 \cdot 152.6}{25.1 + 22} = 225.67 \text{ kN} \tag{6.33}$$

Mode 3

$$F^{I}_{t,3,Rpl} = 2 \cdot 152.6 = 305.2 \text{ kN} \tag{6.34}$$

Resistance of the group with bolt rows 1 and 2

Mode 1

$$M^{Gr}_{pl,1,Rpl} = \frac{0.25 \cdot (111.41 + 111.41) \cdot 12^2 \cdot 385.3}{1.0 \cdot 1000} = 3090.7 \text{ kNmm} \tag{6.35}$$

$$\Rightarrow F^{Gr}_{t,1,Rpl} = \frac{(8 \cdot 22 - 2 \cdot 7.5)3090.7}{2 \cdot 22 \cdot 25.1 - 7.5(25.1 + 22)} = 663.6 \text{ kN} \tag{6.36}$$

Mode 2

$$M^{Gr}_{pl,2,Rd} = \frac{0.25 \cdot (111.41 + 111.41) \cdot 12^2 \cdot 385.3}{1.0 \cdot 1000} = 3090.7 \text{ kNmm} \tag{6.37}$$

$$\Rightarrow F^{Gr}_{t,2,Rpl} = \frac{2 \cdot 3090.7 + 22 \cdot 4 \cdot 152.6}{25.1 + 22} = 416.7 \text{ kN} \tag{6.38}$$

Mode 3

$$F^{Gr}_{t,3,Rpl} = 4 \cdot 152.6 = 610.4 \text{ kN} \tag{6.39}$$

The ultimate resistance is assessed with the full strength of the bolts by suppressing the safety coefficient in eq. 6.28, therefore the ultimate tensile capacity of the bolts becomes:

$$F_{t,Ru} = \frac{f_{ub} A_s}{\gamma_{M2}} = \frac{1080 \cdot 157}{1.0} = 169.56 \text{ kN} \tag{6.40}$$

Consequently, the ultimate resistance of cfb is evaluated for two cases:

Individual resistances of bolt rows 1 and 2

Mode 1

$$M^{I}_{pl,1,Ru} = \frac{0.25 \cdot 140.82 \cdot 12^2 \cdot 539.6}{1.0 \cdot 1000} = 2735.6 \text{ kNmm} \tag{6.41}$$

$$\Rightarrow F^{I}_{t,1,Ru} = \frac{(8 \cdot 22 - 2 \cdot 7.5) \cdot 2735.6}{2 \cdot 22 \cdot 25.1 - 7.5(25.1 + 22)} = 587.3 \text{ kN} \tag{6.42}$$

Mode 2

$$M^{I}_{pl,2,Ru} = \frac{0.25 \cdot 140.82 \cdot 12^2 \cdot 539.6}{1.0 \cdot 1000} = 2735.6 \text{ kNmm} \tag{6.43}$$

$$\Rightarrow F^{I}_{t,2,Ru} = \frac{2 \cdot 2735.6 + 22 \cdot 2 \cdot 169.56}{25.1 + 22} = 274.76 \text{ kN} \tag{6.44}$$

Mode 3

$$F^{I}_{t,3,Ru} = 2 \cdot 69.56 = 339.12 \text{ kN} \tag{6.45}$$

Resistance of the group with bolt rows 1 and 2

Mode 1

$$M^{Gr}_{pl,1,Ru} = \frac{0.25 \cdot (111.41 + 111.41) \cdot 12^2 \cdot 539.6}{1.0 \cdot 1000} = 4328.5 \text{ kNmm} \tag{6.46}$$

$$\Rightarrow F_{t,1,Ru}^{Gr} = \frac{(8 \cdot 22 - 2 \cdot 7.5)4328.5}{2 \cdot 22 \cdot 25.1 - 7.5(25.1 + 22)} = 929.3 \text{ kN} \tag{6.47}$$

Mode 2

$$M_{pl,2,Ru}^{Gr} = \frac{0.25 \cdot (111.41 + 111.41) \cdot 12^2 \cdot 539.6}{1.0 \cdot 1000} = 4328.5 \text{ kNmm} \tag{6.48}$$

$$\Rightarrow F_{t,2,Ru}^{Gr} = \frac{2 \cdot 4328.5 + 22 \cdot 4 \cdot 169.56}{25.1 + 22} = 50.97 \text{ kN} \tag{6.49}$$

Mode 3

$$F_{t,3,Ru}^{Gr} = 4 \cdot 169.56 = 678.2 \text{ kN} \tag{6.50}$$

d) Component 4 - End-plate in bending

Similar to a column flange in bending in a bolted connection, the resistance and the failure mode of *epb* component are assessed once again by referring to the equivalent T-stub model. The fact that the first bolt rows is adjacent to the beam's flange in tension implies the estimation of an additional parameter m_2 as depicted in Figure B7.

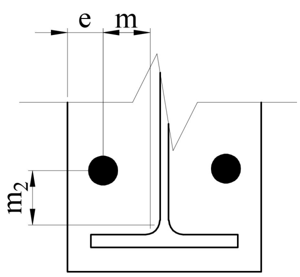

Figure B7: Geometrical parameters for the equivalent T-stub

The effective lengths of the T-stub element are evaluated based on the following parameters:

$$e = 22 \text{ mm}$$
$$m = \frac{p_2}{2} - \frac{t_{wb}}{2} - 0.8a_w\sqrt{2} = \frac{76}{2} - \frac{5.3}{2} - 0.8 \cdot 3 \cdot \sqrt{2} = 31.96 \text{ mm}$$
$$m_2 = \frac{h_b}{2} - \frac{p_1}{2} - t_{fb} - 0.8a_f\sqrt{2} = \frac{179.8}{2} - \frac{82}{2} - 7.8 - 0.8 \cdot 5 \cdot \sqrt{2} = 35.44 \text{ mm}$$
$$n = \min(e_{min};\ 1.25m) = \min(22;\ 1.25 \cdot 31.96) = 22 \text{ mm}$$

The effective lengths for bolt row 1 require the estimation of an α coefficient as this bolt row is under the beam flange in tension; the two following parameters are needed for the estimation of this coefficient (see Figure B8):

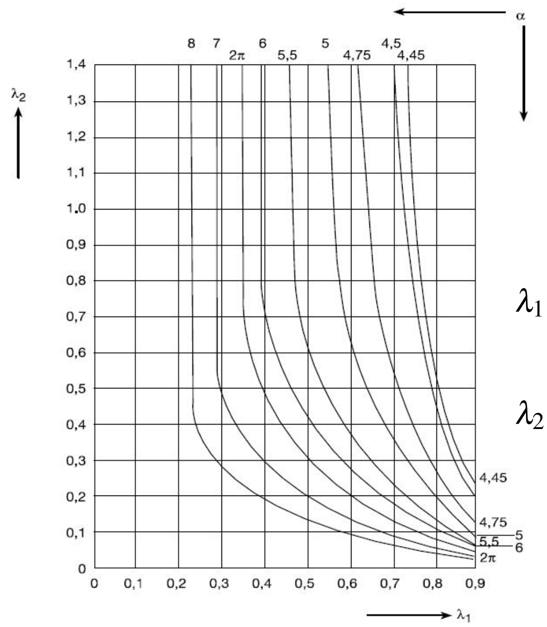

$$\left.\begin{aligned}\lambda_1 &= \frac{m}{m+e} = \frac{31.96}{31.96+22} = 0.59 \\ \lambda_2 &= \frac{m_2}{m+e} = \frac{35.44}{31.96+22} = 0.66\end{aligned}\right\} \Rightarrow \alpha = 5 \quad (6.51)$$

Figure B8: α coefficient (EC3, 2005)

Bolt row 1

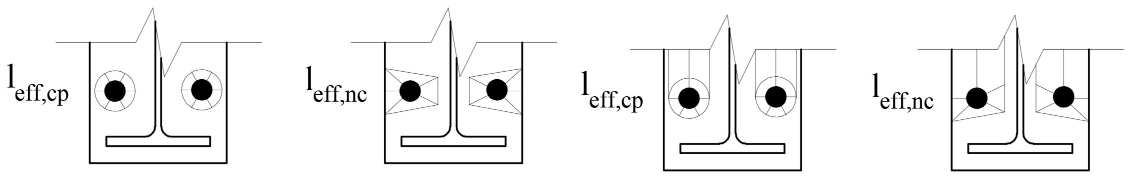

(a) Individual

(b) As first row of a group

Figure B9: Effective lengths for bolt row 1

- Individual effective lengths

$$\begin{aligned} l_{eff,cp} &= 2\pi m + p = 2\pi \cdot 31.96 = 200.8 \text{ mm} \\ l_{eff,nc} &= \alpha m = 5 \cdot 31.96 = 159.8 \text{ mm} \end{aligned} \tag{6.52}$$

-Effective lengths as first bolt row of a group

$$\begin{aligned} l_{eff,cp} &= \pi m + p = \pi \cdot 31.96 + 82 = 182.4 \text{ mm} \\ l_{eff,nc} &= 0.5p + \alpha m - (2m + 0.625e) \\ &= 0.5 \cdot 82 + 5 \cdot 31.96 - (2 \cdot 31.96 + 0.625 \cdot 22) = 123.1 \text{ mm} \end{aligned} \tag{6.53}$$

Bolt row 2

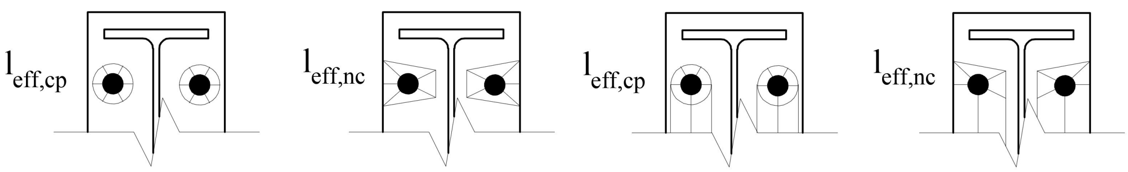

(a) Individual

(b) As first row of a group

Figure B10: Effective lengths for bolt row 2

- Individual effective lengths

$$l_{eff,cp} = 2\pi m + p = 2\pi \cdot 31.96 = 200.8 \text{ mm}$$
$$l_{eff,nc} = \alpha m = 5 \cdot 31.96 = 159.8 \text{ mm} \tag{6.54}$$

-Effective lengths as last bolt row of a group

$$\begin{aligned} l_{eff,cp} &= \pi m + p = \pi \cdot 31.96 + 82 = 182.4 \text{ mm} \\ l_{eff,nc} &= 0.5p + \alpha m - (2m + 0.625e) \\ &= 0.5 \cdot 82 + 5 \cdot 31.96 - (2 \cdot 31.96 + 0.625 \cdot 22) = 123.1 \text{ mm} \end{aligned} \tag{6.55}$$

The plastic and ultimate resistances are determined for two possible cases when the bolts are working individually or in a group:

Plastic individual resistances of bolt rows 1 and 2

Mode 1

$$M_{pl,1,Rpl} = \frac{0.25 \cdot 159.8 \cdot 15.08^2 \cdot 416.6}{1.0 \cdot 1000} = 3784.3 \text{ kNmm} \tag{6.56}$$

$$\Rightarrow F_{t,1,Rpl} = \frac{(8 \cdot 22 - 2 \cdot 7.5)3784.3}{2 \cdot 22 \cdot 31.96 - 7.5(31.96 + 22)} = 608.4 \text{ kN} \tag{6.57}$$

Mode 2

$$M_{pl,2,Rpl} = \frac{0.25 \cdot 159.8 \cdot 15.08^2 \cdot 416.6}{1.0 \cdot 1000} = 3784.3 \text{ kNmm} \tag{6.58}$$

$$\Rightarrow F_{t,2,Rpl} = \frac{2 \cdot 3784.3 + 22 \cdot 2 \cdot 152.6}{31.96 + 22} = 264.7 \text{ kN} \tag{6.59}$$

Mode 3

$$F_{t,3,Rpl} = 2 \cdot 152.6 = 305.2 \text{ kN} \tag{6.60}$$

Plastic resistance of the group with bolt rows 1 and 2

Mode 1

$$M_{pl,1,Ru} = \frac{0.25 \cdot (123.1 + 123.1) \cdot 15.08^2 \cdot 416.6}{1.0 \cdot 1000} = 5831.9 \text{ kNmm} \tag{6.61}$$

$$\Rightarrow F_{t,1,Ru} = \frac{(8 \cdot 22 - 2 \cdot 7.5)5831.9}{2 \cdot 22 \cdot 31.96 - 7.5(31.96 + 22)} = 937.6 \text{ kN} \tag{6.62}$$

Mode 2

$$M_{pl,2,Ru} = \frac{0.25 \cdot (123.1 + 123.1) \cdot 15.08^2 \cdot 416.6}{1.0 \cdot 1000} = 5831.9 \text{ kNmm} \tag{6.63}$$

$$\Rightarrow F_{t,2,Ru} = \frac{2 \cdot 5831.9 + 22 \cdot 4 \cdot 152.6}{31.96 + 22} = 465.1 \text{ kN} \tag{6.64}$$

Mode 3

$$F_{t,3,Ru} = 4 \cdot 152.6 = 610.4 \text{ kN} \tag{6.65}$$

The yield strength is replaced with the ultimate one in the expressions above and the ultimate resistance of *epb* component is evaluated as follows:
Ultimate individual resistances of bolt rows 1 and 2
Mode 1

$$M^I_{pl,1,Ru} = \frac{0.25 \cdot 159.8 \cdot 15.08^2 \cdot 588.7}{1.0 \cdot 1000} = 5347.6 \text{ kNmm} \tag{6.66}$$

$$\Rightarrow F^I_{t,1,Ru} = \frac{(8 \cdot 22 - 2 \cdot 7.5)5347.6}{2 \cdot 22 \cdot 31.96 - 7.5(31.96 + 22)} = 859.8 \text{ kN} \tag{6.67}$$

Mode 2

$$M^I_{pl,2,Ru} = \frac{0.25 \cdot 159.8 \cdot 15.08^2 \cdot 588.7}{1.0 \cdot 1000} = 5347.6 \text{ kNmm} \tag{6.68}$$

$$\Rightarrow F^I_{t,2,Ru} = \frac{2 \cdot 5347.6 + 22 \cdot 2 \cdot 169.56}{31.96 + 22} = 336.5 \text{ kN} \tag{6.69}$$

Mode 3

$$F^I_{t,3,Ru} = 2 \cdot 169.56 = 339.1 \text{ kN} \tag{6.70}$$

Ultimate resistance of the group with bolt rows 1 and 2
Mode 1

$$M^{Gr}_{pl,1,Ru} = \frac{0.25 \cdot (123.1 + 123.1) \cdot 15.08^2 \cdot 588.7}{1.0 \cdot 1000} = 8241.1 \text{ kNmm} \tag{6.71}$$

$$\Rightarrow F^{Gr}_{t,1,Ru} = \frac{(8 \cdot 22 - 2 \cdot 7.5)8241.1}{2 \cdot 22 \cdot 31.96 - 7.5(31.96 + 22)} = 1325 \text{ kN} \tag{6.72}$$

Mode 2

$$M^{Gr}_{pl,2,Ru} = \frac{0.25 \cdot (123.1 + 123.1) \cdot 15.08^2 \cdot 588.7}{1.0 \cdot 1000} = 8241.1 \text{ kNmm} \tag{6.73}$$

$$\Rightarrow F^{Gr}_{t,2,Ru} = \frac{2 \cdot 8241.1 + 22 \cdot 4 \cdot 169.56}{31.96 + 22} = 582 \text{ kN} \tag{6.74}$$

Mode 3

$$F^{Gr}_{t,3,Ru} = 4 \cdot 169.56 = 678.2 \text{ kN} \tag{6.75}$$

e) Component 5 - Beam flange and web in compression

The bending moment applied to the beam leads to the development of compression forces in the proximity of the beam flange and the adjacent part of the web. Due to different lever arms, the concentrated force F_c may differ considerably when compared to the compression force F induced by the same loading at a certain distance from the connection, as depicted in Figure B11.

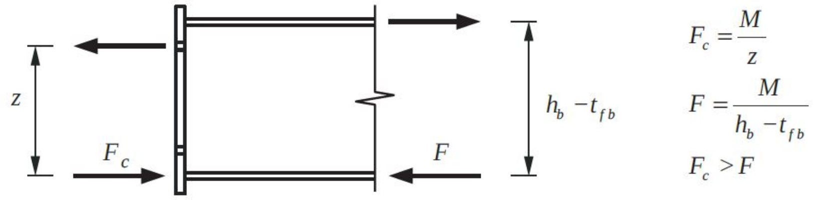

Figure B11: Concentrated force F_c and compression force F (Jaspart and Weynand, 2016)

The design compression resistance of the combined beam flange and web is given by the following expression:

$$F_{c,fb,Rd} = \frac{M_{c,Rd}}{h - t_{fb}} \tag{6.76}$$

where h is the depth of the connected beam and $M_{c,Rd}$ is the moment resistance of the beam cross-section.

For an IPE 180 profile, being a cross-section class 2, the plastic resistance for bending about the principal axis of the cross-section is evaluated as:

$$M_{c,Rpl} = M_{pl,Rpl} = \frac{W_{pl} f_y}{\gamma_{M0}} = \frac{169640.5 \cdot 435.5}{1.0 \cdot 10^3} = 73870 \text{ kNmm} \tag{6.77}$$

The plastic compression resistance of the bfc component yields:

$$F_{c,fb,Rpl} = \frac{73780}{(179.8 - 7.8)10^3} = 429.5 \text{ kN} \tag{6.78}$$

The ultimate resistance yields from eqs. 6.79 and 6.80:

$$M_{c,Ru} = M_{pl,Ru} = \frac{W_{pl} f_u}{\gamma_{M0}} = \frac{169640.5 \cdot 545.2}{1.0 \cdot 10^3} = 92488 \text{ kNmm} \tag{6.79}$$

The plastic compression resistance of the bfc component yields:

$$F_{c,fb,Ru} = \frac{92488}{(179.8 - 7.8)10^3} = 537.7 \text{ kN} \tag{6.80}$$

f) Component 6 - Beam web in tension

For the beam web in tension, the resistance is estimated with the following expression:

$$F_{t,wb,Rd} = \frac{b_{eff,t,wb}\, t_{wb}\, f_{y,wb}}{\gamma_{M0}} \tag{6.81}$$

The effective width $b_{eff,t,wb}$ is considered to be equal to the equivalent length l_{eff} of the T-stub evaluated for epb component. Therefore, the effective width to compute the resistance of the bolt rows acting individually or as a group is estimated as follows:
- for bolt rows 1 and 2 acting individually

$$b_{eff,t,wb} = \min(l_{eff,cp};\; l_{eff,nc}) = \min(200.8;\; 159.8) = 159.8 \text{ mm}$$

- for bolt rows 1 and 2 acting as a group

$$b_{eff,t,wb} = \min(\Sigma l_{eff,cp};\ \Sigma l_{eff,nc}) = \min(182.4 + 182.4\ ; 123.1 + 123.1) = 246.2 \text{ mm}$$

The plastic individual resistance of bolt rows 1 and 2 yields:

$$F^{I}_{t,wb,Rpl} = \frac{159.8 \cdot 5.3 \cdot 435.5}{1.0 \cdot 1000} = 368.8 \text{ kN} \tag{6.82}$$

For the bolt rows acting as a group:

$$F^{Gr}_{t,wb,Rpl} = \frac{246.2 \cdot 5.3 \cdot 435.5}{1.0 \cdot 1000} = 568.3 \text{ kN} \tag{6.83}$$

The ultimate individual resistance of bolt rows 1 and 2 is:

$$F^{I}_{t,wb,Ru} = \frac{159.8 \cdot 5.3 \cdot 545.2}{1.0 \cdot 1000} = 461.7 \text{ kN} \tag{6.84}$$

For the bolt rows acting as a group:

$$F^{Gr}_{t,wb,Rd} = \frac{246.2 \cdot 5.3 \cdot 545.2}{1.0 \cdot 1000} = 711.5 \text{ kN} \tag{6.85}$$

Assembly of the components

The assembly of the basic active components of the joint allows for to assess its bending resistance, the latter being derived from from the equilibrium condition between tensile and compressive forces within the joint.Thereofre, the sum of the tensile forces corresponding to each bolt row has to be smaller than the resistance of the compressed group of components. Accordingly, the tensile capacity of each bolt row is initially estimated as follows:

Plastic resistance

- Load which can be supported by row 1 and 2 considered individually

Column flange in bending - *cfb*:	225.67 kN
Column web in tension - *cwt*:	382.89 kN
End-plate in bending - *epb*:	264.7 kN
Beam web in tension - *bwt*:	368.8 kN
$F_{1,min} =$	225.67 kN

- Account for group effect between rows 1 and 2

The sum of the individual resistances of rows 1 and 2 is equal to:

$$F_{1,min} + F_{2,min} = 225.67 + 225.67 = 451.34 \text{ kN} \tag{6.86}$$

Afterwards, this value should be compared to the tensile force that can be supported by bolt rows

1 and 2 acting as a group:

Column flange in bending - *cfb*:	416.67 kN
Column web in tension - *cwt*:	605.85 kN
End-plate in bending - *epb*:	465 kN
Beam web in tension - *bwt*:	568.3 kN
$F_{1+2,min} =$	416.67 kN

As the group resistance is smaller than the sum of the individual resistances, the tensile individual resistance of each row cannot be reached, thus a reduction of the forces distributed on the elevation of the joint is required. The load which can be supported by the 2$^{\text{nd}}$ bolt row is estimated as follows:

$$F_{2,min,red} = F_{1+2,min} - F_{1,min} = 416.67 - 225.67 = 191 \text{ kN} \tag{6.87}$$

Thus, the sum of the maximum tensile resistances of rows 1 and 2 will take the value of their resistance acting as a group:

$$F_{1,min} + F_{2,min,red} = F_{1+2,min} = 416.67 \text{ kN} \tag{6.88}$$

In order to ensure the equilibrium of the internal forces in the joint, this value has to be compared to the resistances of the components in compression:

Column web in compression - *cwc*:	450.4 kN
Beam web and flange in compression - *bfc*:	429.48 kN
$F_{glob,min} =$	429.48 kN

Since the resistance of the components group in compression is higher than $F_{1+2,min}$, the individual resistances of the bolts (reduced by the group resistance) can be reached. Therefore, the tensile forces within the joint can be expressed as shown in Figure B12b.

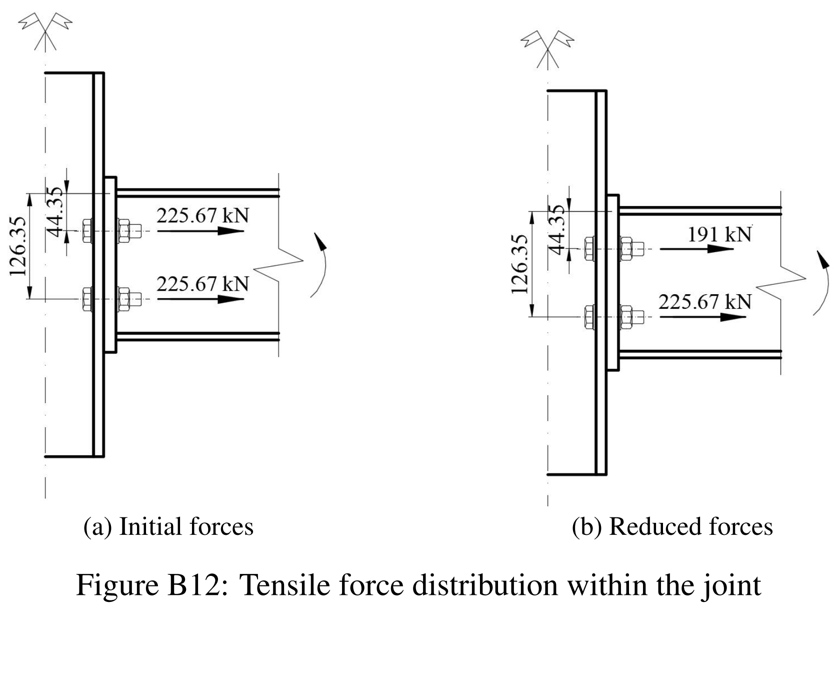

(a) Initial forces (b) Reduced forces

Figure B12: Tensile force distribution within the joint

Ultimate resistance

- Load which can be supported by row 1 and 2 considered individually

Column flange in bending - *cfb*:	274.76 kN
Column web in tension - *cwt*:	480.3 kN
End-plate in bending - *epb*:	336.5 kN
Beam web in tension - *bwt*:	461.7 kN
$F_{1,min} =$	274.76 kN

- Account for group effect between rows 1 and 2

The sum of the individual resistances of rows 1 and 2 is equal to:

$$F_{1,min} + F_{2,min} = 274.76 + 274.76 = 549.52 \text{ kN} \tag{6.89}$$

Afterwards, this value is compared to the tensile force that can be supported by bolt rows 1 and 2 acting as a group:

Column flange in bending - *cfb*:	500.97 kN
Column web in tension - *cwt*:	760.02 kN
End-plate in bending - *epb*:	582.02 kN
Beam web in tension - *bwt*:	711.51 kN
$F_{1+2,min} =$	500.97 kN

The load which can be supported by the 2$^{\text{nd}}$ bolt row is reduced once again as follows:

$$F_{2,min,red} = F_{1+2,min} - F_{1,min} = 500.97 - 274.76 = 226.21 \text{ kN} \tag{6.90}$$

The resistance of row 1 and row 2acting as a group becomes:

$$F_{1,min} + F_{2,min,red} = F_{1+2,min} = 500.97 \text{ kN} \tag{6.91}$$

In order to ensure the equilibrium of the internal forces in the joint, this value has to be compared to the resistances of the components in compression:

Column web in compression - *cwc*:	565.02 kN
Beam web and flange in compression - *bfc*:	537.72 kN
$F_{glob,min} =$	565.02 kN

Since the resistance of the components in compression is higher than the sum of the reduced individual resistance of the bolt rows, the bolt rows resistances can be reached.

Bending resistance

Considering the distribution of forces illustrated in Figure B12b and the lever arms corresponding to each bolt row, the plastic bending resistance is estimated using the following expression.

$$M_{Rpl} = \Sigma h_r F_{tr,Rpl} = [225.67 \cdot 126.35 + 191 \cdot 44.35] \cdot 10^{-3} = 36.98 \text{ kNm} \tag{6.92}$$

Subsequently, the ultimate bending resistance of the joint yields:

$$M_{Ru} = [274.76 \cdot 126.35 + 226.21 \cdot 44.35] \cdot 10^{-3} = 44.75 \text{ kNm} \tag{6.93}$$

Rotational stiffness

Initial stiffness

The initial rotational stiffness of the joint is assessed by estimating the stiffness coefficients for the different components of the joint. The latter are determined according to the prescriptions of EN 1993-1-8 as follows:

- *Column web in compression:*

$$k_2 = \frac{0.7 b_{eff,c,wc}\, t_{wc}}{d_c} = \frac{0.7 \cdot 165.7 \cdot 7.27}{89.5} = 8.1 \text{ mm} \tag{6.94}$$

- *Column web in tension:*

$$k_{3,1} = k_{3.2} = \frac{0.7 b_{eff,t,wc}\, t_{wc}}{d_c} = \frac{0.7 \cdot 140.8 \cdot 6.27}{89.5} = 5.5 \text{ mm} \tag{6.95}$$

- *Column flange in bending:*

$$k_{4,1} = k_{4,2} = \frac{0.9 l_{eff}\, t_{fc}^3}{m^3} = \frac{0.9 \cdot 111.41 \cdot 12^3}{25.1^3} = 11 \text{ mm} \tag{6.96}$$

- *End-plate in bending:*

$$k_{5,1} = k_{5,2} = \frac{0.9 l_{eff}\, t_p^3}{m^3} = \frac{0.9 \cdot 123.1 \cdot 15.08^3}{31.96^3} = 11.6 \text{ mm} \tag{6.97}$$

- *Bolts in tension:*

$$k_{10} = \frac{1.6 A_s}{L_b} = \frac{1.6 \cdot 157}{12 + 15 + 2 \cdot 3 + (10 + 13)/2} = 5.6 \text{ mm} \tag{6.98}$$

Taking into account the distribution of tensile forces on the elevation of the joint, it is easily noticeable that both bolt rows are subjected to tension. For such a case, Eurocode 3 prescribes the following expression to evaluate the equivalent stiffness coefficient for the two bolt rows:

$$k_{eq} = \frac{\sum_r k_{efff,r}\, h_r}{z_{eq}} \tag{6.99}$$

where, the effective stiffness coefficient $k_{eff,r}$ for bolt row r is determined from:

$$k_{eff,r} = \frac{1}{\sum_i \frac{1}{k_{i,r}}} \tag{6.100}$$

Because all stiffness coefficients for the two bolt rows are identical, the value for $k_{eff,1}$ and $k_{eff,2}$ will be the same and more specifically:

$$k_{eff,1-2} = \frac{1}{\frac{1}{5.5}+\frac{1}{11}+\frac{1}{11.6}+\frac{1}{5.6}} = 1.86 \text{ mm} \tag{6.101}$$

the equivalent lever arm z_{eq} is estimated as follows:

$$z_{eq} = \frac{\sum_r k_{eff,r}\, h_r^2}{\sum_r k_{eff,r}\, h_r} = \frac{1.86 \cdot 126.35^2 + 1.86 \cdot 44.35^2}{1.86 \cdot 126.35 + 1.86 \cdot 44.35} = 105 \text{ mm} \tag{6.102}$$

Therefore, the equivalent stiffness coefficient k_{eq} yields:

$$k_{eq} = \frac{1.86 \cdot 126.35 + 1.86 \cdot 44.35}{105} = 3 \text{ mm} \tag{6.103}$$

The initial rotational stiffness of the joint is then computed from eq. 6.104.

$$S_{j,ini} = \frac{Ez^2}{\sum_i \frac{1}{k_i}} = \frac{210000 \cdot 105^2}{\frac{1}{3}+\frac{1}{8.1}} \cdot 10^{-6} = 5107.2 \text{ kNm/rad} \tag{6.104}$$

Strain-hardening stiffness

The bending resistance associated to each individual component of the joint has to be compared to the value of bending resistance corresponding to the "elastic contribution" boundary.

The limit value of the bending capacity is:

$$M_{Rpl,limit} = 1.65 M_{Rpl} = 1.65 \cdot 36.98 = 61.02 \text{ kNm} \tag{6.105}$$

The plastic bending resistance associated to all components that may contribute to the strain-hardening stiffness is computed as listed below:

- *Column web in compression:*

$$M_{Rpl,cwc} = 450.4 \cdot 105.05 \cdot 10^{-3} = 47.31 \text{ kNm} \tag{6.106}$$

- *Column web in tension:*

$$M_{Rpl,cwt} = [382 \cdot 126.35 + (605.85 - 382) \cdot 44.35] \cdot 10^{-3} = 58.2 \text{ kNm} \tag{6.107}$$

- *Column flange in bending:*

$$M_{Rpl,cfb} = [225.67 \cdot 126.35 + (416.67 - 225.67) \cdot 44.35] \cdot 10^{-3} = 36.98 \text{ kNm} \tag{6.108}$$

- *End-plate in bending:*

$$M_{Rpl,epb} = [264.72 \cdot 126.35 + (465.07 - 264.72) \cdot 44.35] \cdot 10^{-3} = 42.33 \text{ kNm} \tag{6.109}$$

- *Bolts in tension:*

$$M_{Rpl,bt} = [2 \cdot 152.6 \cdot 126.35 + 2 \cdot 152.6 \cdot 44.35] \cdot 10^{-3} = 52.10 \text{ kNm} \tag{6.110}$$

Since the plastic bending resistance associated to each of the joint's components, all components will contribute to the post-plastic stiffness with their strain-hardening coefficients. Therefore, the strain hardening stiffness is estimated as follows:

$$S_{j,st} = \frac{Ez^2}{\sum \frac{1}{k^*}} \tag{6.111}$$

It is reasonable to assume that the ratio between the strain-hardening and the elastic moduli of steel is:

$$\frac{E_{st}}{E} = \frac{1}{50}$$

Therefore, the strain-hardening stiffness coefficient for each individual component are evaluated as listed below:

- *Column web in compression:*

$$k_{2,st} = \frac{E_{st}}{E} k_2 = \frac{1}{50} \cdot 8.1 = 0.16 \text{ mm} \tag{6.112}$$

- *Column web in tension:*

$$k_{3,1,st} = k_{3,2,st} = \frac{E_{st}}{E} k_3 = \frac{1}{50} \cdot 5.5 = 0.109 \text{ mm} \tag{6.113}$$

- *Column flange in bending:*

$$k_{4,1,st} = k_{4,2,st} = \frac{E_{st}}{E} k_4 = \frac{1}{50} \cdot 11 = 0.22 \text{ mm} \tag{6.114}$$

- End-plate in bending:

$$k_{5,1,st} = k_{5,2,st} = \frac{E_{st}}{E} k_5 = \frac{1}{50} \cdot 11.6 = 0.233 \text{ mm} \tag{6.115}$$

- Bolts in tension:

$$k_{10,st} = \frac{E_{st}}{E} k_{10} = \frac{1}{50} \cdot 5.6 = 0.113 \text{ mm} \tag{6.116}$$

Accordingly, the equivalent strain hardening stiffness coefficient $k^*_{eff,1-2}$ yields :

$$k^*_{eff,1-2} = \frac{1}{\frac{1}{0.109} + \frac{1}{0.22} + \frac{1}{0.233} + \frac{1}{0.113}} = 0.037 \text{ mm} \tag{6.117}$$

And the equivalent lever arm z^*_{eq}:

$$z_{eq} = \frac{\sum_r k^*_{eff,r} h_r^2}{\sum_r k^*_{eff,r} h_r} = \frac{0.037 \cdot 126.35^2 + 0.037 \cdot 44.35^2}{0.037 \cdot 126.35 + 0.037 \cdot 44.35} = 105 \text{ mm} \tag{6.118}$$

The initial rotational stiffness of the joint is then computed from eq. 6.119.

$$S_{j,st} = \frac{Ez^2}{\sum \frac{1}{k^*}} = \frac{210000 \cdot 105^2}{\frac{1}{0.037} + \frac{1}{0.16}} \cdot 10^{-6} = 102.14 \text{ kNm/rad} \tag{6.119}$$

Rotational capacity

The plastic rotational capacity $\phi_p l$ can be estimated easily on the basis of M_{Ru}, $M_{R,pl}$ and $S_{j,st}$ from eq. 6.120.

$$\phi_{pl} = \frac{M_{Rpl} + 2/3 M_{Rpl}}{S_{j,ini}/7} - \frac{2/3 M_{Rpl}}{S_{j,ini}} = \frac{36.98 + 2/3 \cdot 36.98}{5107.2/7} - \frac{2/3 \cdot 36.98}{5107.2} = 0.0217 \text{ rad} \tag{6.120}$$

Subsequently, the ultimate rotational capacity ϕ_u yields:

$$\phi_u = \frac{M_{Ru} - M_{Rpl}}{S_{j,st}} = \frac{44.75 - 36.98}{102.14} = 0.076 \text{ rad} \tag{6.121}$$